



ALMA MATER STUDIORUM - UNIVERSITA' DI BOLOGNA

FACOLTÀ DI AGRARIA

**Dottorato di Ricerca in Scienze degli Alimenti
(CHIM/06)**

***NMR Study of Meat as Related to its
Structural Organisation***

Coordinatore:

Prof. Claudio Cavani

Presentata da:

Luca Venturi

Tutors:

Prof. Claudio Cavani

Dr. Mauro Andrea Cremonini

XX Ciclo - Esame Finale - A.A.2007/08

*This work is dedicated to the memory of my father Andrea
and to all the members of my family, my mother Laura, Pino, Rocco
and my beloved wife Chiara*

INDEX**CHAPTER 1**

	Introduction.....	9
1.1	Muscle Architecture.....	9
1.2	NMR Relaxation Studies on Muscle Tissue and Meat.....	11
1.3	Relationships Between NMR Transverse Relaxation Times Distribution and Post Mortem events in Muscle Tissue.....	16
1.4	Quality Evaluation of Meat by NMR Transverse Relaxation Studies.....	18
1.4.1	<i>Water Holding Capacity (WHC).....</i>	18
1.5	Aim of the Study.....	19
	References.....	21

CHAPTER 2

	NMR Investigation of Relaxation and Magnetisation Transfer Process in Meat Through the Analysis of a Model Protein System: BSA.	
	<i>Part I: Monodimensional Approach.....</i>	23
2.1	Bovine Serum Albumin (BSA): a Model to Study the Transverse Relaxation Distribution of Meat.....	23
2.2	Assignment of the Fast Relaxing Proton Pool in Cross-Linked BSA: CPMG and One Pulse Experiments.....	25
2.3	Assignment of the Fast Relaxing Proton Fraction in Meat.....	27
	Materials and Methods.....	29
	References.....	31

CHAPTER 3

	NMR Investigation of Relaxation and Magnetisation Transfer Process in Meat Through the Analysis of a Model Protein System: BSA.	
	<i>Part II: Multidimensional Approach.....</i>	33
3.1	Multidimensional Relaxation Studies on BSA.....	33
3.1.1	<i>Cross Relaxation in a 24% w/w Native BSA Solution.....</i>	37

3.1.2	<i>Cross Relaxation in a Thermally Denatured 24% BSA Gel.....</i>	41
3.1.3	<i>Three-Dimensional Field-Cycled Cross-Correlation Relaxometry.....</i>	45
3.1.4	<i>Native BSA Systems over a Range of Water Contents.....</i>	46
3.2	Multidimensional Relaxometry and Diffusometry of Meat.....	52
3.2.1	<i>T₁-T₂ Spectra of Cod Meat.....</i>	53
3.2.2	<i>T₂-store-T₂ Cod Meat Spectra.....</i>	54
	Materials and Methods.....	57
	Appendix A.....	59
	References.....	63

CHAPTER 4

Study of Water Availability and Mobility in Meat: a NMR-DSC-a_w Multianalytical Approach..... 65

4.1	Measurements of Water Availability in Food Systems.....	65
4.2	Aim of the Study.....	67
4.3	Sorption Isotherm Approach.....	67
4.4	DSC Measurements.....	69
4.5	NMR Measurements.....	70
4.6	Multianalytical Comparison.....	72
	Materials and Methods.....	75
	References.....	81

CHAPTER 5

NMR Diffusion Studies on Meat. Part I: Probing Meat Microstructure through Bulk ¹H NMR Diffusion Measurements..... 85

5.1	Water Diffusive Studies and Microstructural Organisation of Compartmentalized Biological Samples.....	85
5.2	The Choice of an Appropriate Fitting Model for Meat.....	86
5.3	Microstructure and Diffusive Consideration on Turkey Fresh Samples.....	89

5.4	Effect of Freezing on Meat Structure and Organisation.....	91
	Materials and Methods.....	95
	References.....	97

CHAPTER 6

NMR Diffusion Studies on Meat.		
<i>Part II: DTI Measurements of Meat Anisotropic Diffusion Properties upon Freezing.....</i>		
		99
6.1	Previous NMR Meat Authentication Studies.....	99
6.2	Effect of Different Freezing Methods and Storage Time on Meat DTI Parameters.....	100
	Materials and Methods	107
	Appendix B.....	111
	References.....	125
	Conclusions and Perspectives.....	127
	Acknowledgments.....	131

CHAPTER 1

INTRODUCTION

1.1 Muscle Architecture

Muscles are organs of the muscular system. Each organ or muscle consists of muscle tissue (i.e. skeletal or smooth), connective tissue, nerve tissue, and blood or vascular tissue. Skeletal muscle is the major component of lean tissue that is used for food thus its structure and organisation is of great importance to food animal agriculture and industrial processing. Skeletal muscles vary considerably in size, shape, and arrangement of fibers. Each skeletal muscle fiber is a single cylindrical muscle cell. An individual skeletal muscle may be made up of hundreds, or even thousands, of muscle fibers bundled together and wrapped in a connective tissue covering.

Each muscle is surrounded by a connective tissue sheath called the **epimysium** (see figure 1). Since the muscle fibers are organized into bundles (fasciculi) portions of the epimysium known as the **perimysium** project inward to surround each fasciculus. Within the fasciculus, each individual muscle cell, called a muscle fiber, is surrounded by connective tissue known as the **endomysium**. The connective tissue covering furnishes support and protection to the delicate cells and allows them to withstand the forces of contraction. The coverings also provide pathways for the passage of blood vessels and nerves [1].

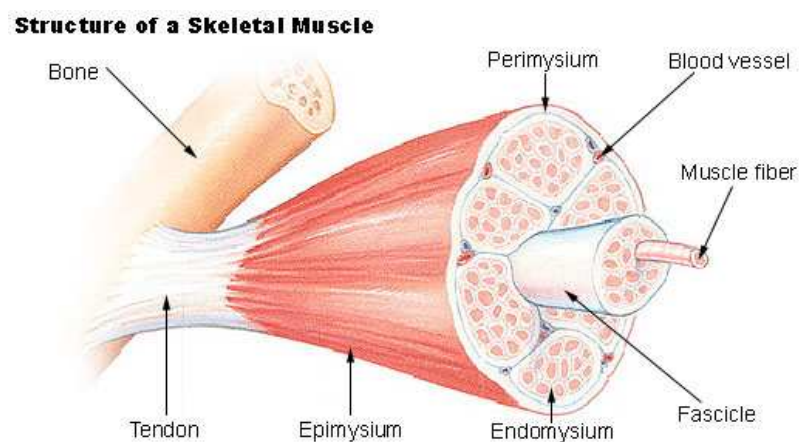


Figure 1. Schematic representation of the skeletal muscle organisation.

(Figure taken from www.web-books.com/.../Skeletal_Structure.htm)

Each muscle fiber cell comprises (see figure 2) [1]:

- a plasma membrane sheath which is called the **sarcolemma**;
- **transverse tubules** ("T Tubules"), tunnel-like extensions that from the sarcolemma pass through the muscle fibre from one side of it to the other in transverse sections through the diameter of the fibre;
- **nuclei** that are located at the edges of the diameter of the fibre, adjacent to the sarcolemma. A single muscle fibre may have many nuclei;
- a cytoplasm called **sarcoplasm** containing very many **mitochondria**, which are the energy-producing units within the cell. These mitochondria produce large amounts of a chemical called "Adenosine Triphosphate", which is usually referred to in abbreviated form as "**ATP**";
- a **sarcoplasmic reticulum** that is a network of membrane-enclosed tubules similar to smooth endoplasmic reticulum (SER). Sarcoplasmic reticulum extends throughout the **sarcoplasm** of the cell and it has the function of storing calcium ions, which are necessary for muscle contraction;

In addition, **myoglobin** is present in the sarcoplasm of muscle fibres/cells. This is a reddish pigment that not only results in the distinctive colour of skeletal muscle, but also stores oxygen - until it is required by the mitochondria for the production of ATP.

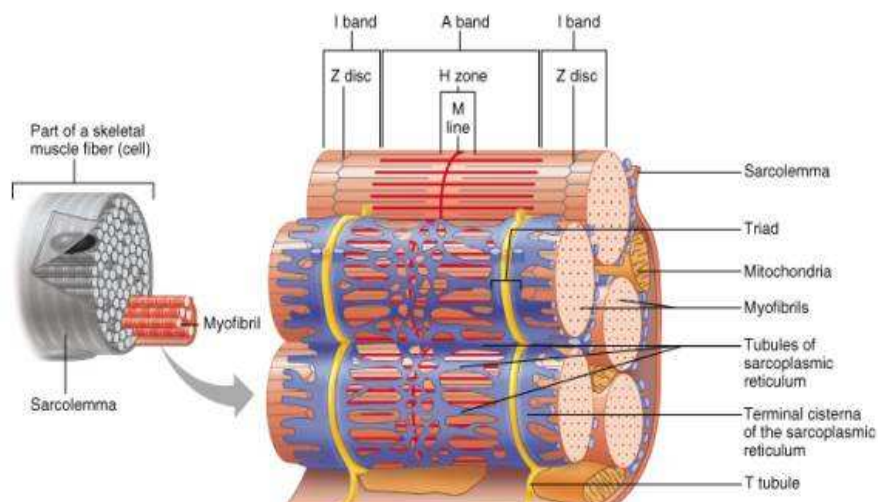


Figure 2. Structure of a skeletal muscle cell
(Figure taken from www.etsu.edu/.../Histologyofmuscleforweb.htm)

Within each muscle cell there are also numerous **myofibrils**, which extend for the length of the cell. Actin and myosin are the two principal muscle proteins, and they are found in myofibrils. They are arranged in a ring-like structure, usually with

six (**thin**) actin strands surrounding a (**thick**) myosin fibril. Again, they run parallel and lengthwise. Thick and thin filaments within myofibrils overlap in a structured way, forming units called **sarcomeres**. Sarcomeres are sections of myofibril that are separated from each other by areas of dense material called "**Z discs**". The sarcomeres are also described in terms of the bands/zones within which one or both of the two filaments occur. These bands/zones are illustrated in terms of:

- "**A band**", a relatively darker area within the sarcomere where there is an overlapping of the thin and thick filaments of the myofibril. This area approximately extends along the total length of the thick filaments;
- "**H zone**" located at the centre of the A band of each sarcomere. In this region there are only thick filaments, and no thin filaments;
- "**I band**", a region between adjacent A bands, in which there are only thin filaments, and no thick filaments (each I band extends across two adjacent sarcomeres).

The myofibrils occupy approximately 80% of the muscle volume and the water, which makes up about 75% of the muscle weight, is located in the spaces between thin and thick filaments. Structural organisation of muscle is therefore not only important for contraction but also capable of influencing the processing and eating attributes of meat after muscle *post mortem* conversion.

1.2 NMR Relaxation Studies on Muscle Tissue and Meat

Meat contains approximately 75% of water whose organization is of utmost importance for its quality. Water has an essential role in almost every aspect of meat science, including the processing response of raw material, its organoleptic properties as well as its microbial safety. Nevertheless, the fundamental understanding of the role of water in meat remains largely empirical. The problem mainly lies in the extreme complexity of meat as its micro-heterogeneous, multicomponent and multiphase characteristics make hard to predict how water interacts and partitions between the various components and micro-phases. Therefore, the production of clear cut-models and simple quality parameters readily applicable in the meat industry require a deeper understanding of the mobility and availability of water in terms of migration among compartments as well as biopolymer-solute interactions at the molecular level.

NMR proton relaxometry is a unique technique for studying meat quality because it gives direct information about physical (distribution, compartmentalisation) and chemical (mobility, interactions with macromolecules) water properties. The interpretation of meat and muscle relaxation times has been the matter of dispute since the initial stage of research. Early NMR proton relaxation studies on muscle tissue showed that [2]:

- a) the ^1H and ^2H T_2 relaxation in muscle water is much faster than T_2 relaxation of pure water;
- b) the T_2 relaxation of protons in muscle tissue is non-monoexponential.

The multiexponential property of meat transverse relaxation time (T_2) has usually been solved by decomposing the relaxation decay into a discrete sum of components according to the following:

$$I(2\tau n) = \sum_{i=1}^M I_{0,i} \cdot \exp(-2\tau n / T_{2,i}) \quad n=1 \dots N \quad (1)$$

where $I(2\tau n)$ is the intensity of magnetisation during its decay, $I_{0,i}$ is the signal intensity of component i , and $T_{2,i}$ the corresponding relaxation time. The application of this *a priori* model has usually led to the detection of three transverse relaxation components: (i) a major population characterized by a time constant of 35-50 ms accounting approximately for 85-95% of the signal (namely T_{21}); (ii) a slower relaxing component with a T_2 relaxation time of 100-250 ms representing about 5-15% of the relaxation (namely T_{22}) and (iii) a fast relaxing pool with a T_2 of 0-10 ms corresponding to 5% of the total signal (namely T_{2b}). However, in the literature the investigation of muscle and meat relaxation times has mainly focused on the slower and most abundant relaxing components (T_{21} and T_{22}). The presence of these two populations has also been confirmed by the application of a more appropriate fitting model based on the inverse Laplace transformation [3] of the raw CPMG (**C**arr-**P**urcel-**M**eiboom-**G**ill) decay [4]. This approach known as the "continuous fitting" leads to the least biased distribution of transverse relaxation times that fits the CPMG decay at best according to eq (2):

$$I(2\tau n) = \sum_{i=1}^M I_{0,i} \cdot \exp(-2\tau n / T_{2,i}) \quad n=1 \dots N \quad (2)$$

where 2τ is the CPMG interpulse spacing, n is the index of a CPMG echo, and $I_0(T_{2,i})$ provides a distribution of signal intensities for each T_2 component extrapolated at $\tau = 0$ (the relaxogram), sampled logarithmically in the interval $T_{2,\min} - T_{2,\max}$ as shown in eq (3):

$$T_{2,i} = T_{2,\min} \cdot \exp\left[\frac{(i-1)\ln(T_{2,\max}/T_{2,\min})}{(M-1)}\right] \quad (3)$$

In comparison with the discrete model, it has been demonstrated that the continuous approach offers a less biased and reliable method since the number of relaxation components included in the fitting procedure is a result of the regularization parameter incorporated in the algorithm and not an arbitrary choice set by the user.

In figure 3 is reported a typical continuous muscle sample T_2 distribution. It can be observed that the relaxogram is dominated by the presence of two populations (i.e. T_{21} and T_{22}) while a third pool (T_{2b}) is detectable in the fast relaxing region of the graph in agreement to what previously discussed in this section.

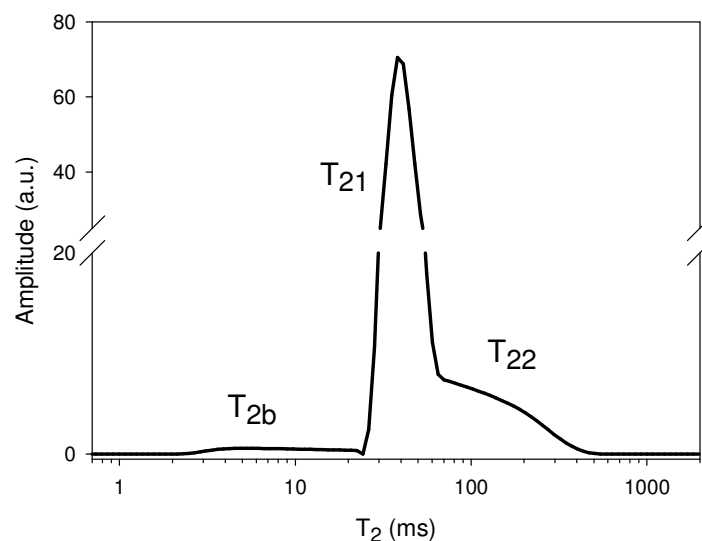


Figure 3. Typical continuous T_2 distribution of an *ex-vivo* muscle sample.

According to the available theory [5-7] the multiexponential character of muscle transverse relaxation decays depends on water compartmentalisation and slow exchange between the two major transverse relaxing components, assigned to intra (T_{21}) and extra-cellular water (T_{22}). The intra and extra-cellular water would be in a slow chemical exchange regime owing to the presence of the plasmatic membrane which acts as proper physical barrier. In addition, the evidence of faster

relaxation rates exhibited by the intra and extra-cellular proton pools in comparison with pure water was explained by assuming fast proton exchange between structural (s), hydration (m) and bulk water (b) within each water compartment. In light of this, the observed relaxation rates (T_{22}^{-1} and T_{21}^{-1}) would be described by the following:

$$T_{2,obs}^{-1} = F_s T_{2,s}^{-1} + F_m T_{2,m}^{-1} + F_b T_{2,b}^{-1} \quad (4)$$

where $T_{2,s}^{-1}$, $T_{2,m}^{-1}$ e $T_{2,b}^{-1}$ are the transversal relaxation rates of structural water (i.e. which comprises all those water molecules more strongly hydrogen bonded within the interior of the proteins and which are essential for maintaining the proteins conformational integrity [8-9]), hydration water (i.e. consisting of one or two molecular layers of hydration water whose correlation times are lengthened by hydrogen bonding to hydrophilic groups on the surface of the proteins molecules [8-9]) and bulk water (i.e. water slightly interacting with solutes and macromolecules) while F_s , F_m e F_b represent the inherent molar fractions which in turn depends on compartment size and shape.

However, some researchers [10-11] raised questions about the correctness of this interpretation arguing that the multiexponential character of muscle relaxation decay could be just a consequence of slow hydrogen exchange and not a direct evidence of water compartmentalisation within the cell.

Further studies [12-13] were conducted to test if the anatomical features of a muscle cell were sufficient to explain the multiexponentiality of the relaxation decay regardless of whether or not the assignment of intra and extra-cellular water was correct.

In particular, Brownstein and Tarr [12] considered if the non-monoexponential relaxation rate exhibited by muscle tissue could be explained by taking into account the size of a muscle cell. According to their theory, the water relaxation rates could be calculated by the probability of water molecules to interact with the macromolecules described as relaxation sink "agents" present at the boundary surface of a cell:

$$T_{2,i}^{-1} = \mu(S/V) \quad (5)$$

where μ is the relaxation sink strength of the macromolecules, S is the exchanging surface with water and V the compartment volume while S/V ratio represents the

probability that a water molecule “experiences” the surface. In agreement with their studies, for sample size ranging from 1 to 30 μm , under conditions of slow diffusion regime and planar geometry, only a discrete amount of water molecules would experience the surface thus leading to a multiexponential transverse relaxation behaviour. This is also the case of muscle cells whose diameter has been estimated to be around 10-100 μm as reported in the literature. [13].

The intra/extra-cellular model in muscle tissue and meat was finally tested by manipulation of its macroscopic features through glycerination and treatment with DMSO [11, 14, 15] which are known to disrupt the cellular membrane. According to theory advocating the intra/extra-cellular assignment, the loss of membrane integrity should have led to a fast proton exchange regime between the two water populations resulting in a monoexponential behaviour of the relaxation decay. However, all these studies showed unaltered relaxation behaviour upon membrane disruption, which suggests that intact cell membranes *per se* are not necessary for a non-monoexponential relaxation [2].

These findings were also supported by studies which investigated the influence of overall structure disruption through homogenisation in muscle tissue and meat on transverse relaxation times. In particular, Bertram *et al.* [15] still observed multiexponential relaxation decay in meat after homogenisation with a decrease in the fraction of the slowest relaxing component (T_{22}) as well as a minor decrease in the relaxation rate of the fastest proton pool (T_{21}) in comparison to intact meat samples. Since homogenisation causes disruption of membrane integrity the presence of the two water populations reveals once again that the multiexponential character of meat relaxation is not ascribable to the mechanism of intra/extra-cellular compartmentalisation induced by cellular membrane but more likely to its overall structural organisation. In light of this, a new assignment of the proton relaxation pools in meat has been proposed [15] where:

- the major T_2 population (T_{21}) represents water entrapped and interacting with the dense myosine and actin contractile protein network;
- the slowest relaxing component (T_{22}) is ascribable to water located outside the myofibrillar protein reticulum characterized by a lower interacting grade with proteins and, for this reason, more susceptible to be lost as drip;
- the minor population (T_{2b}) reflects water tightly associated with macromolecules therefore characterized by a very short transverse relaxation time (0-10 ms).

The hypothesis of interpreting the proton relaxation decay in meat in terms of its structural organisation has been further tested through studies conducted on muscle and meat samples. Yamada [16] noticed that T_{21} relaxation rate was faster in stretched skinned fibers in comparison with relaxed skinned ones suggesting that the observed difference could be due to an increase in the water-protein interactions within the myofilamentous lattice of stretched muscles. Analogous results were also reported in meat [17] where relationships between myofilament lattice spacing and T_2 relaxation parameters were investigated. Specifically, significant correlations were found between the T_{21} population and the myofilament length where the T_{21} rate showed to be influenced by the I- and the A-band ratio of the sarcomere. The assignment of the T_{21} proton pool to myofibrillar water was further confirmed by a research where pork meat samples of animals slaughtered at different ages (thus weight) were analyzed 24 h *post mortem*. Since protein density increases during growth of animals a dependence of T_{21} on animal weights is expected and this is exactly what was found in the study [18]. In addition, during the progress of *rigor mortis* a decrease in the T_{21} population was observed followed by a concomitant increase of the T_{22} proton pool. This is in agreement with the interpretation that T_{22} reflects the extra-myofibrillar water because during the conversion of muscle to meat a lateral shrinkage of myofibrils occurs thus a redistribution of water outside the protein lattice is expected.

1.3 Relationships Between NMR Transverse Relaxation Times Distribution and Post Mortem events in Muscle Tissue

In the previous section it was shown that the relaxation behaviour of muscle systems can be better rationalized by taking into account their inherent structural organization. Nevertheless, because of the profound changes that characterize the conversion of muscle to meat it could be unwise to adopt a single model to describe both systems. For example, the intra/extra-cellular interpretation, although controversial, could still be applied to explain the relaxation properties of muscle, as they still possess an active membrane system that ensures physical separation of compartments. On the other hand, this explanation seems to be less applicable to meat where *post mortem* events induce changes in membrane integrity, in particular permeability as well as on the overall original structure of the muscle.

The relation between transverse relaxation times and *post mortem* events was investigated by Bertram et al.[19]. In this research NMR T_2 relaxometry was combined with impedance, muscle contraction and water holding capacity measurements to follow the physical/chemical process leading to *rigor mortis* in porcine *m. longissimus dorsi*. These parameters were continuously monitored from 20 minutes to 24 h after animal death. According to what has been reported in the study the entire process of muscle conversion to meat can be summarized in the following stages:

- a) initially, the hormonal stimulation induced by animal slaughtering in addition with anaerobic conditions lead to an increase of the cellular volume and its ionic strength (osmotic pressure) exerting a driving force to water that migrates within the cell space. This physical process, known as *pre-rigor* swelling, causes a redistribution of water resulting in an increase of the T_{21} population accompanied by an obvious reduction of the T_{22} water pool;
- b) approximately 2h after the animal death, membrane denaturation takes place as confirmed by the drop in the impedance measurements and a new water redistribution occurs as a consequence of cellular homeostasis debilitation. In particular, the process is characterized by expulsion of water from the cellular volume into the outside of the cell reflecting in a decrease of the relative T_{21}/T_{22} percentages registered by NMR. At this stage, it seems more reasonable to interpret the T_{21} and T_{22} populations in terms of intra and extra-myofibrillar water since the water compartmentalisation model does not hold anymore, because of membrane disruption;
- c) the production of lactate as a consequence of glycolysis under anaerobic conditions induces pH drop leading to a series of modification know as protein denaturation. This stage is characterized by an increase of longitudinal muscle contraction (shortening) and by a transversal shrinkage causing reduction in muscle diameter. Both processes are responsible for a further expulsion of water outside the protein lattice (additional decrease of the T_{21} population) with formation of extra-myofibrillar water compartments with mobile water found to reflect potential drip loss (increase of the T_{22} proton fraction). Furthermore, the longitudinal contraction of cell has been related to a shortening of the T_{21} relaxation time supporting the theory that ascribed this pool to the water entrapped in the contractile reticulum.

1.4 Quality Evaluation of Meat by NMR Transverse Relaxation Studies

1.4.1 Water Holding Capacity (WHC)

Water holding capacity (i.e. WHC) is a qualitative parameter of primary importance for meat. It indicates the ability of meat to retain its own water thus it is responsible of meat textural and sensorial attributes as well as its yielding and storage quality traits. There are three different methods commonly used to measure WHC in meat:

- 1) **Honikel's bag method**: a sample of approximately 100g is suspended in a metallic net inside a plastic bag and keep refrigerated at 4°C for 48h. The percentage of drip loss is evaluated as the difference in the sample weight before and after the analysis [20];
- 2) **filter paper press**: a force of approximately 1kg is exerted for 5 minutes on a meat sample (about 300 mg) placed on a Whatman filter paper of know weight. The percentage of drip loss is calculated as the ratio between the weight of expelled water and that one of the sample [21-22];
- 3) **centrifugation loss**: a meat sample of known weight is placed inside a centrifugation tube equipped with a bottom filter (pore diameter approximately 90 µm) in order to keep separated meat from the expelled water. The sample is then centrifuged for 1h at 500rpm. Centrifugation loss are expressed as the difference in the sample weight before and after centrifugation [23].

Unfortunately, the response of these approaches is strongly dependent on operator skills and experience. In addition, these methods does not allow reproducibility of the measurements because of the impossibility of recovering the sample at the end of the analysis. Due to its non-invasiveness and destructiveness, NMR has been advocated as a valuable tool to measure WHC in meat [24] since it gives information on water mobility and compartmentalisation as discussed in previous sections. In this regard, several studies have tried to correlate the measurement of WHC with proton NMR transverse relaxation times measured at low field.

Renou *et al.*[25] first demonstrated that both T_1 and T_2 relaxation times correlate with WHC. Other authors [26] reported a dependence of WHC on T_2 relaxation rate in porcine meat classified as PSE (pale, soft, exudative, characterized by low WHC) and DFD (dark, dry and firm, i.e. high WHC) in animals affected by genetic anomalies and exposed to *pre mortem* stressing conditions. Correlations between NMR transverse relaxation curves and 14 of the most common meat quality and technological parameters influencing WHC were also investigated by Brown *et al.* on pork meat [27] By application of the statistical analysis of variance (ANOVA) the study individuated the portions of the raw T_2 decay capable of being more influenced by a variation of the considered technological parameter. Higher correlations were found between drip loss (0.74), filter paper press (0.71), pH_1 (0.71) and NMR by performing a multivariate Principal Component Regression (PCR) on the whole T_2 spin-echo decay. The highest correlation between WHC and T_2 NMR parameter was obtained by Bertram *et al.* [26, 28]. In this study, the T_{22} population displayed a correlation coefficient of 0.77 with WHC measured as drip loss while a slightly smaller correlation (0.75) was found between the T_{22} relative fraction and WHC determined by centrifugation. The relative fraction of amplitude ascribed to the T_{22} component correctly predicted the 57 and 59% respectively of the WHC variation of meat samples. These findings strongly support the water extra-myofibrillar origins of the T_{22} proton pool whose lower interacting grade with proteins reflects in a higher susceptibility to be lost as drip.

1.5 Aim of the Study

Despite significant improvements have been achieved in clarifying the relations between the NMR parameters and water properties /structural attributes of meat the development of generally industrial applicable models and simple quality parameters is far to be achieved. The correlations found between the relaxometric NMR parameters and some meat quality traits in response to specific technological, environmental and genetic factors (for a complete review on NMR applications in meat science see [2]) is undoubtedly a prove of the sensitiveness of this technique in detecting the physico-chemical changes occurring upon perturbation of the structural organisation of meat system. Nevertheless, in the author's opinion these correlations represent an oversimplification rather than a

valuable tool readily applicable for the control of meat quality. The reasons for that rely on the extreme complexity of meat that displays a multicomponent, multiphase organisation giving raise to a dynamic heterogeneity and structure which is usually time-dependent thus exhibiting phase, water distribution and compositional changes during processing and storage.

The aim of this study was therefore that of achieving a deeper and broader understanding of the mechanisms underlying the mobility and availability of water in meat in relation to its structural architecture. In particular, NMR relaxation and diffusion experiments were carried out to clarify the water-biopolymer interactions at the molecular level and characterize the moisture migration process between meat compartments.

First, theoretical studies have been conducted on reference concentrated protein (BSA) solutions and gels to rationalize to what extent the NMR relaxation analysis of a model system can be used to explain the complexity of a real multiphase, multicomponent system such as meat. In particular, BSA and meat transverse relaxation distribution has been re-investigated focusing on the role played by magnetisation transfer either by proton exchange or by secular dipolar interactions. Evidence for water compartmentalisation in BSA gels has been found by extending the conventional monodimensional relaxometric approach to higher dimensions and the potentials of the multidimensional cross-correlation NMR relaxometry in elucidating water-biopolymer interactions in more complex heterogeneous biopolymer systems as meat will be discussed.

Pulsed-gradient spin-echo (PGSE) NMR measurements were also performed to characterized the water mobility in meat samples through the measure of its effective diffusion coefficient (ADC). Since the high degree of organisation of meat, whose fibers are mainly aligned in a specific direction, the directional dependence of water diffusion (anisotropy) has been taken into account by measuring the water diffusion coefficient axially and radially with respect to the fiber orientation. The anisotropic diffusion properties of water in meat has more rigorously been treated by application of the diffusion tensor MRI (DTI-MRI) technique. The opportunity of obtaining diffusion parameters that are rotationally invariant have been exploited to infer structural information in meat and how its overall organisation changes upon perturbation induced by low temperature treatments (i.e. freezing) conducted at different regimes.

REFERENCES

1. N. F. S. Gault, "Structural Aspects of Raw Meat", in "The Chemistry of Muscle-Based Foods", Royal Society of Chemistry, London, (1992), 79-105.
2. H.C. Bertram and H. J. Andersen, *Annu. Rep. NMR Spectros.*, **53**, (2004) 157.
3. G. C. Borgia, R. J. S. Brown and P. Fantazzini, *J. Magn. Reson.*, **132**, (1998), 65.
4. S. Meiboom and D. Gill, *Rev. Sci. Instrum.*, **29**, (1958), 688.
5. C. F. Hazelwood, D. C. Chang, B. L. Nichols and D. E. Woessner, *Biophys. J.*, **14**, (1974), 583.
6. P. S. Belton, R. R. Jackson and K. J. Packer, *Biochem. Biophys. Acta*, **286**, (1972), 16-25.
7. R. T. Pearson, I. D. Duff, Derbyshire and J. M. V. Blanshard, *Biochim. Biophys. Acta*, (1974), **362**, 188.
8. B. P. Hills, C. E. Manning and J. Godward, "A multistate theory of water relations in biopolymer systems", in "Advances in Magnetic Resonance in Food Science", Royal Society of Chemistry, Cambridge, (1999).
9. B.P. Hills, "Water transport and dynamics in food", in "The Chemical Physics of Food", Oxford (in press).
10. B. M. Fung and T. W. McGaughy, *Biophys. J.*, **28**, (1979), 293.
11. B. M. Fung and P. S. Puon, *Biophys. J.*, **3**, (1981), 27.
12. K. R. Brownstein and C. E. Tarr, *Phys. Rev.*, **19**, (1979), 2446.
13. H. E. Huxley, *Sci. Am.*, **213**, (1965), 18.
14. W. C. Cole, A. D. LeBlanc and S. G. Jhingran, *Magn. Reson. Med.*, **29**, (1993), 19.
15. H. C. Bertram, A. H. Karlsson, M. Rasmussen, S. Dønstrup, O. D. Petersen and H. J. Andersen, *J. Agric. Food Chem.*, **49**, (2001), 3092.
16. T. Yamada, *Mechanisms of Work Production and Work Absorption in Muscle*, Plenum Press, New York, (1998), 145.
17. H. C. Bertram, P. P. Purslow and H. J. Andersen, *J. Agric. Food Chem.*, **50**, (2002), 824.
18. H.C. Bertram, M. Rasmussen, H. Busk, N. Oksbjerg, A. H. Karlsson and H. J. Andersen, *J. Magn. Reson.*, **157**, (2002), 267.

19. H.C. Bertram, K. Rosenvold, A. Schäfer and H. J. Andersen, *Meat Sci.*, **66**, (2004), 915.
20. Honikel K.O., *Meat Sci.*, **49**, (1998), 447.
21. Grau, R., and R. Hamm, *Fleischwirtsch*, **8**, (1956), 733.
22. Hoffman, K., R. Hamm, and E. Bluchel, *Fleischwirtsch*, **62**, (1982), 87.
23. Wierbicki E., Tiede M.G., Burrell R.C., *Fleischwirtschaft*, **42**, (1962), 948.
24. M. Bianchi, F. Capozzi, M. A. Cremonini, L. Laghi, M. Petracci, G. Placucci and C. Cavani, *J. Sci. Food. Agric.*, **84**, (2004), 1535.
25. J. P. Renou, G. Monin and P. Sellier, *Meat Sci.*, **15**, (1985), 225.
26. E. Tornberg, A. Andersson, Å. Göransson and G. von Seth, *Pork Quality: Genetic and Metabolic Factors*, CAB International, UK, 239.
27. R. J. S. Brown, F. Capozzi, C. Cavani, M. A. Cremonini, M. Petracci and G. Placucci, *J. Magn. Reson.*, **147**, (2000) 89.
28. H. C. Bertram, A. H. Karlsson and H. J. Andersen, *Meat Sci.*, **57**, (2001), 125.

CHAPTER 2

NMR INVESTIGATION OF RELAXATION AND MAGNETISATION TRANSFER PROCESS IN MEAT THROUGH THE ANALYSIS OF A MODEL PROTEIN SYSTEM: BSA

Part I: Monodimensional Approach

2.1 Bovine Serum Albumin (BSA): a Model to Study the Transverse Relaxation Distribution of Meat

It is well documented in the literature that the NMR relaxation behaviour of biological samples can be modelled by systems containing immobilized protein in contact with water such as protein cross-linked by thermal denaturation [1], or chemical methods [2], and protein powders [3]. The reason is that most part of the relaxation in tissues involves exchange of magnetization between water and proteins. The major contribution to the longitudinal relaxation rate ($1/T_1$) of water in biological tissues is transfer of longitudinal magnetisation (because of dipolar and/or chemical mechanisms) between the solvent and protein proton ensembles. Chemical exchange of transverse magnetisation between water and labile protons of protein aggregates, or between different types of water having different correlation times [4-5], is also the primary mechanism accounting for water proton transverse relaxation rate ($1/T_2$) in tissues. Generally, proton exchange rate will decrease with decreasing water content and depends on the pH and temperature. Therefore, the study of the proton magnetisation transfer process, also known as "cross relaxation", in native and cross-linked protein systems represents a valid model to elucidate relaxation in more complex matrixes such as tissues and foodstuffs.

BSA was proposed as a model to study the transverse relaxation times distribution in muscle [6-8] and meat [9]. In particular, it was found that the thermal denaturation of a 24% BSA solution leads to an ordered protein gel structure very similar to the intra-myofibrillar architecture of meat, as confirmed by confocal microscopy observations [9]. The analysis of BSA gel transverse relaxation times confirms these similarities from the NMR point of view and reveals presence of three different proton pools (see figure 1a), resembling the transverse relaxation times distribution previously discussed for meat in chapter 1.

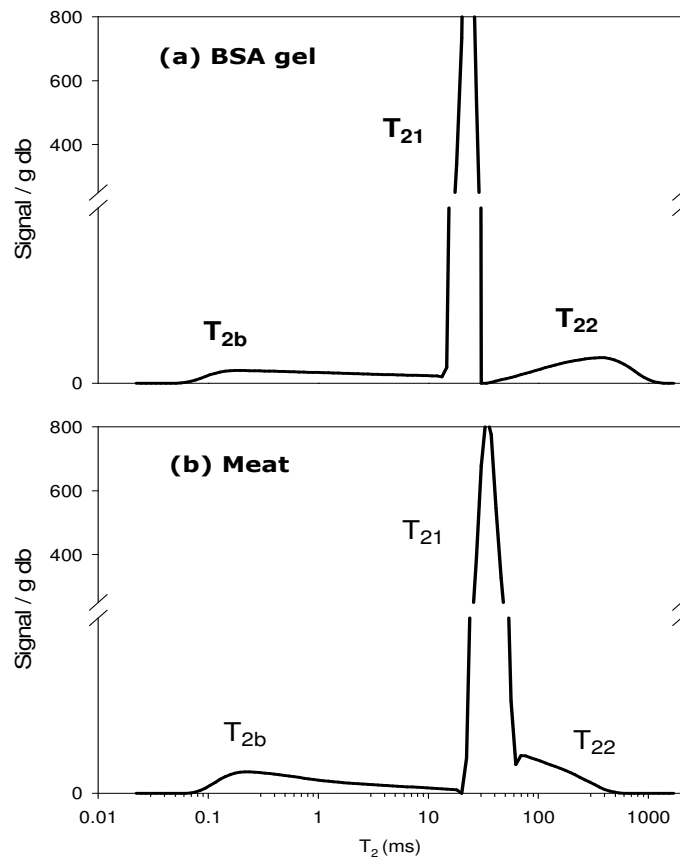


Figure 1. Comparison of (a) BSA gel and (b) meat T_2 relaxograms samples highlighting the similarities in the transverse proton distribution of these two systems.

In particular, the T_2 decay obtained from gels of denaturated BSA is dominated by a water fraction identical to the T_{21} population observed in meat and associated to intra-myofibrillar water (see section 1.2). In BSA gels this proton pool was assigned to water located into rich cross-linked protein domains. The extension of this BSA finding to meat was used as a proof to infer the assignment of meat T_{21} population to water located inside tertiary and quaternary protein structures and other structured parts of the muscle characterized by high myofibrillar protein density [9].

However, some problems are still open in the interpretation of the T_2 -relaxation behaviour of both BSA gels and meat. First, the assignment of the very fast relaxing proton fraction (T_{2b}) to “structural water” has been never properly supported with clear-cut experiments that may finally accept or reject this hypothesis. Second, the role played by magnetisation transfer processes in the BSA system has been only seldom studied [10-11] and needs to be reinvestigated by means of up-to-date methods (such as 2D relaxation experiments) to confirm the

conclusions drawn long ago. Third, no thorough study of the magnetization transfer in meat has ever been attempted.

In the following sections these three aspects will be addressed and discussed.

2.2 Assignment of the Fast Relaxing Proton Pool in Cross-Linked BSA: CPMG and One Pulse Experiments

As reported above, the continuous relaxogram obtained from the CPMG relaxation decay of a highly concentrated cross-linked BSA solution in water closely resembles that of meat. In this part of my Ph.D. work I concentrated on the fastest relaxing part of meat and BSA relaxograms, that is the one whose T_2 is lower than 1 ms and which is usually assigned to "structural water". Structural water is a loosely defined term, but roughly it can be used to identify water so strongly held by the macromolecular environment that (i) has a very limited mobility and (ii) for this reason does not exchange with other labile protons. Systems containing cross-linked BSA gels are quite useful in this respect because normal water can be replaced with deuterated water *before* cross-link of the protein takes place (see methods). Once the gel is formed in D_2O , structural water (if present) is also deuterated and therefore the intensity of the corresponding part of the relaxogram should be close to null.

The results for two samples of cross-linked BSA gels obtained in H_2O and D_2O are reported in figure 2. It is apparent that the deuteration process mainly affects the T_{21} and T_{22} BSA gel populations whose total signal (% dry base) decreases by an overall percentage of 93% (92.8 and 94.5% respectively). On the other hand, only a minor decrease (21.2 %) is found in the T_{2b} population, indicating that this proton pool cannot belong to water, let alone "structural water". One possible hypothesis is that the T_{2b} population belongs to mobile macromolecular protons, for example protein side chains, whose mobility remains sufficiently high, despite cross-linking, and that for this reason can be detected in a CPMG decay, provided that the interpulse spacing is short (here it was 80 μs). Under this view, the 21.2% decrease of the T_{2b} population is but an effect of the deuteration of the labile protons present on the mobile chains, as this figure is comparable to the actual percentage of exchangeable protons in BSA (19.3 %) [12]. This explanation of course that separate populations for water and exchangeable protein protons are visible in a CPMG experiment. This is however not a contradiction, because a proton

exchange constant of the order of 2000 s^{-1} has been reported for cross-linked BSA [11], which is quite slow with respect to either the fast relaxing protons average relaxation rate (about $1 \times 10^4\text{ s}^{-1}$) or to the reciprocal 2τ space used for the CPMG experiments ($1.25 \times 10^4\text{ s}^{-1}$), thus allowing for slow exchange between the two pools considered.

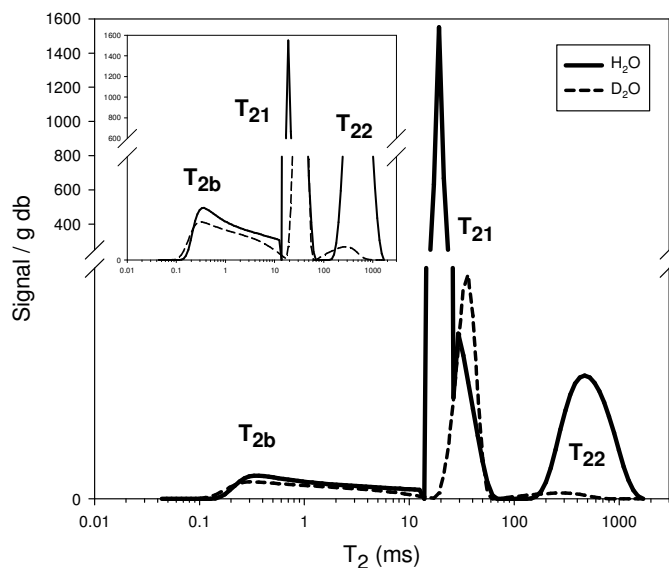


Figure 2. T_2 relaxograms of protonated (solid line) and deuterated (dashed line) 24% (w/w) BSA gels. A close-up view of the fast relaxing part is shown in the inset.

The effect of deuteration was also studied by normal “one-pulse” experiments where the FIDs of the samples used for the CPMG experiments described above were obtained at 20 MHz and compared. The use of a low resolution relaxometer for recording FIDs in place of a high resolution spectrometer was dictated by the lower “dead time” (i.e. the time elapsed between the end of the RF pulse and the beginning of the FID acquisition) of the former with respect to the latter equipment (7 vs 20 μs , respectively). On the other side, using a relaxometer equipped with a permanent magnet and with no shimming facilities results in FIDs which are heavily and unpredictably distorted by field inhomogeneities and that cannot be approximated by meaningful fitting functions. Fitting of the FIDs was thus carried out by a techniques called “reference convolution” [13], using the FID of a water sample as a “template FID” (see materials for further details).

The results of the analysis of cross-linked BSA samples are reported in figure 3. Black curves represent the experimental FID points of protonated (panel a) and

deuterated (panel b) BSA gels samples respectively while the red lines correspond to fitting points.

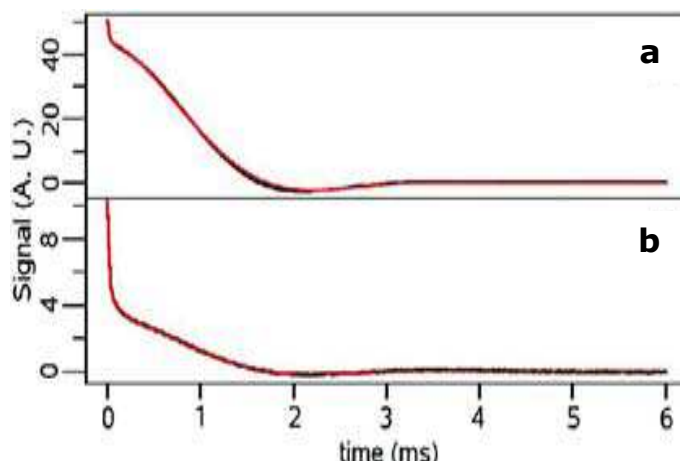


Figure 3. Results of the *reference deconvolution FIDs* fitting of (a) protonated and (b) deuterated 24% BSA gels. Black curves represents experimental points while red ones correspond to fitted values.

The reference convolution fitting of the FID revealed the presence of a fast and relatively slow component accounting respectively for 17.49 and 82.51% of the signal. Overall, the FID data confirm and complete the CPMG findings. In fact, the ratio between the intensity of the fast and the slow FID components in the H₂O sample (23.7) matched the ratio between the BSA and water protons (24.1), thus confirming that labile BSA protons form a separate pool from water because of slow chemical exchange and behave as their non exchangeable counterparts. As expected, on passing from H₂O to D₂O, the fast signal decreased by about 17%, an amount again comparable to the percentage of exchangeable protons in the BSA.

2.3 Assignment of the Fast Relaxing Proton Fraction in Meat

Since BSA gels have been proposed as models for the study of the NMR relaxation properties of tissues [6] previous BSA findings (section 2.2) have been extended to meat in order to reinvestigate its relaxation behaviour. The small population characterized by a fast transverse relaxation rate of meat (indicated as T_{2b}) has usually been assigned to hydration/structural water or water tightly associated with macromolecules, although it has been noted that some part of this signal may also come from protons of the macromolecular matrix [9,14]. This

hypothesis has been tested through hydration of lyophilized chicken meat samples in protonated and deuterated buffer solution at pH8 (see material and methods for details).

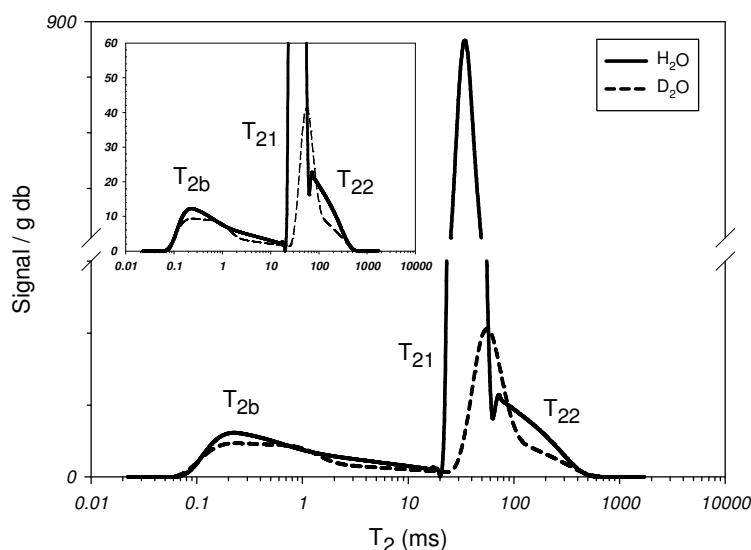


Figure 4. T_2 relaxograms of two samples of the same freeze-dried chicken breast meat rehydrated in H_2O (solid line) and D_2O (dashed line). A close-up view of the fast relaxing part is shown in the inset.

The results of this analysis are shown in figure 4. As much as 83.4% of the T_{2b} signal persists in the meat relaxogram after deuteration (inset of figure 4). A similar experiment has been recently reported [15] where no difference in the population of the fast relaxing signal fraction was detected upon deuteration; it was concluded that this fraction originated from protons not susceptible to exchange, "i.e. hydration water" [15]. However, it is worth to mention that this fraction is also minimally affected by meat homogenization which disrupts the overall meat structure [9] and should indeed significantly modify the amount of the "hydration water" held by the matrix. It is therefore reasonable to believe that another explanation of the origin of the fast relaxing fraction in meat is possible. By comparison with model BSA gels findings it seems consistent to assign the T_{2b} in meat to protons located to macromolecular structures plasticized by water. In addition, again by comparison with BSA experiments, the fraction disappearing in D_2O is assigned to exchangeable protons located on the plasticized structures.

MATERIALS AND METHODS

Deuteration Experiments

The effect of deuteration on the T_2 distribution of rehydrated chicken meat was studied using two freeze-dried samples weighing about 100 mg. The first sample was submitted to five consecutive hydration/freeze-drying cycles. In each cycle the sample was hydrated with a phosphate buffer solution in D_2O at pH 8 (to enhance H/D exchange), equilibrated in D_2O for about 15 min, and freeze-dried again. At the end of the fifth cycle the sample was weighed and rehydrated with the deuterated buffer solution so as to obtain a final moisture concentration typical of fresh meat ($\approx 300\%$). The second sample (which we used as protonated reference) was treated in the same way as the first but used water instead of D_2O .

A similar procedure was applied in the studies related with BSA. A total of four BSA samples were used to carry out the FID and CPMG relaxation experiments (two for each batch). Each trial comprised the preparation of two solutions by dissolving approximately 90 mg of BSA powder in a proper amount of distilled H_2O and a deuterated phosphate buffer solution at pH 8 in order to obtain a final concentration of 24% (w/w). The sample in D_2O was submitted to five consecutive hydration/freeze-drying cycles to ensure a complete hydrogen replacement with deuterium. The two BSA gels were finally obtained through heating the samples at $85^\circ C$ for 12 minutes in a water bath.

NMR Relaxation Measurements

Meat and BSA CPMG experiments have been conducted at $24^\circ C$ with a Bruker Minispec PC/20 spectrometer operating at 20 MHz. Each measurement comprised 3000 points, corresponding to 3000 echoes, with a 2τ interpulse spacing (i.e., between each couple of 180° pulses) of $80\ \mu s$ and a recycle delay of 3.5 s. The number of scans was varied depending on the nature of sample analyzed (BSA in H_2O or D_2O) to obtain a S/N ratio in the range 900–1400. The CPMG decays were then normalized to the BSA weight and the signal intensity of each T_2 component was extrapolated after inversion of the raw CPMGs with the UPEN program.

The FID relaxation curves of BSA samples have been acquired on a Bruker Minispec PC/20 spectrometer operating at 20 MHz and analyzed through the application of the reference convolution technique. This approach starts from the hypothesis that the effect of the magnetic field inhomogeneity on the FID is independent of the sample; an experimental FID (FID_{exp}) is thus the point-by-point multiplication of the undistorted FID (FID_{und}) by an unknown distortion function D [13]:

$$FID_{\text{exp}} = FID_{\text{und}} D \quad (1)$$

To get rid of D , the FID of a water sample with the same geometry of the BSA ones has been recorded in the same experimental conditions. The experimental water FID (FID_w) can be expressed as:

$$FID_w = I_{0w} e^{-R_{2w} t} D \quad (2)$$

where R_{2w} is the water transverse relaxation rate. Considering all the components of BSA FID_{und} exponential, Eq. (1) can be rewritten as:

$$FID_{\text{exp}} = \sum_i \frac{I_{0i}}{I_{0w}} e^{-(R_{2i} - R_{2w}) t} FID_w \quad (3)$$

Of course, this is equivalent to convolution in frequency domain between the BSA undistorted FID and the water FID acting as a distortion reference, whence the name.

REFERENCES

1. S. H. Koenig and R. D. Brown III, *Invest. Radiol.*, **23**, (1988), 495.
2. R.G. Bryant and D. A. Medelson and C.C. Lester, *Magn. Reson. Med.*, **21**, (1991), 17.
3. C.C.Lester and R. G. Bryant, *Magn. Reson. Med.*, **22**, (1991), 143.
4. F. V. Chávez and B. Halle, *Magn. Res. Med.*, **56**, (2006), 73.
5. F. V. Chávez, E. Persson and B. Halle, *J. Am. Chem. Soc.*, **128**, (2006), 4902.
6. S. K. Koenig and R. D. Brown III, *Magn. Reson. Med.*, **30**, (1993), 685.
7. S. K. Koenig, R. D. Brown III and R. Ugolini, *Magn. Reson. Med.*, **29**(3), (1993), 311.
8. S. K. Koenig, R. D. Brown III and R. Ugolini, *Magn. Reson. Med.*, **29**(1), (1992), 77.
9. H.C. Bertram, A. H. Karlsson, M. Rasmussen, O. D. Pedersen, S. Dønstrup and H. J. Andersen, *J. Agric. Food Chem.*, **49**, (2001), 3092.
10. B. P. Hills, S. F. Takacs, P. S. Belton, *Mol. Phys.*, **67**, (1989), 903.
11. B. P. Hills, S. F. Takacs, P. S. Belton, *Mol. Phys.*, **67**, (1989), 919.
12. E. S. Benson, B. E. Hallaway and R. W. Lumry, *J. Bio. Chem.*, **239**(1), (1964), 122.
13. M. A. Cremonini, D. Tacconi, V. Clementi and C. Luchinat, *J. Agric. Food Chem.*, **46**, (1998), 3943.
14. H. Peemoeller and M. M. Pintar, *Biophys. J.*, **28**, (1979), 339.
15. H. C. Bertram and H. J. Andersen, *In Modern Magnetic Resonance*, Webb, G. A. Ed., Springer: Dordrecht, Netherlands, (2006), 1707.

CHAPTER 3

NMR INVESTIGATION OF RELAXATION AND MAGNETISATION TRANSFER PROCESS IN MEAT THROUGH THE ANALYSIS OF A MODEL PROTEIN SYSTEM: BSA

Part II: Multidimensional Approach

3.1 Multidimensional Relaxation Studies on BSA

In the following sections of this chapter it will be reported for the first time the use of multidimensional cross-correlation relaxometry to a model aqueous BSA system over a wide range of water contents from the solution to glassy states. The 2-dimensional pulse sequences (for a detailed description see Appendix A), T_1 - T_2 [1], T_1 - T_2^* and T_2 -store- T_2 were employed to support the proton-exchange cross relaxation model of water relaxation. The dependence of the water proton relaxation rates on moisture content is also explored and rationalized with the multistate theory of water dynamics in protein systems. Evidence for water compartmentation in BSA gels is presented and the potential of multidimensional cross-correlation NMR relaxometry in elucidating water-biopolymer interactions in more complex heterogeneous systems such as meat is also discussed.

The advantage of extending the conventional monodimensional approach to a second dimension is illustrated in figure 1 for a 24% native BSA solution acquired at 23 MHz. Both relaxograms are dominated by a main peak accounting approximately for the 86% of the total signal and ascribable to the hydrogen water pool (namely H_2O). The main differences in the fitting output arising from the fast relaxing part of the signal coming from the BSA proton pools. In particular, the inherent relaxation times of the BSA pools are too similar to be completely resolved by a conventional continuous distribution of the CPMG decay and they will thus appear as a single and broad peak (i.e. F) spanning the T_2 region 1-10 ms (figure 1a). On the other hand, the extension of the conventional CPMG to a second dimension (figure 1b), represented by T_1 , leads to a clean separation of all the BSA proton pools (i.e. F2-F4) on the basis of their different intrinsic longitudinal relaxation times (T_1). Therefore, it should not be surprising if a higher number of peaks is generally detected in the multidimensional relaxation analysis of BSA since

the better “resolving power” exhibited by this technique in comparison with conventional relaxation methods.

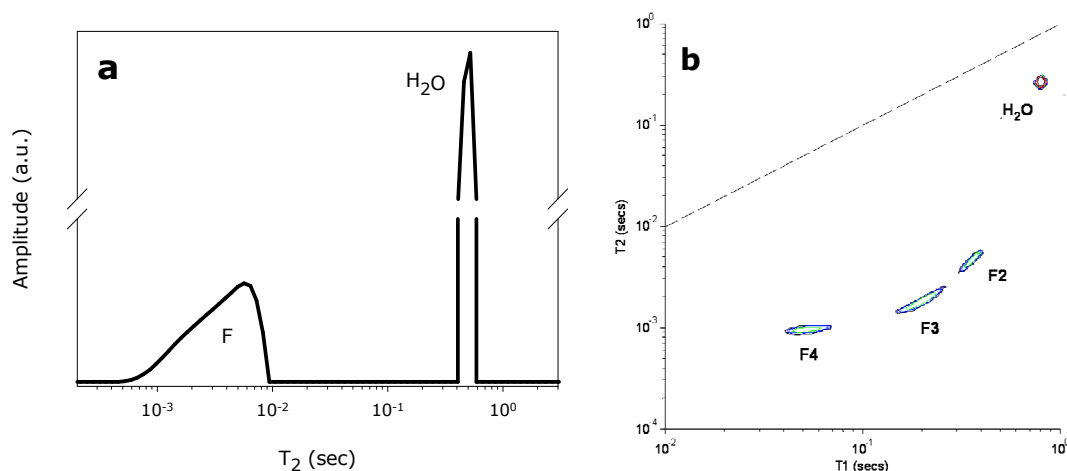


Figure 1. Comparison of (a) monodimensional (T_2) vs (b) multidimensional (T_1 - T_2) analysis of a 24% native BSA solution.

To explain the reported multidimensional BSA data it is necessary to take into consideration the role of 2-site magnetisation transfer, either by proton exchange or secular dipolar interactions, in T_1 - T_2 spectra [2-6]. If the two exchanging sites are labelled a and b , then under intermediate exchange conditions four peaks are predicted at the corners of a square at locations (s_1^+, s_2^+) , (s_1^+, s_2^-) , (s_1^-, s_2^+) and (s_1^-, s_2^-) where

$$s_i^{+/-} = -0.5(R_{ai} + K_{ai} + R_{bi} + K_{bi}) \pm 0.5 \left[(R_{ai} + K_{ai} + R_{bi} + K_{bi})^2 - 4((R_{ai} + K_{ai})(R_{bi} + K_{bi}) - K_{ai}K_{bi}) \right]^{1/2} \quad (1)$$

are the effective relaxation rates.

Similar (but more complex) calculations have been made for the T_2 -store- T_2 sequence [4] where the variable store period allows exchange of longitudinal magnetisation. These calculations show that in slow 2-site exchange at short storage times only two peaks on the diagonal appear close to the intrinsic T_{2a} and T_{2b} . In the fast exchange regime only a single peak on the diagonal appears at the weighted average T_2 . However, at intermediate exchange rates, comparable to the reciprocal storage time, two off-diagonal cross-peaks appear, thereby forming what could be called a symmetric “exchange square” [4]. In practice, experimental imperfections, noise and sub-optimum regularisation in the inverse Laplace

transform mean that the exchange cross peaks observed in T_1 - T_2 spectra may not actually form a perfect square showing a distortion that it can make difficult to distinguish exchange cross peaks from those arising from non-exchanging proton pools. Replacement of H_2O with D_2O can help in this regard since this eliminates the exchangeable proton peaks as well as the proton exchange mechanism while leaving only longitudinal dipole-dipole cross relaxation.

According to the available theory, BSA protons can be classified into five separate pools. The major proton pool is represented by water while the remaining four are BSA protons (i.e. F1-F4) comprising non-exchanging and labile protons in intermediate or slow exchange regime with water. The four pools are distinguished by their dynamic state, as measured by their decreasing intrinsic T_2 's, and can therefore be labelled as F1 to F4 in order of decreasing flexibility (or transverse relaxation time). Figures 2a and 2b show the various exchange pathways for transfer of transverse and longitudinal magnetisation respectively between these various proton pools [6]. Proton exchange between water and the EP (i.e. Exchangeable Protons) pool is the principle water proton transverse relaxation mechanism, though the proton exchange rate will decrease with decreasing water content and depend on the pH and temperature. In the absence of cross-relaxation a fully resolved T_2 -store- T_2 spectrum should therefore reveal five peaks, namely H_2O pool together with four peaks corresponding to F1 to F4. Figure 13b, which corresponds to an 8% native BSA solution in D_2O acquired at 100 MHz with a short storage time to minimise cross-relaxation, shows that this is indeed the case. However peak F1 is of low intensity and is usually only observed when the water signal is partly suppressed by dilution in D_2O and at good signal/noise, which is the case at high frequency (e.g. 100 MHz).

The situation with longitudinal magnetisation is more complicated because, in addition to the proton exchange pathway, there is the possibility of transfer by secular dipolar interactions (the so-called flip-flop term in the Hamiltonian giving rise to spin-diffusion in solids). This is increasingly effective as the system becomes more rigid and correlation times for molecular motion become longer [7]. Clearly the exchange processes depicted in figure 2b will operate during the inversion recovery step of T_1 - T_2 sequence as well as during the store time of T_2 -store- T_2 sequence.

To facilitate the analysis of native BSA solution data the cross-peaks between each of the proton pools in the T_2 -store- T_2 spectrum have been labelled according to the scheme illustrated in 2c. CP denotes "Cross Peak" and W the (H_2O) proton

pool. To distinguish off-diagonal cross peaks in opposite corners of the exchange square the numbers (or letters) are reversed. In anticipation of the results for thermally denatured BSA gels, where there are two distinct microscopic domains, it has been introduced an analogous nomenclature in figure 2d.

It will now be tested to what extent this model succeeds in rationalising the multidimensional cross-correlation relaxation data.

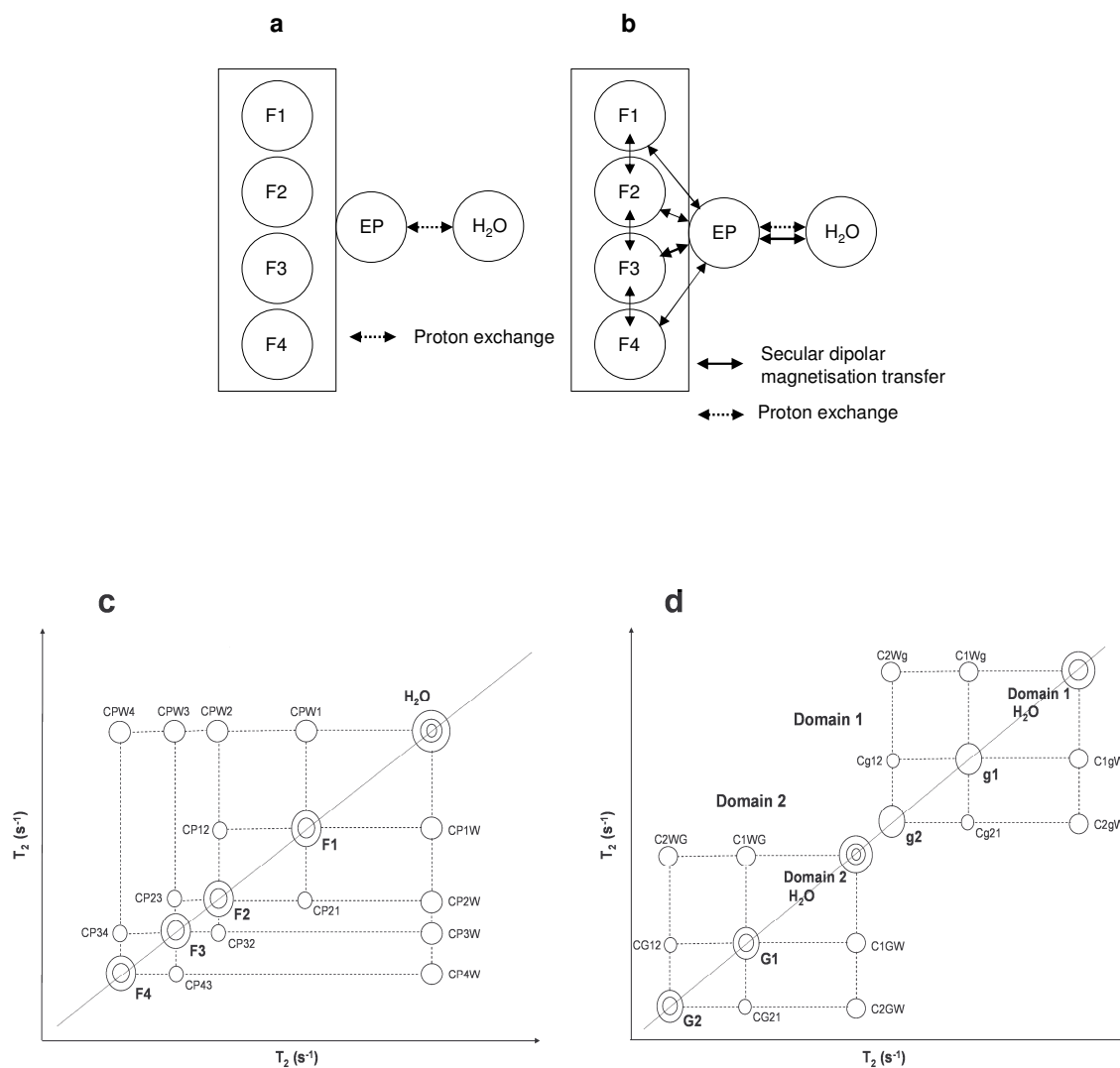


Figure 2. Schematics for the cross relaxation of water proton magnetisation in BSA. a) Transverse and b) longitudinal magnetisation. F1-F3 exchanging and non-exchanging BSA protons of decreasing mobility. Dashed arrow denotes proton exchange, solid arrows denotes secular dipolar cross relaxation. c) A schematic showing the cross-peak nomenclature for native BSA solutions. d) A schematic showing the cross-peak nomenclature for the two domains of thermally denatured BSA gels.

3.1.1. Cross Relaxation in a 24% w/w Native BSA Solution

Figure 3 shows the T_1 - T_2 spectrum of a 24% w/w BSA solution acquired at 23.4 MHz and with a CPMG 180-180⁰ pulse spacing of 200 μ s, together with provisional assignments based on figure 2a. Previous studies [6] have shown that at neutral pH the water and BSA EP proton pools (comprised in the F1 to F4 peaks) exchange at a rate of the order of 10^3 s⁻¹. Of course, because of the chemical shift difference between the exchanging water and BSA EP protons, the water T_2 does, in general, exhibit a dispersion as the CPMG pulsing rate is varied, and the amplitude of this dispersion increases with increasing spectrometer frequency [6]. This dispersion can therefore be exploited in peak assignment in the T_1 - T_2 and T_2 -store- T_2 spectra as it will be shown in the next sections. The F1 pool is not present in figure 3 because is of too low intensity to be observed at 23.4 MHz without water suppression by dilution in D₂O. The remaining peaks in figure 3 are labelled F2 to F4 in anticipation of later data showing that the F1 pool exists, but is of too low intensity to be observed at 23.4MHz without water suppression by dilution in D₂O.

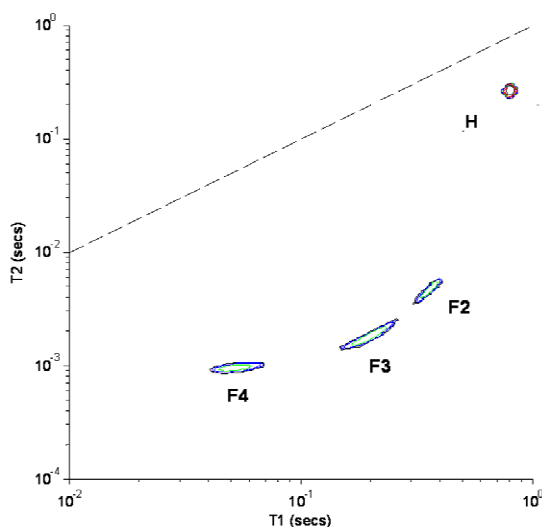


Figure 3. The T_1 - T_2 cross relaxation spectrum of a 24% w/w native BSA solution at 298K acquired at 23.4 MHz with a CPMG 90-180 pulse spacing of 100 μ s.

Further information is available in the T_2 -store- T_2 spectrum of the same sample (figure 4). At a very short storage time of 200 μ s at 23.4 MHz (figure 4a) and a short 180-180⁰ CPMG pulse spacing of 200 μ s the peaks lie on the diagonal and F2, F3 and F4 proton pools can be resolved. The slight off-diagonal shift of the F4 peak might be attributable to poor characterisation because its very short T_2 is

comparable to the CPMG pulse spacing. If the store time is increased to 10 ms (figure 4b) off-diagonal cross-peaks between the water and F2/F3 peaks appear, showing that the effective exchange rate is of the order of 100 s^{-1} . These cross-peaks are most probably a result of a 2-step exchange process, involving proton exchange between the water and EP proton pools followed by secular dipolar exchange between the EP and F2 and F3 proton pools. This follows because the correlation times of the hydration water are known to be on the sub-nanosecond timescale which is far too short to permit direct secular dipolar exchange of longitudinal magnetisation between the hydration water and the non-exchanging BSA protons F1 to F4.

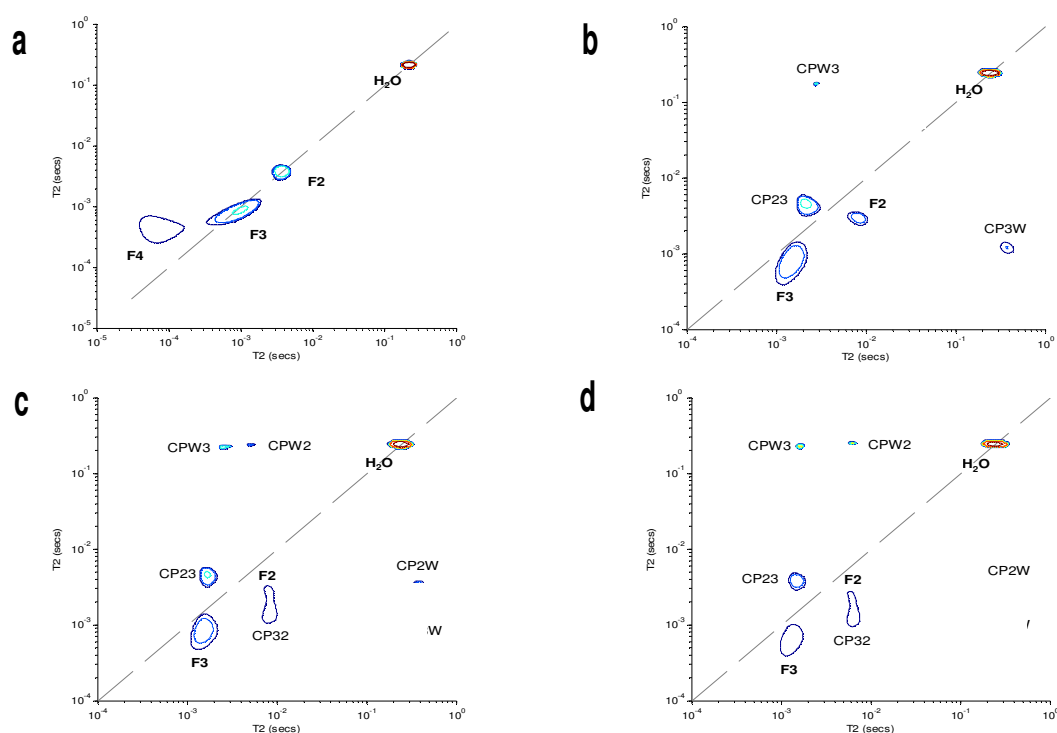


Figure 4. T_2 -store- T_2 cross relaxation spectra of a 24% w/w native BSA solution in H_2O at 298K acquired at 23.4 MHz with a CPMG 90-180⁰ pulse spacing of 100 μs and a store time of a) 200 μs . b) 2 ms c) 12 ms d) 100 ms.

However the possibility remains that the F1-F4 proton pools contain slowly or intermediate-exchanging protons with lifetimes of the order of 10 ms and these could also contribute to the observed cross-peaks. It is interesting to note that figure 4b shows the emergence of an additional cross-peak, CP23, between the F2 and F3 proton pools presumably by secular dipolar interaction. The cross peaks are fully developed with a longer storage time of 40 ms (figure 4c) where the cross

peaks CPW3 and CP3W in figure 4b have now split into pairs, presumably because of the different dipolar cross-relaxation rates from the EP protons to F2 and F3. There is also a hint of the second cross peak (labelled CP32) between F2 and F3. Increasing the mixing time to 100 ms produces no more significant change (figure 4d).

To test this interpretation the experiments were repeated in D₂O rather than H₂O while keeping the spectrometer frequency fixed at 23.4 MHz (see figure 5). At a short storage time of 25 μ s (figure 5a) no off-diagonal cross-peaks are observed and, as expected, the relative intensity of the peak from residual HOD is greatly reduced compared to F1-F4 peaks. It is also interesting to see the appearance of the F1 peak in this water-suppressed spectrum.

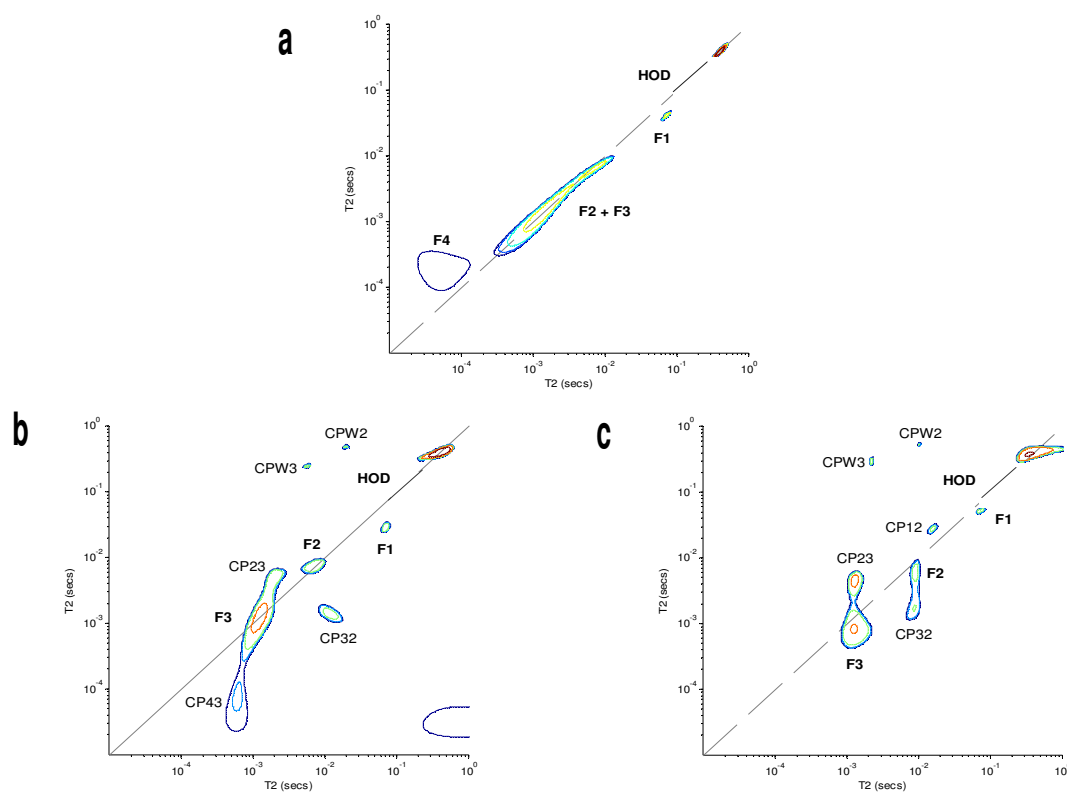


Figure 5. T₂-store-T₂ cross relaxation spectra of a 24% w/w native BSA solution in D₂O at 298K acquired at 23.4 MHz with a CPMG 90-180° pulse spacing of 100 μ s and a store time of a) 25 μ s. b) 2 ms c) 50 ms.

As the storage time is increased it has not only seen the cross peak CPW3 appear between the residual protons in the water and the F3 pools (as in figure 4c) but also a cross peak labelled CPW2 with the F2 protons. An incipient cross peak,

CP43, between the F3 pool and F4 also appears, though F4 itself is missing because its relaxation times are shorter than the storage time. At an even longer storage time of 50 ms (figure 5c) these cross peaks become more fully developed and a new peak, labelled CP32, presumably a cross peak between the F2 and F3 pools appears. An exchange square between the water and F1 proton pools has also been seen with this 24% sample but is more clearly seen in the 2.5% BSA solution (figure 12).

Because the chemical exchange between water and EP BSA protons, the increase of the CPMG 90-180⁰ pulse spacing in the T₂-store-T₂ sequence at fixed store time and at a suitably high spectrometer frequency (100 MHz) should give rise to a strong dispersive dependence of the T₂ of the water peak on CPMG pulsing frequency; while leaving its T₁ as well as the relaxation times of the other peaks, such as F1-F4, unchanged. This effect arises from the frequency difference between the EP and water proton pools which, through proton exchange results in an enhanced dephasing [6].

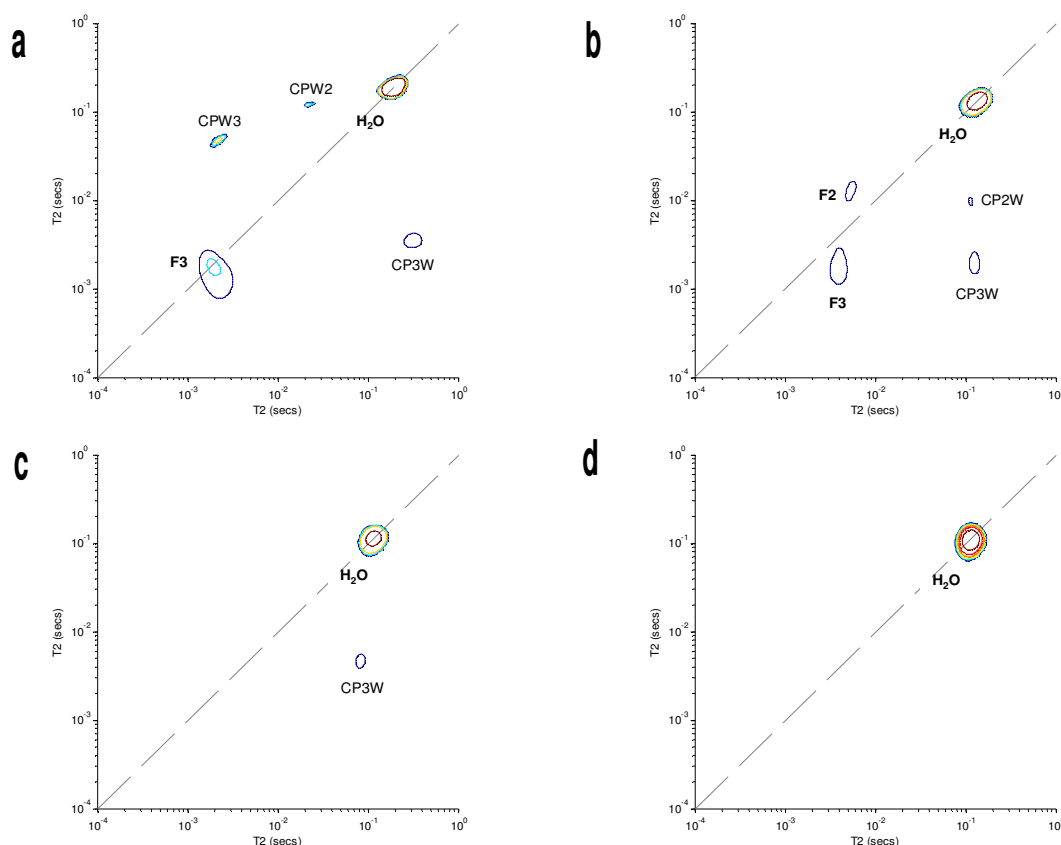


Figure 6. T₂-store-T₂ cross relaxation spectra of a 24% w/w native BSA solution in H₂O at 298K acquired at 100 MHz with a fixed mixing time of 40ms and CPMG 90-180⁰ pulse spacings of a) 200 μs b) 700 μs c) 2 ms d) 4 ms.

The off-diagonal cross peaks intensity between the water and F2 protons should be independent of the pulsing rate and appear at the corners of a contracting exchange square as the pulse spacing increases. Figure 6 shows the anticipated effect, although the F3 peak eventually disappears from the spectrum when the CPMG pulse spacing is comparable to its intrinsic T_2 of ca. 2 ms, so the peak can no longer be reliably deconvoluted (see figures 6c and 6d). Note how previously missing cross peaks, CP3W and CP2W which make up the “exchange square” now appear in the spectra. Figure 7 shows the dispersion of the water peak on pulsing frequency derived from the spectra in figure 6. The pulsing rate at the midpoint of this dispersion gives the effective exchange rate between the water and EP protons which is approximately $2 \cdot 10^3 \text{s}^{-1}$, in agreement with earlier work [6].

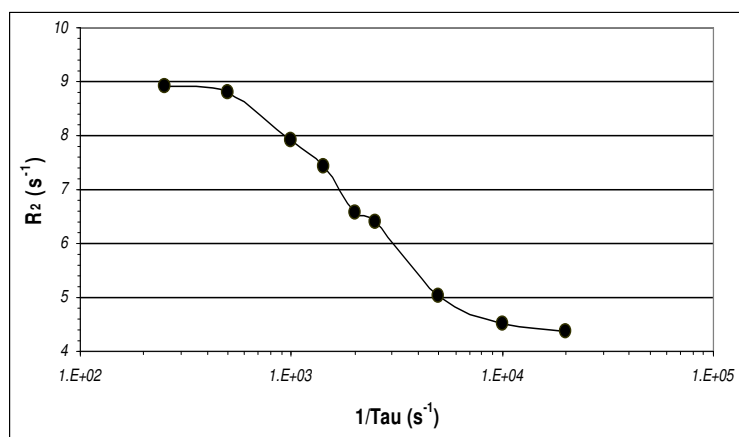


Figure 7. The dispersive dependence of the transverse relaxation rate of the water proton peak in figure 6 on CPMG pulsing frequency.

3.1.2 Cross Relaxation in a Thermally Denatured 24% BSA Gel

Heating native BSA above its denaturation temperature (60-65°C) causes protein unfolding and exposes buried cysteine residues (especially the cysteine-34 residue) permitting intermolecular cross-linking through disulphide bonding [8]. The extent of aggregation through disulphide linking depends on the BSA concentration. The BSA gel formed by heating the 24% w/w native BSA solution is indeed a cross-linked “gel” but it is also opaque showing that microscopic phase separation has occurred creating microscopic BSA-rich and BSA-poor domains on

the 1-100 micron distance scale. This sample is therefore not just a useful model system of protein denaturation but also of more complex microstructured food systems. Of particular interest is the possibility of detecting a third cross-relaxation mechanism caused by molecular diffusion of water between the two microdomains.

In figure 8 are reported the results of the monodimensional (T_2) vs multidimensional (T_1 - T_2) analysis of a 24% w/w gelled BSA in H_2O sample, acquired at 23.4 MHz, together with provisional peak assignments. As previously reported in section 3.1 for native BSA solution, the multidimensional BSA analysis leads to a higher number of proton pools in comparison with the monodimensional counterpart. In particular, panel b of figure 8 shows that the broad shoulder (namely g) appearing at the right side of the main population in conventional T_2 analysis (panel a) is now split into 3 peaks (i.e. domain 1 H_2O + g1 +g2) due to the differences in their intrinsic T_1 values.

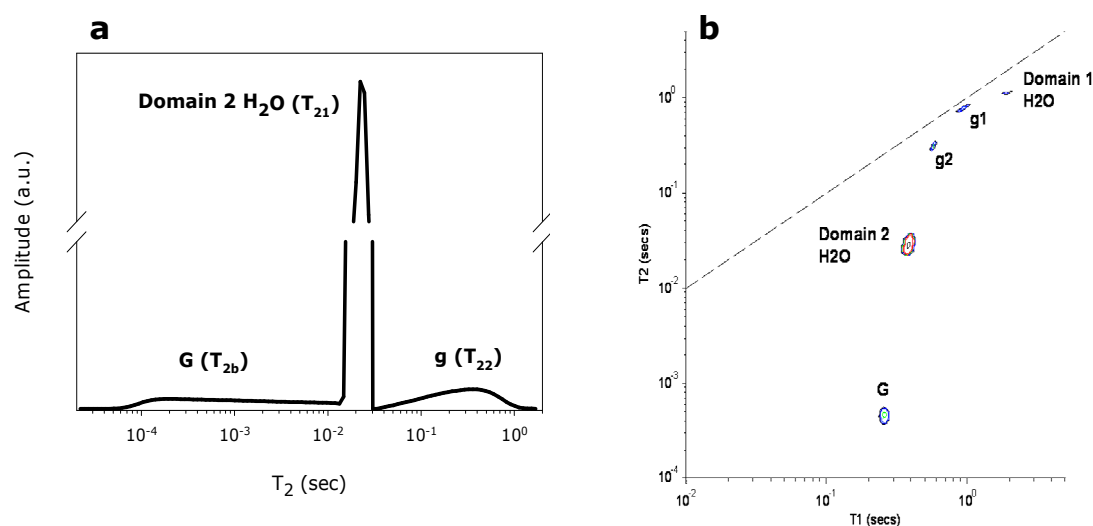


Figure 8. Comparison of (a) monodimensional (T_2) vs (b) multidimensional (T_1 - T_2) analysis of a 24% gel BSA at 298K acquired at 23 MHz with a CPMG 90-180 pulse spacing of 100 μ s. Brackets in panel **a** refers to the assignments of the 24% gel BSA proton pools previously discussed in chapter 2 to allow readers easy comparison with multidimensional data.

It can be seen that cross-linking decreases the BSA chain flexibility and therefore reduces the T_2 's of the EP and F1-F4 proton pools and because of proton exchange this also reduces the T_2 of the water peak. The net result is to shift the whole solution spectrum (figure 3) to shorter T_2 's with the result that the F3 and F4 pools can no longer be properly characterised even with a short CPMG pulse

spacing and appear at the extreme bottom of the spectrum. The labels have been changed from F's to a G in figure 8b because one cannot assume they refer to the same proton pools in the gelled, cross-linked state.

It is especially interesting to note that 2 water peaks now appear in the T_1 - T_2 spectrum, which can be assigned to water protons in the more dilute and more concentrated BSA microphases (labelled domains 1 and 2) respectively. The peaks labelled g1 and g2 in figure 8b are presumably the non-exchanging and slowly/intermediate exchanging protons [9] on the denatured BSA in domain 1. C

Cross relaxation in this 2-domain gel can be investigated with the T_2 -store- T_2 protocol. Figure 9a shows the T_2 -store- T_2 spectrum of the 24% BSA gel in H_2O acquired at 23.4 MHz with a short store time of 200 μs , together with provisional assignments. Increasing the store time to 40 ms (figure 9b) reveals the expected cross-peaks between the water protons and the slowly/intermediate exchanging G protons in domain 2.

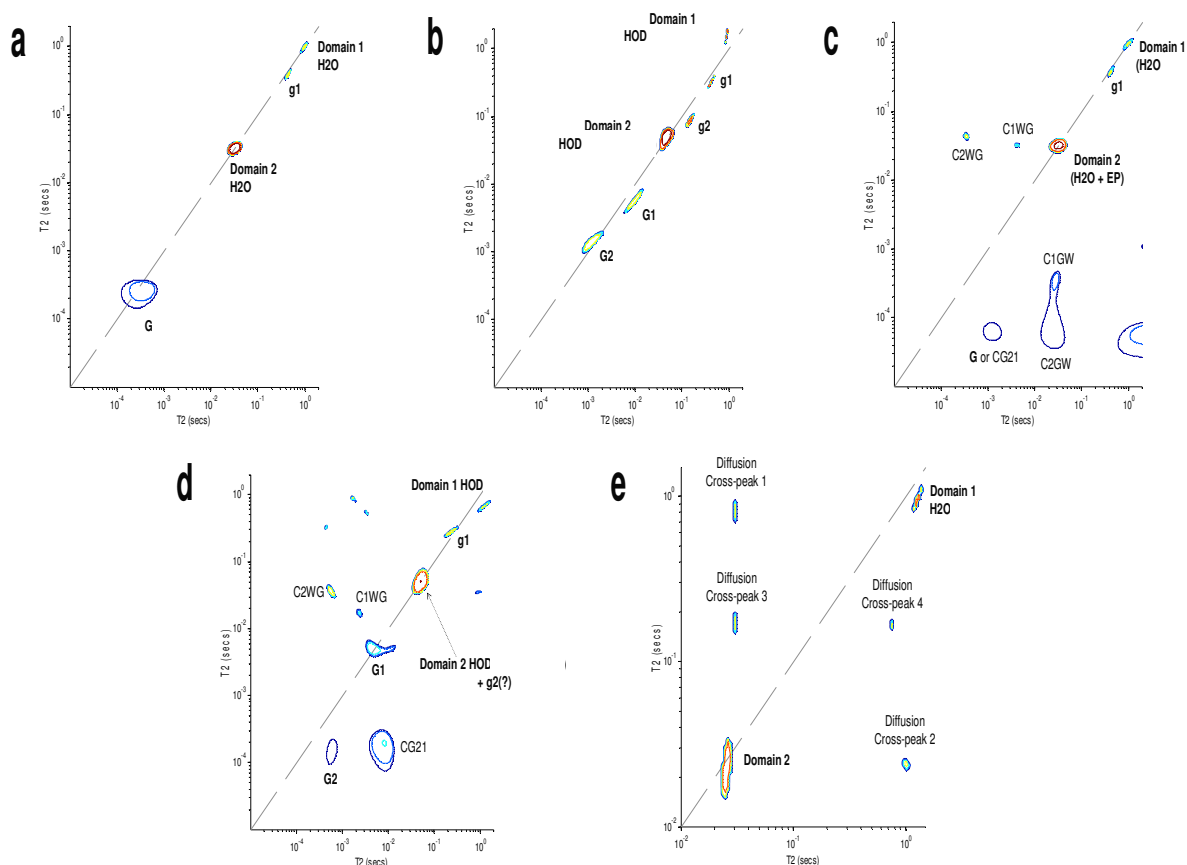


Figure 9. T_2 -store- T_2 cross relaxation spectra of a 24% w/w thermally denatured BSA gel at 298K acquired at 23.4 MHz with a CPMG 90-180° pulse spacing of 100 μs and store times of a) 200 μs in H_2O b) 40 ms in H_2O c) 200 μs in D_2O d) 40 ms in D_2O e) 1 second store time in H_2O at 100 MHz.

The observation of 2 sets of cross peaks labelled C1WG and C2WG and C1GW, C2GW and CG21 suggests that they are cross-relaxing with missing G1 and G2 peaks which would have appeared on the diagonal but whose T_1 relaxation times are too short compared to the 40 ms store time, for this to be possible. This doubling of the off-diagonal cross-peaks again suggests that the peak labelled "G" in figure 9a is actually a composite peak containing the G1 and G2 pools. Figures 9c and 9d show the effect of replacing H_2O with D_2O . At a short storage time (200 μs) each domain gives rise to two BSA protons (comprising both non-exchanging and slowly/intermediate proton exchanging) pools, labelled g1 and g2 (for domain 1) and G1 and G2 (for domain 2). Increasing the store time to 40 ms (figure 9d) introduces the expected cross-peaks between the domain 2 proton pools, but one cannot be certain about their assignment to particular diagonal peaks.

The possibility of directly detecting exchange between domains 1 and 2 by water diffusion was investigated by stepping out the store time in the T_2 -store- T_2 experiment to one second. In this time bulk water diffuses about 100 μm so diffusive cross peaks should appear, though we expect to have lost the signal from all peaks with T_1 's shorter than about 200 ms. Figure 9e shows that this is indeed the case. The scale has been expanded in figure 9e because no other peaks appear outside this expanded region and the only two peaks on the diagonal are those from the water protons in domains 1 and 2 together with off-diagonal diffusive cross peaks (labelled Diffusion Cross Peak 1 and 2) between them. Curiously a second set of cross peaks labelled Diffusion Cross-peak 3 and 4 also appears in figure 9e and their origin is less clear. Diffusion Cross-peak 4 would appear to be part of an exchange square between Domain 1 (H_2O) and a missing diagonal peak, presumably the (g1+g2) proton pool. If this is the case then Diffusion Cross-peak 3 would form part of a second exchange square between (g1+g2) of domain 1 with Domain 2 (H_2O). Because direct magnetisation transfer between domains 1 and 2 is impossible without an intervening water diffusion process it would appear that Diffusion Cross-peaks 3 and 4 are an indirect result of magnetisation transfer by diffusion. Regardless of the mechanism creating the cross peaks 3 and 4, the observation of diffusion cross peaks in a two-domain system is particularly significant because such cross-peaks will only appear when the effective diffusive exchange time is comparable to the store time, so this, in principle, provides a new method for probing water diffusion in microstructured systems without the need for applied magnetic field gradients.

Although these results nicely demonstrate the power of cross-correlation relaxometry to probe exchange processes in complex systems, the interpretation and peak assignment in even model BSA systems is far from straightforward and must be regarded, for the moment, as provisional. Additional tests of the interpretation arise if the spectra are extended into a third dimension by systematic variation of the spectrometer frequency in the T_1 - T_2 and T_2 -store- T_2 sequences, which is possible using a field-cycling relaxometer.

3.1.3 Three-Dimensional Field-Cycled Cross-Correlation Relaxometry

Conventional field-cycling NMR uses field-switching to measure the dispersive dependence of T_1 on spectrometer frequency and such dispersions directly probe the spectral density functions giving rise to the longitudinal relaxation and, in simple cases, permit the correlation times of the molecular processes contributing to the relaxation to be extracted [10]. In the field-cycled versions of the T_1 - T_2 spectrum each peak should exhibit its own characteristic frequency dispersion, thereby identifying the spectral density function(s) contributing to it. The field-cycling can be implemented during the inversion recovery and/or the CPMG dimensions depending on the type of information required.

Figure 10 shows the results of a field-cycled T_1 - T_2 experiment on the 24%w/w BSA gel in H_2O where the field cycling was only applied to the inversion recovery step. Figure 10a is the "control" result because the polarisation, relaxation and acquisition fields are all equal and equivalent to a proton frequency of 8 MHz. However figure 10b shows the same spectrum where the relaxation field, (B_{relax} in figure 10c) has been dropped to 1 MHz while the polarisation and acquisition fields remain at 8 MHz. Not only has the water peak shifted to a shorter T_1 but the G1-G2 peaks have shifted to such short T_1 s that only a single peak remains. This preliminary result serves to demonstrate the feasibility of field-cycled 2-D cross correlation methods but the result, for BSA is somewhat disappointing. The very long acquisition times of these 3-dimensional experiments is a major disadvantage and prevented a complete determination of the dispersion curve for the separate peaks. Faster versions of the experiment are therefore under development. Certainly, a repeat study in D_2O would help clarify this observation and further field-cycling cross-correlation experiments are planned. It would also be of interest

to try a field-cycled T_2 -store- T_2 experiment because both the secular dipolar cross-relaxation rate as well as the intrinsic T_1 's depend, in general, on field strength.

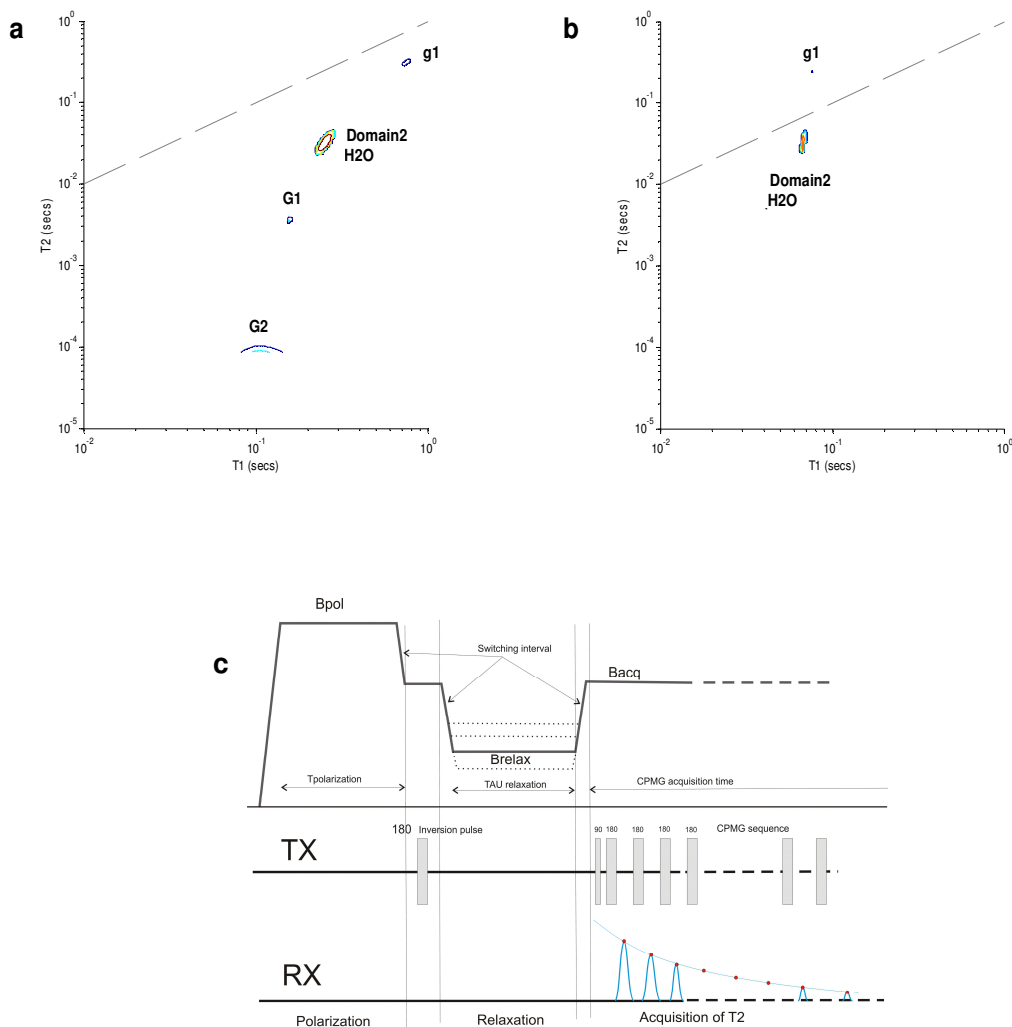


Figure 10. The field-cycled T_1 - T_2 spectra of a 24% w/w BSA gel in H_2O at 298K acquired using the pulse sequence in figure 10c with relaxation fields of a) 2 MHz and b) 1 MHz.

3.1.4 Native BSA Systems over a Range of Water Contents

Figure 11 shows a plot of the water proton transverse relaxation rate *versus* water content for native BSA measured at a resonance frequency of 100 MHz at 295K.

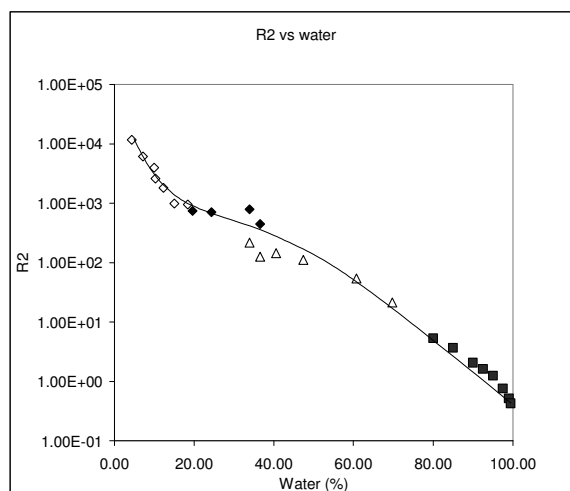


Figure 11. The dependence of the water proton transverse relaxation rate measured with the CPMG and FID sequences at 100 MHz on water content for native BSA at 298K. CPMG on solutions (solid squares); CPMG on osmotically squeezed solutions (hollow triangles); FID on osmotically squeezed samples (solid diamonds); FID on desiccated samples (hollow diamonds).

To see the changing dynamic state of the water a very wide concentration range between a dilute 0.5% w/w BSA solution to a rigid “glass”-like material containing 95.65% BSA was used. At concentrations above 80% BSA the transverse relaxation time became too short to be reliably characterised by the CPMG pulse sequence, even with a short 90-180° pulse spacing of 100 μ s so the FID was used instead. It is noteworthy that the plot shows a similar sigmoidal dependence to that previously observed for gelatine [11] and this sigmoidal shape would be even more pronounced if the FID points (solid diamonds in figure 11) were lowered to superimpose with the corresponding CPMG points (hollow triangles) to correct for the difference between T_2^* and T_2 caused by dephasing in B_0 inhomogeneities

This characteristic sigmoidal shape finds a ready interpretation in the multistate theory of hydration water [12-13]. According to this theory the water in a globular protein system such as BSA exists in at least three distinct dynamic states, namely, a bulk water phase, a “multilayer” phase consisting of one or two molecular layers of hydration water whose correlation times are lengthened by hydrogen bonding to hydrophilic groups on the surface of the globular BSA molecule; and “structural” water, which comprises all those water molecules more

strongly hydrogen bonded within the interior of the biopolymer and which are essential for maintaining the biopolymers conformational integrity. All three states of water can exchange with each other via molecular diffusion although the exchange rates will obviously decrease with decreasing water content. According to this multistate model the three regions forming the sigmoidal shape in figure 11 correspond to the progressive removal of bulk water from the dilute solution down to about 40% water content; then, with further drying, the removal of multilayer water down to water contents of ca. 20% and this corresponds to the plateau region and finally, with further desiccation the progressive removal of increasingly strongly hydrogen bonded structural water down to the completely dry material. At some point during the progressive removal of bulk water the native globular BSA molecules become rotationally immobile and “jammed” together in a pseudo-glassy state [13] and the exchange between water and BSA protons as well as the diffusive exchange between bulk and multilayer water becomes increasingly slow. While this qualitative description succeeds in rationalising the one-dimensional relaxation data in figure 11, multidimensional relaxation methods allow a more rigorous test of this theory. Unfortunately a systematic application of several 2- and 3-dimensional pulse sequences at every BSA concentration in both H₂O and D₂O for both the native and denatured forms, though desirable, would have been too much time consuming, so, the analysis have been limited to a few concentrations and appropriate pulse sequences to map out the unexplored territory.

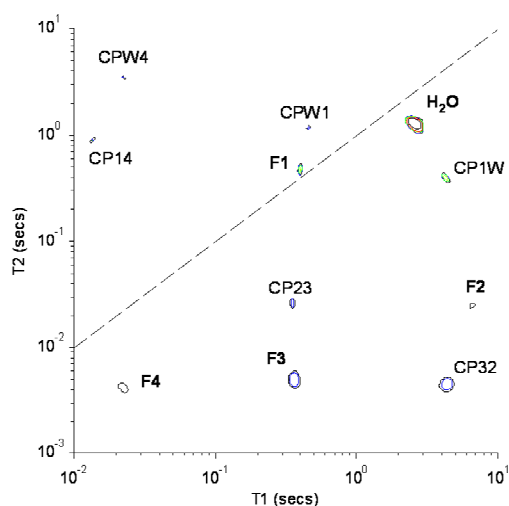


Figure 12. The T₁-T₂ cross relaxation spectrum of a 2.5% w/w native BSA solution in H₂O at 298K acquired at 100 MHz with a CPMG 90-180 pulse spacing of 100 μs.

Figure 12 shows the nine peaks in the T_1 - T_2 spectrum of a dilute 2.5% w/w native BSA solution acquired at 100 MHz, together with provisional peak assignments.

A comparison with the corresponding 24% w/w BSA spectrum acquired at 23.4 MHz in figure 13 shows that the F1 peak is now observable at the higher spectrometer frequency. It is particularly noteworthy that distinct exchange squares with off-diagonal cross peaks, CPW1 to CPW5, now appear between the water pool and each of the four F1 to F4 pools. This is interesting because it implies the cross-relaxation is in the intermediate exchange regime. This suggests that fast rotational diffusion of the BSA molecule must be reducing the rate of secular dipolar cross relaxation between the EP and F1-F4 pools so that the combined proton exchange plus secular dipolar exchange is now on the intermediate timescale.

The off-diagonal exchange cross peaks CPW1 and CPW2 are still observed in the T_1 - T_2 spectrum of a more concentrated 4% w/w BSA solution at 100 MHz, but disappear with a more concentrated 8% BSA solution at the same frequency leaving only a single water-dominated peak and a spectrum (figure 13a) resembling that in figure 3.

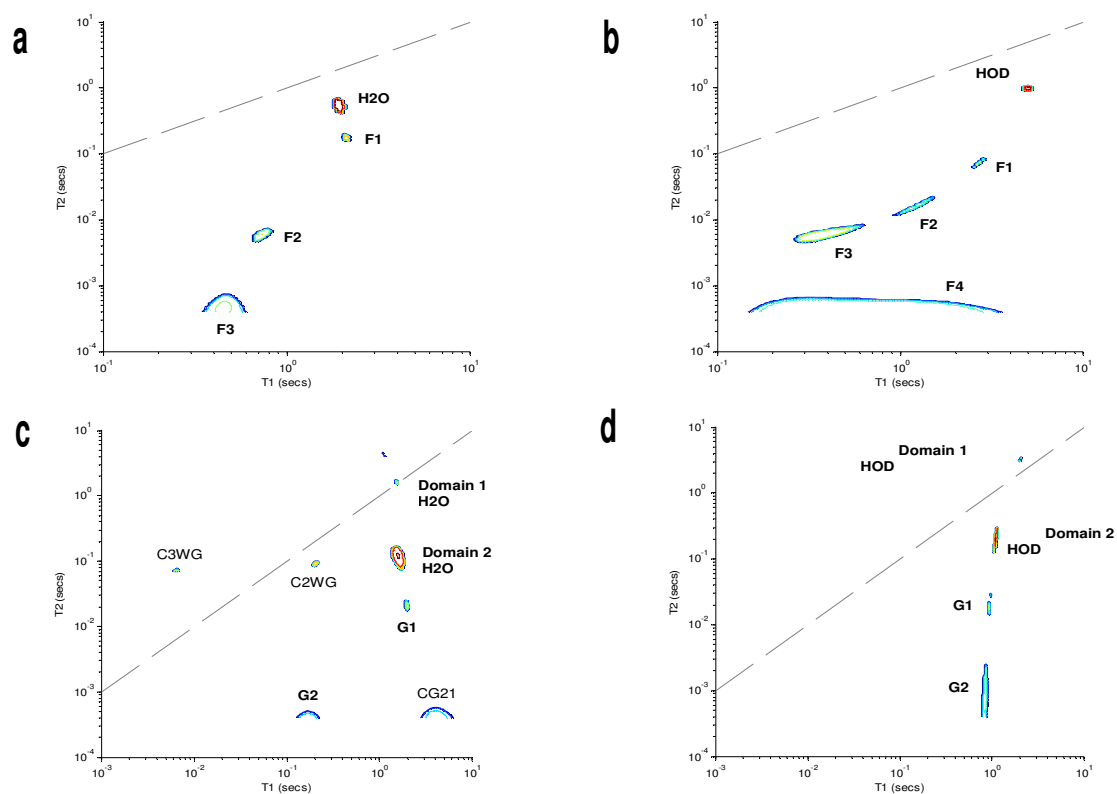


Figure 13. The T_1 - T_2 cross relaxation spectrum of a 8% w/w BSA systems at 298K acquired at 100 MHz with a CPMG 90-180 pulse spacing of 100 μ s. a) native BSA in H_2O b) native BSA in D_2O c) thermally denatured BSA gel in H_2O c) thermally denatured BSA gel in D_2O .

This disappearance of the off-diagonal cross-peaks with increased concentration may indicate that the overall exchange rate has shifted into the fast regime as a result of a faster secular dipolar EP-Fn exchange and would be expected with slower BSA dynamics at higher viscosities. Figure 13b shows the corresponding T_1 - T_2 spectrum of the 8% native BSA in D_2O , with provisional assignments and it is noteworthy that all four F1-F4 peaks are now clearly resolved. Figure 13c shows the dramatic effect of thermally denaturing the 8% solution in H_2O which not only shifts the peaks to shorter T_2 's but introduces new peaks for the two gel domains already seen in the 24% BSA gel. The spectrum is simplified in D_2O because the cross peaks are removed (see figure 13d).

Figure 14 shows the effect of removing most of the bulk water and corresponds to a 30% w/w BSA solution acquired at a spectrometer frequency of 100 MHz. The higher concentration and higher frequency means that the F1 proton pools now clearly seen, but, not surprisingly the much longer BSA rotational correlation time in this highly viscosity solution causes the F1-F4 peaks to shift to much shorter T_2 's and longer T_1 's. Unlike the 24% w/w BSA solution at 23.4 MHz (figure 3) secular dipolar cross peaks between F1, F2 and F3 are now clearly seen.

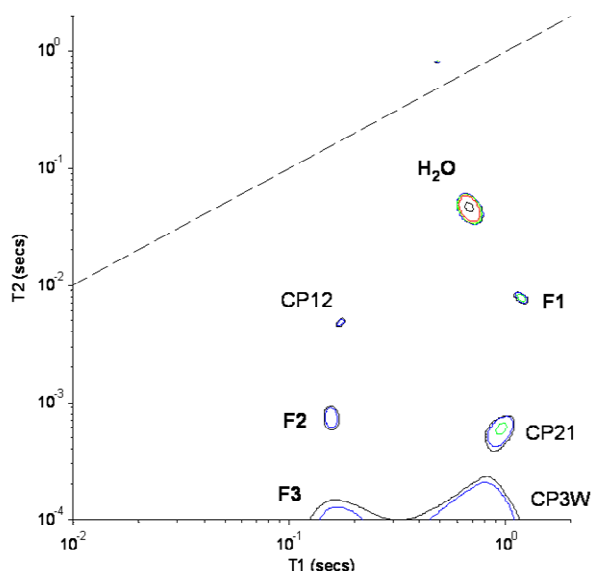


Figure 14. The T_1 - T_2 cross relaxation spectrum of a 30% w/w native BSA solution in H_2O at 298K acquired at 100MHz with a CPMG 90-180 pulse spacing of 100 μ s.

Removing the bulk water completely by reducing the water content to 34% (66% w/w BSA) has the very interesting consequence that a new "exchange

square" appears in the T_1 - T_2 spectrum (see figure 15). Assuming that the F2-F4 peaks now have such short T_2 's that they no longer appear in the spectrum, there are two possible assignments for this exchange square. One possibility assumes it is an exchange square between the F1 and water pools; the other assumes that proton exchange is so slow at this low water content that the water and EP proton pools have at last separated and the observed exchange square corresponds to proton exchange between the water and EP proton pools. In the later case it is assumed that the F1 pool is also unobserved because of its fast relaxation. It would be interesting to probe this system further with other 2 and 3-dimensional cross-correlation sequences to try to distinguish these alternative interpretations. The one-dimensional relaxation spectrum derived from the FID of the same sample shows a peak with a very short T_2 of 19 μ s, which undoubtedly arises from the more rigid non-exchanging BSA protons. A T_1 - T_2^* spectrum obtained by replacing the CPMG sequence with the FID showed two F_n peaks with solid-like transverse relaxation times of the order of 20 microseconds. However the longer T_2 's of the EP and water peaks were poorly characterised by the FID, so the distorted spectrum has not been reproduced here.

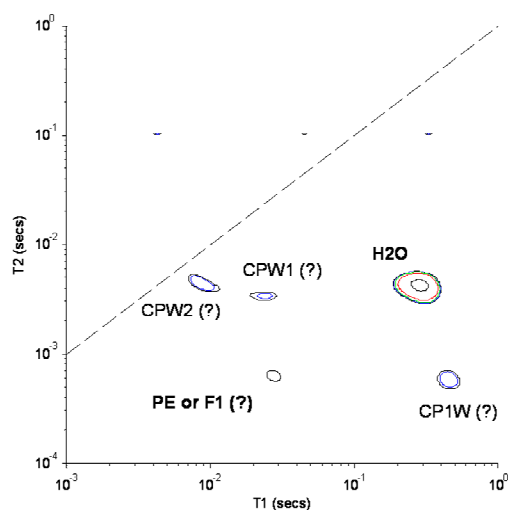


Figure 15. The T_1 - T_2 cross relaxation spectrum of a 66% w/w native BSA solution in H_2O at 298K acquired at 100 MHz with a CPMG 90-180 pulse spacing of 100 μ s.

As expected, removal of both the bulk and most of the multilayer water by further drying to a water content of 20% water (80% BSA) shifts the exchange square seen in the 66% spectrum (figure 15) to even shorter T_2 's (see figure 16). The intermediate regime exchange cross-peaks are still evident, although the T_2 's

of the Fn (and EP?) protons are now too short to be seen in figure 16. Whether the cross-relaxation mechanism giving rise to the CPW1 and CPW2 exchange peaks still involves proton exchange or is completely dominated by secular dipolar interactions remains to be investigated.

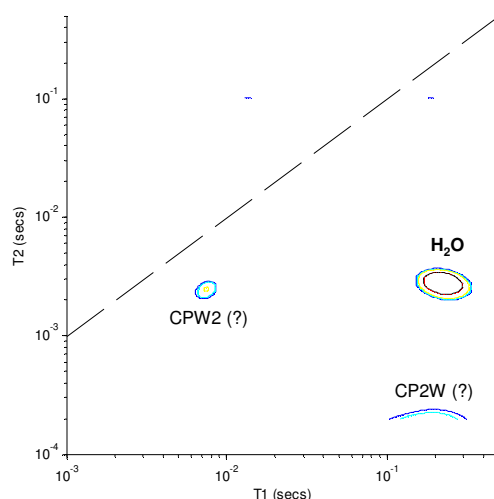


Figure 16. The T_1 - T_2 cross relaxation spectrum of an 80% w/w native BSA solution in H_2O at 298K acquired at 100 MHz with a CPMG 90-180 pulse spacing of 100 μ s.

3.2 Multidimensional Relaxometry and Diffusometry of Meat

The multidimensional studies conducted on ideal BSA systems have highlighted the important advantages of extending even in relatively “simple” systems the conventional relaxometric and diffusion experiments to a second or third dimension. In particular, the BSA findings can represent an important step towards the application of this multidimensional approach on more complex systems since the gels of this protein have been proposed as models to study the NMR relaxation properties of tissues (see chapter 2, section 2.1). In principle, it is therefore possible to extend the previous BSA experimental results to meat whose multidimensional spectra would be much more difficult to be interpreted without a reference model system. In the next sections will be reported some multidimensional relaxation spectra acquired on cod meat samples particularly focusing on aspects related to transfer of magnetisation between exchangeable protein protons and water. Aspects concerning water diffusion between meat domains will also be highlighted since these physical phenomena are capable of influencing the shelf life as well as texture and microbial stability of the product.

3.2.1 T_1 - T_2 Spectra of Cod Meat

Figure 17a shows the T_1 - T_2 spectrum of a cod fish sample acquired at 23.4 MHz with a CPMG 180-180⁰ pulse spacing of 200 μ s. The T_1 - T_2 spectrum has been interpreted basing on previous 1-D T_2 relaxometric studies [15-16] in terms of three different water pools characterized by a slow diffusional exchange on the NMR time scale and an increasing mobility level as follows: (P1) protons of macromolecular matrix (T_{2b} : 0.1-10 ms, 5-10%) more specifically assigned to protein mobile side-chains comprising non-labile and labile protons in intermediate or slow exchange with water (see also section 2.3 of chapter 2); (P2) myofibrillar water (T_{21} : 20-60 ms, 80-90%) or water entrapped in the contractile protein reticulum and (P3) extra-myofibrillar water (T_{22} : 60-500 ms, 10-15%) or water physically located outside the protein network characterized by a lower interacting grade with proteins and, for this reason, more susceptible to be lost as drip. The poorly resolved peak appearing at short T_2 's -comparable to CPMG pulse spacing- might be attributed to the solid non-exchanging protein protons or it might simply be an artefact introduced by the fitting process.

Conducting the same T_1 - T_2 experiment at higher frequency leads to the appearance of new features not visible at 23 MHz. In figure 17b is reported a T_1 - T_2 spectra of cod fish acquired at 100 MHz with a CPMG 90-180⁰ pulse spacing of 100 μ s. The spectrum resembles that one obtained at 23MHz with the addition of new peaks (named CP12 and CP21) forming a very distorted square between the P1 and P2 pools.

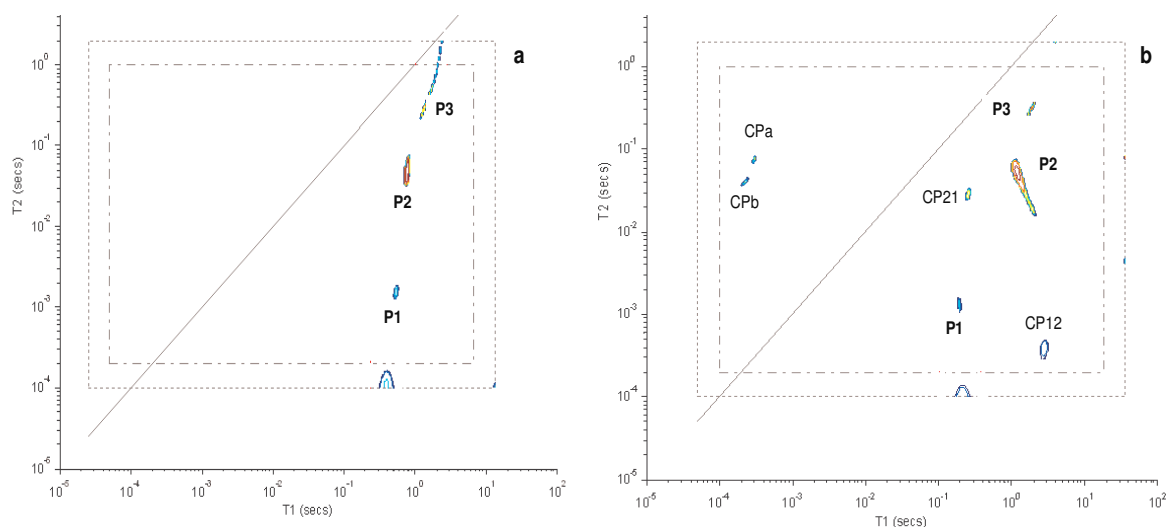


Figure 17. The T_1 - T_2 cross relaxation spectrum of a cod fish sample acquired at (a) 23 and (b) 100 MHz with a CPMG 90-180 pulse spacing of 100 μ s.

Furthermore, other peaks (CPa and CPb) appear in a “forbidden” region of the spectrum where the $T_1 < T_2$. Similar findings were also encountered when the effect of magnetization transfer was simulated in T_1 - T_2 sucrose spectra [17].

3.2.2 T_2 -store- T_2 Cod Meat Spectra

As seen in the previous sections dealing with BSA samples the role of magnetization transfer in T_1 - T_2 spectra can be clarified by performing a T_2 -store- T_2 sequence. Figure 18 shows the T_2 -store- T_2 spectrum of a cod fish sample acquired at 100 MHz with a variable store time, together with provisional assignments. Even at very short storage time of 200 μ s (figure 18a) cross peaks appear between the P1 and P2 pools indicative of an intermediate exchange regime between the labile protein protons comprised in the P1 protein pool and the myofibrillar interacting water of the sample. Stepping out the store time to longer delays (figure 18b and figure 18c) doesn't affect the appearance of the spectrum as theoretically predicted for a 2-site intermediate exchange [4]. Basing on this evidence the peaks CP12 and CP21 of figure 17b can therefore be attributed to chemical exchange phenomena occurring between P1 and P2 proton pools while the origins of peaks CPa and CPb still remain unclear. These findings also support the results reported in section 2.3 of chapter 2 where it was proposed that the P1 pool could arise from the contribution of both non-labile and slow/intermediate exchanging protein protons.

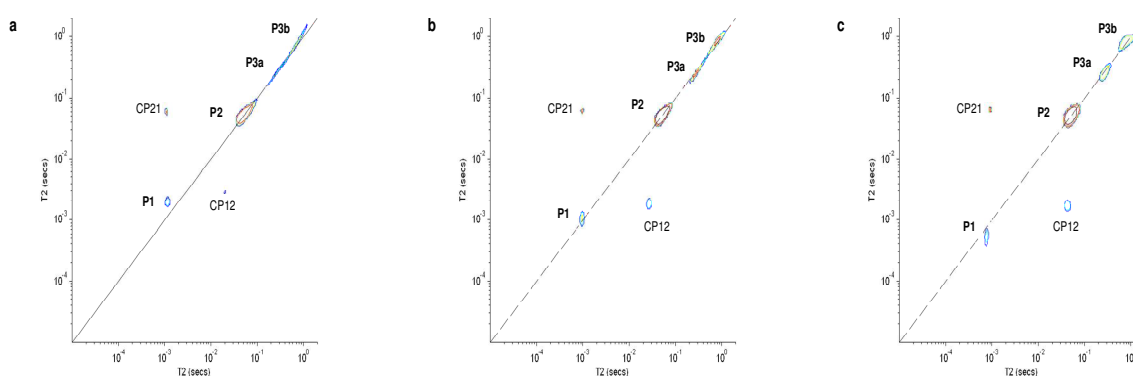


Figure 18. T_2 -store- T_2 cross relaxation spectra of a cod fish sample acquired at 100 MHz with a store time of (a) 200 μ s; (b) 10 ms and (c) 40 ms with a CPMG 90-180 pulse spacing of 50 μ s.

It could be apparently surprising that the presence of cross peaks at 100 MHz vanishes at 23 MHz (figure 17a) but this has already been reported in [17]. where it was explained that the absence of off-diagonal cross-peaks does not imply there is no magnetisation exchange.

The possibility of directly detecting diffusion exchange between intra and extra-myofibrillar water was investigated by stepping out the store time in the T_2 -store- T_2 experiment to one second. By comparison of previous BSA gel findings, it can be hypothesized that in this time, assuming a free diffusion regime, intra and extra-myofibrillar water (now curiously split into two peaks labelled P3a and P3b as also seen in figure 18) would diffuse about $100\ \mu\text{m}$ so diffusive cross peaks should appear. This is indeed the case as shown in figure 19. These results are in perfect agreement with a previous research by Landis *et al.* [18] which estimated the average lifetime of a water molecule in a muscle cell to be around 1.1 s. Diffusive exchange between on-diagonal water peaks P2, P3a and P3b is proved by the appearance of off-diagonal cross peaks (labelled DCP 23b and DCP 3a3b) in figure 19. It can be noted that the exchanging square of figure 19 lacks of symmetry since the complete absence of its upper right corner. In addition, peak P3a is characterized by a slight off-diagonal position in comparison with pool P2 and P3b. These anomalies are responsible of the pronounced exchanging square distortion seen in figure 19. Thought additional work is needed to better clarify the role played by experimental procedure and fitting method on T_2 -store- T_2 spectra, these results demonstrate for the first time the possibility of probing water diffusion in microstructured food systems such as meat without the application of magnetic field gradients.

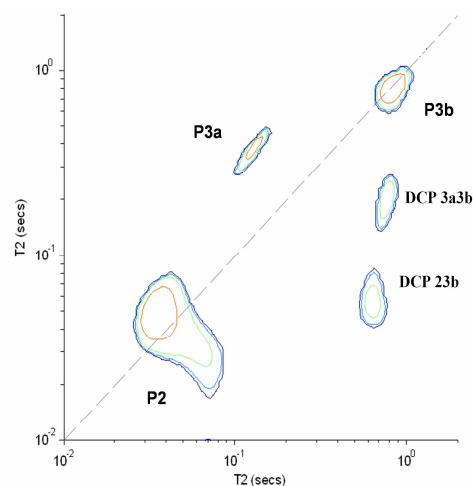


Figure 19. T_2 -store- T_2 cross relaxation spectra of a cod fish sample acquired with a CPMG 90- 180° pulse spacing of $50\ \mu\text{s}$ and store time of 1s at 100 MHz.

MATERIALS AND METHODS

BSA and Meat Samples

Dilute BSA solutions were prepared by dissolving lyophilised BSA powder (Sigma, A-2153, Lot 39h1099) in a 0.2 M NaCl solution. The pH was adjusted to neutrality (6.8) with NaOH 0.1N. More concentrated solutions up to 70%w/w BSA were made by osmotic squeezing against solutions of polyethylene glycol (PEG) (Fluka, 81300, MW 20k). In this way it was possible to attain a maximum concentration of 70% w/w BSA which required dialysis against a 45.8%w/w PEG solution for 40 hours. Higher BSA concentrations were prepared by storing the 70% BSA pellet in a desiccator at controlled relative humidity (RH). The most concentrated sample examined here (95.65% w/w BSA) required 40 hours of equilibration in a RH of 11.3. Final water contents were checked by heating the samples to dry weight. BSA solutions in D₂O were made in 0.2M NaCl-D₂O and stored refrigerated for one night. The pH was then adjusted to 6.8 with a NaOD solution concentrate in D₂O at 0.4%w/w. BSA gels were made by heating the solution at 80⁰C for 30 minutes.

Cod fish was bought from a local retailer (White Rose, UK) and kept refrigerated at 4°C prior to the analysis. The NMR samples were prepared by excising cylindrical samples of approximately 300 mg with a designed die-cutter, thermostated at 24°C and finally analyzed.

NMR Measurements

NMR measurements were performed on samples thermostated at 295K using Resonance Instruments DRX spectrometers operating at either 23.4 or 100 MHz. Field cycling T₁-T₂ measurements were undertaken at Stelar srl. in Mede (PV), Italy. The T₂-store-T₂ sequence was undertaken with full phase cycling. In particular, +M_z and -M_z were added during the store period to minimise the effects of longitudinal relaxation during the store period. The data were analysed with a MATLAB script incorporating the fast 2-D inverse Laplace transform algorithm [1]. The default value (unity) of the regularisation parameter was used in the inversion algorithm.

APPENDIX A

Monodimensional (1-D) versus Multidimensional NMR Relaxometry and Diffusometry

To date, the majority of low-field relaxometry and diffusion studies on foods could be classified as “one-dimensional” (1-D), “fixed spectrometer frequency” and “single nucleus” measurements [19]. Typically a CPMG or inversion recovery pulse sequence would be used at a fixed spectrometer frequency to report the dependence of the proton transverse or longitudinal relaxation on some quality factor, processing or storage variable [19]. With this regard, when a standard CPMG or Inversion Recovery experiment is acquired the information related with the intrinsic relaxation times of the sample is obtained by simply deconvolving the signal with an inverse Laplace transformation (i.e. UPEN software package) leading to a continuous relaxation times distribution or by fitting the signal as a discrete sum of exponential functions thus assuming *a priori* distribution of relaxation pools.

Basing on these relatively “simple” 1-D NMR experiments some NMR manufactures have developed over the years protocols that can be applied on low resolution bench top NMR used in industrial quality control for the determination of solid-to-liquid and oil-to-water ratios in food system such as food emulsions and plant seeds. However, the results are most reliable when the degree of compositional complexity is minimal [19]. In fact, when more complex multicomponent, multiphase food systems (such as dough, chocolate, creams, biscuits, ecc) are taken into observation these simple NMR protocols break down and the results can even be more biased if the system is characterized by cellular and sub-cellular compartmentalization of the aqueous component as it happens in the majority of solid-like tissue-based food systems.

The most common problems may arise from the impossibility of resolving components with similar intrinsic relaxation times by conventional multiexponential or continuous distribution. Clean separation of relaxation time peaks may also be impossible if water is compartmentalized and gives rise to several peaks overlapping with organic compounds such as lipids and proteins. Even a simple FID experiment employed to determine the solid-to-liquid ratio can be problematic since the solid component can comprise both biopolymers and fat signals or if there is not

a clear dynamic separation because the “solid” phase has mobile side-chain contributions [19].

In principle, these problems can be overcome by extending the conventional 1-D relaxometric and diffusion experiments to higher dimensions. The advent of fast algorithms for 2-D inverse Laplace transformation [1] has made this further step possible promoting the development of the so called 2- and even 3-D relaxation and diffusion correlation spectra on conventional low-field bench-top NMR [5,20-21]. The basic idea of this approach is to combine together the conventional 1-D relaxometric and diffusion experiment with the optional addition of a third dimension to exploit the huge amount of information potentially available to characterize the sample.

Theoretical Basis of Multidimensional Relaxometry and Diffusometry

T₁-T₂ and T₁-T₂* Cross Correlation Spectra

In a T₁-T₂ experiment an inversion recovery step with a variable recovery time, t₁, is followed by a CPMG acquired in a time t₂. The resulting 2-D array of CPMG echo trains, M(t₁,t₂), is given as:

$$M(t_1, t_2) = \iint dT_1 dT_2 F(T_1, T_2) k_1(T_1, t_1) k_2(T_2, t_2) \quad (2)$$

where F(T₁,T₂) is the desired “spectrum”, which, more precisely, is the probability density of protons having relaxation time T₁ and T₂. The kernels are, in this case, those for relaxation during the inversion recovery and CPMG steps, respectively

$$k_1(T_1, t_1) = 1 - 2 \exp(-t_1 / T_1) \quad (3)$$

$$k_2(T_2, t_2) = \exp(-t_2 / T_2) \quad (4)$$

The relaxation spectrum, F(T₁,T₂) is obtained from M(t₁,t₂) by a 2-D inverse Laplace transformation.

When the intrinsic transverse relaxation times are too short to be measured via a conventional CPMG sequence a different approach can be employed by

replacing the CPMG part of the T_1 - T_2 sequence with an FID. The so called T_1 - T_2^* sequence is particularly appropriate to study solid-like systems with very short intrinsic transverse relaxation times otherwise the FID would be dominated by dephasing effects induced by magnetic field inhomogeneity.

D- T_2 and Multidimensional Diffusometry Correlation Spectra

The simplest 2D sequence is composed by a CPMG sequence followed by a PGSE sequence (either a Han echo or a stimulated echo) in the second dimension. The kernels are the following:

$$k_1 = \exp(-q^2 D \Delta) \text{ with variable } q^2 \Delta \quad (5)$$

$$k_2 = \exp(-t_2 / T_2) \text{ with variable } t_2 = 2n\tau \quad (6)$$

The 2-D Laplace transformation yields the D- T_2 spectrum as that one reported in [20] for avocado tissue. It is important bearing in mind that the kernel in Eq. (5) is formally valid only for unrestricted diffusion. In cases where diffusion is restricted it may be better to perform a higher dimensional analysis by varying both q and Δ independently. First, a 2-D spectrum $D(q)$ - T_2 could be obtained by varying Δ at fixed q then, a 3D stacked plot would be create by exploring the q -dependence as a useful indicator of the nature of restricted diffusion.

Also 2-D diffusion correlation spectra of the type D_1 - D_2 can be acquired via double Laplace inversion of the echoes arising from independent double gradient encoding steps in the q_1 - q_2 dimension with the \mathbf{q} -vectors in either collinear or orthogonal directions. The so called DEXSY-PGSE sequence is particularly suited in detecting correlations between diffusivities before and after a well-defined mixing time, tm . In principle, with this sequence it is possible to characterized diffusive exchange between domains connected to one another by simply stepping out the mixing time of the sequence. Callaghan et al. [22] tested this sequence on the polydomain lamellar phase of the lyotropic liquid crystal, 25% aerosol OT/water demonstrating its reliability in detecting diffusion exchange process between the small domains of the system.

Other Multidimensional Cross Correlation Relaxation Techniques

Because of proton exchange and intercompartmental diffusion in biopolymer systems and cellular tissue, T_2 , displays in general a dependence on both spectrometer frequency and CPMG pulse spacing, τ . A similar dependence on magnetic field strength is also shown by T_1 whose values are a function of spectrometer frequency, decreasing with decreasing frequency. Therefore, it is possible to extend to a third or even to a fourth dimension the standard T_1 - T_2 sequence as a function of both ω_0 and τ $-T_1(\omega_0)$ - $T_2(\omega_0, \tau)$ -. The ω_0 dimension could be explored by implementing the sequence on a field cycling spectrometer where peaks that overlap at higher frequencies in a T_1 - T_2 spectrum can be resolved at lower frequencies where the T_1 differences get amplified.

When operating at high spectrometer frequency it is also possible to exploit the spectral resolution of peaks to obtain a T_1 - T_2 -chemical shift resolved spectrum. Instead of acquiring only a single point at the echo maximum in the CPMG dimension, whole echo train can be recorded in the third dimension and Fourier transformed in order to separate spectral peaks, such as those of water, lipids and sugar by their different chemical shifts.

Additional multidimensional applications can be thought to combine $T_{1\rho}$ and T_2 measurements by replacing the initial inversion recovery sequence with a spin-locking sequence of a hard 90_x pulse followed by a phase shift for a variable t_1 before the subsequent CPMG or FID are acquired in the t_2 dimension. The kernel for the t_1 dimension is in this case:

$$k_1(T_1, t_1) = \exp(-t_1 / T_{1\rho}) \quad (7)$$

Furthermore, the dependence of $T_{1\rho}$ on both spectrometer frequency (ω_0) and the radiofrequency field strength (ω_1) can be exploited to extend the $T_{1\rho}$ - T_2 protocol to a third or fourth dimension.

It is also possible to weight the T_1 - T_2 , T_1 - T_2^* and $T_{1\rho}$ - T_2 sequences with various additional preparation sequences [19]. For example various degree of water suppression could be introduced with a PGSE sequence in order to suppress the mobile water protons allowing to better characterized slower diffusion molecules at higher receiver gain.

REFERENCES

1. M. D. Hurlimann, L. J. Venkataramanan, *J. Magn. Reson.*, **157**, (2002), 31.
2. N. Marigheto, S. Duarte, and B. P. Hills, *Applied Magn. Reson.*, **29**, (2005), 687.
3. P. J. McDonald, J. P. Korb, J. Mitchell, L. Monteilhet, *Phys. Rev. E.*, **72**, (2005), 011409.
4. L. Monteilhet, J. P. Korb, J. Mitchell, P. J. McDonald, *Phys. Rev. E.*, **74**, (2006), 061404.
5. B. P. Hills, J. E. M. Snaar, *Mol. Phys.*, **76**, (1992), 979.
6. B. P. Hills, K. M. Wright, P. S. Belton, *Mol. Phys.*, **67**, (1989), 1309.
7. H. T. Edzes and E. T. Samulski, *J. Magn. Reson.*, **31**, (1978), 207.
8. I. Hayakawi, J. Kajihara, M. Oda and Y. Fujio, *J. Food Sci.*, **57**, (1992), 288.
9. M. A. Cremonini, L. Venturi, S. Sykora, C. Cavani, and G. Placucci, *Magn. Reson. Imag.*, **25**, (2007), 555.
10. B. P. Hills, Y. L. Wang and H. R. Tang, *Molecular Phys.*, **19**, (2001), 1679.
11. M. C. Vackier, B. P. Hills and D. N. Rutledge, *J. Magn. Reson.*, **138**, (1999), 36.
12. B. P. Hills, C. E. Manning and J. Godward, A multistate theory of water relations in biopolymer systems, in "Advances in Magnetic Resonance in Food Science", Ed. P. S. Belton, B. P. Hills and G. A. Webb, 1999. Royal Soc. of Chemistry, Cambridge, U.K.
13. B. P. Hills, "Water transport and dynamics in food", in "The Chemical Physics of Food", Ed. P. S. Belton, Blackwells, Oxford, (in press).
14. G. J. Brownsey, T. R. Noel, R. Parker and S. G. Ring, *Biophys. J.*, **85**, (2003), 3943.
15. R. J. S. Brown, F. Capozzi, C. Cavani, M. A. Cremonini, M. Petracchi and G. Placucci, *J. Magn. Reson.*, **147**, (2000) 89.
16. H. C. Bertram, A. H. Karlsson and H. J. Andersen, *Meat Sci.*, **57**, (2001), 125.
17. N. Marigheto, L. Venturi, D. Hibberd, K.M. Wright, G. Ferrante and B.P. Hills, *J. Magn. Reson.*, **187**, (2007), 327.
18. C. S. Landis, X. Li, F. W. Telang, P. E. Molina, I. Palyka, G. Vetek and C. S. Springer, *Magn. Reson. Med.*, **42**, (1999), 467.
19. B. P. Hills, *Annual Reports on NMR Spectroscopy*, **58**, (2005), 178.

20. B. P. Hills, S. Benamira, N. Marigheto and K. M. Wright, *Applied Magn. Reson.*, **26**, (2004), 543.
21. N. Marigheto, K. Wright, and B. P. Hills, *Applied Magn. Reson.*, **30**, (2006), 13.
22. P. T. Callaghan and I. Furò, *J. Chem. Phys.*, **120**, (2004), 40032.

CHAPTER 4

STUDY OF WATER AVAILABILITY AND MOBILITY IN MEAT: A NMR-DSC- a_w MULTIANALYTICAL APPROACH

4.1 Measurements of Water Availability in Food Systems

The mobility and availability of water in food systems depend on the extent of interactions between the aqueous phase and the biopolymers matrix [1]. These parameters are of the utmost importance in food technology as the amount and physico-chemical behavior of water embedded in foods may trigger microbiological growth or even unwanted chemical reactions, thus lowering food quality and shelf-life [2]. It is thus highly desirable to attain a deep understanding of the interactions between water and food components to be able to produce clear-cut models and simple quality parameters that can be readily applied in the food industry.

A partial solution to the problem of assessing the degree of availability of water in food materials is known since the 1950s when Scott and Salwin independently introduced the nowadays well known concept of "water activity" (a_w), whereby "boundness" to a food matrix is related to the relative vapor pressure of water (for a recent historical review see [3] and references therein); the studies on a_w led to the description of a "food stability map" [4] that is still widely used by the food industry as a stability indicator for food quality control and shelf-life prediction. Although it is common referring to the mobility and availability of water in foods or hygroscopic polymers with the expression "state of water" (see for example [5-8]) it must be borne in mind that here water is always as liquid as in the common liquid state and it is hold back by the capillary forces generated by the physical structure of the matrix beyond condensation.

As simple as it is (a single parameter describes the status of the whole embedded water), a_w suffers from a number of drawbacks that have been discussed in the literature along the years, many of them thoroughly reviewed in a famous paper by Slade and Levine [9]. These researchers based their criticisms on the following points: (i) for a_w to be a meaningful descriptor of the water status it is necessary that at thermal equilibrium the partial vapor pressure above the food system is the same as that of the embedded water (i.e. thermodynamic equilibrium

is reached). This condition is generally fulfilled in diluted food systems, but hardly met in concentrated food systems, owing to the low diffusion rate of water with respect to the time scale of measurement. In these systems only a kinetic steady state is reached which is at the basis of the known hysteresis effect in sorption and desorption isotherms; (ii) even if thermodynamic equilibrium were reached, no way would exist for extracting meaningful information from the sorption or desorption isotherms because the widely used BET [10] or GAB [11] equations are based on assumptions that do not hold good for food materials; (iii) a_w is not an absolute food stability predictor because spoilage at a certain measured a_w depends on food composition, physical structure, temperature, prior sample history and even isotherm measurement methodology; (iv) a_w defined as relative vapor pressure can reflect only the surface properties of a system but not necessarily the molecular dynamics that take place in its interior. However, a_w and the parameters obtained from the isotherms may still retain some usefulness, provided they are used as mere empirical indicators for foods at well defined pressure and temperature conditions.

Given the theoretical weaknesses of the a_w and related isotherms approach, but also considering its widespread use in food engineering, it would be interesting to compare the data obtained from the sorption isotherm of a complex food matrix with those coming from other well established techniques like differential scanning calorimetry (DSC) and low-field nuclear magnetic resonance (LF-NMR). These techniques offer a different but complementary point of view for studying the dynamics of water in foods as it was recently demonstrated for several systems [12-16].

DSC is particularly well-suited for the characterization of water at a structural level. From the calorimetric point of view, water is studied in its "free" or "bound" state to the solid food matrix. "Bound" water is determined by DSC as the amount of unfrozen water left in a sample after it is cooled at low temperature below zero [17]. As explained by Wolfe [18], the amount of unfrozen water depends in general on three effects: (i) presence of small solutes, e.g. ions; (ii) presence of macromolecules and membranes and (iii) viscosity of the solution. The first two effects are thermodynamic in origin, while the latter is clearly related to the kinetic of the freezing process. While the presence of small solutes depresses the freezing point because of the entropy of mixing and it is roughly proportional to the number of solutes, the effect of mesoscopic objects (which are much less numerically) on the freezing point is related to the decreased energy of water in the vicinity of the

hydrophilic groups (e.g. because of slower reorientation and hydrogen bonding). This effect extends “within a nanometer or so” from a hydrophilic surface so that “the quantity of unfrozen water may exceed the expected amount of ‘water of hydration’ or ‘hydration shell’” [18]. DSC has been used to monitor the gross phase changes of water in polymeric networks [15] and in food systems, like honey [19], and meat [20].

Compared to DSC, foodstuff analysis *via* LF-NMR yields an additional degree of details for the description of the embedded water, albeit at the price of a more difficult interpretation of the results (for a recent review see [21]). The measure of the transverse relaxation times (T_2) often reveals a multicomponent behavior which reflects the existence of different proton pools within the sample (e.g. protons from the macromolecular matrix or fat, or arising from water contained in different food compartments). A difficulty here arises about the assignment of each proton population to the corresponding chemical species, especially when no previous knowledge of the sample is available.

4.2 Aim of the Study

In the following sections of the chapter the description of the water status provided by LF-NMR was compared to a_w and DSC measurements during hydration of freeze-dried chicken breast meat taken here as a model. Not only can meat be driven to span a large a_w range from complete dryness to complete hydration (a_w of fresh meat is 0.99), but it is also well characterized from both the NMR [22] and the DSC [23] point of view. To the best of the author’s knowledge this is the first time that this kind of multianalytical approach is applied to the hydration of freeze-dried meat.

4.3 Sorption Isotherm Approach

The sorption isotherm for freeze-dried chicken breast meat at 25 °C is shown in figure 1 together with the best-fit curves obtained through the BET or the GAB model (Table 1).

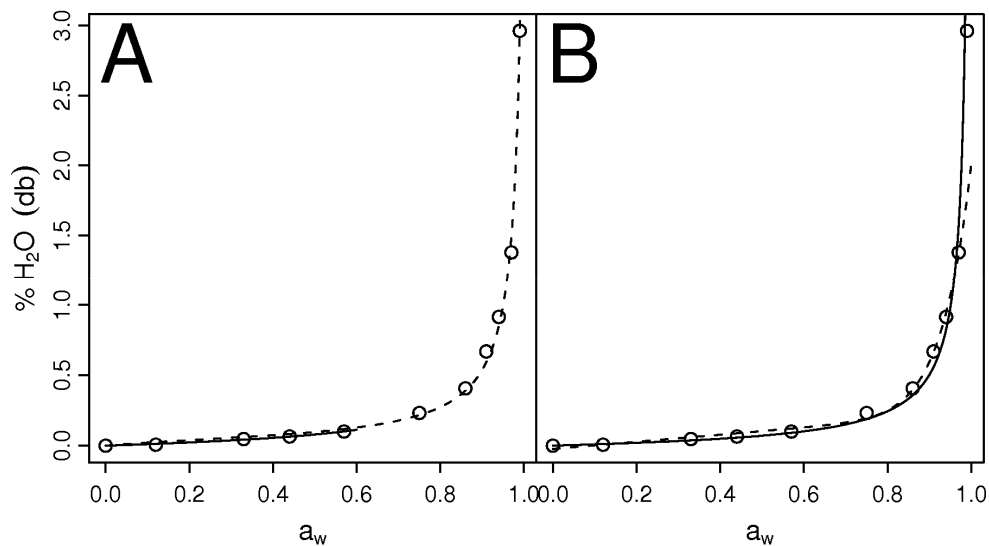


Figure 1. Moisture sorption isotherm of freeze-dried chicken breast meat at 25 °C. Experimental values (\circ); calculated values according to the GAB and BET model (respectively dashed and solid curves in panel A); calculated values according to the Ali-Asbi-Baianu and Caurie model (respectively dashed and solid curves in panel B).

The monolayer values are in both cases smaller than found recently by Delgado and Sun [24] for the same foodstuff and temperature (7.34% and 6.75% for BET and GAB, respectively), probably because their data were obtained from a desorption isotherm.

Type of equation	Best fit parameters	Onset of Moisture Condensation
BET	$X_m=6.31\%$ $C_g=1.715$	--
GAB	$X_m=6.04\%$ $K=0.9894$ $C_g=4.552$	--
Caurie	$X_m = 4.00\%$ $C^{1/n}=1.78$ $n=2.25$	$a_w=0.83$ (29.2%)
Ali Asbi and Baianu	$n_I = 6.060 \times 10^{-3}$ $C=0.214$ $A=1.843$ $B=14.92$	$a_w=0.86$ (39.7%)

Table 1. Parameters obtained from the fitting of Eqs. 1-4 (see materials) to chicken breast meat sorption isotherm data.

Although GAB equation is by far the most used mathematical model for the fitting of isotherm data, a plethora of other models exists, some of which yield physically meaningful parameters, while others are totally empirical, whose only aim is reconstructing the isotherm shape at best for engineering purposes. The recently modified Caurie equation [25] belongs to the first group of models. It is based on a modification of the BET equation, but, contrary to BET, Caurie model does not allow an infinite number of water layers to be adsorbed over the first. Consequently, an end-point for adsorption of water molecules can be marked, which corresponds to the a_w point at which bulk water appears. On the opposite side, one of the simplest empirical models able to describe the shape of an isotherm is that of Ali-Asbi and Baianu [26]. They noted that most food isotherms are of type II in the Brunauer classification [3] and fitted the experimental points with a simple equation (Eq. 4 in material and methods). Ali-Asbi and Baianu model is useful in that provides a simple way for marking the beginning of the isotherm upswing from the intersection between the linear and the power-law part of Eq. 4.

The best-fit parameters for Caurie and Ali-Asbi and Baianu models are reported in Table 1, together with the estimated water activities at which moisture condensation takes place. It appears that above $a_w = 0.83-0.86$ meat water should be considered as bulk-like; given the difference between the two models the agreement is remarkable. Note that our Caurie monolayer value is lower than both BET and GAB estimates, as also recently found for goat meat [27] and spent hen meat [28]. Therefore Caurie [29] notion that monolayer values obtained from Eq. 3 are usually larger than BET values must not be taken for granted, at least for meat samples.

4.4 DSC Measurements

Heating scans of the same chicken meat samples used for sorption isotherm are shown in figure 2. It is apparent that up to $a_w=0.86$ (26.2 % water content) no endothermic peak is detected, meaning that only "unfrozen water" (usually believed to be water "bound" to the macromolecular matrix with a mobility so limited that it cannot freeze) exists in those samples. Only above $a_w=0.86$ is an endothermic peak detected at about $T=-15$ °C, which gradually increases and moves towards $T = 0$ °C with sample hydration.

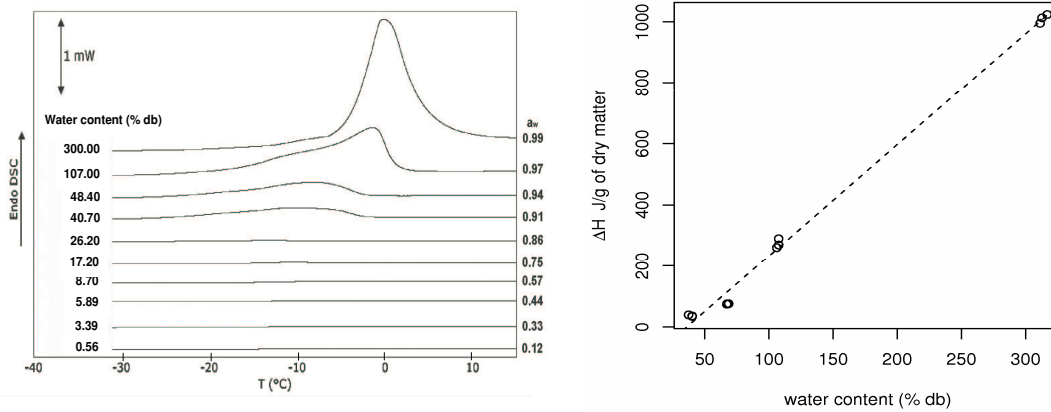


Figure 2. Sample heating scans of freeze-dried breast chicken meat hydrated at several water contents (left) and linear fit of the corresponding melting enthalpies (in triplicate) vs water content (right).

According to Quinn et al. [30] total bound water corresponds to the maximum water content for which no enthalpic peak is detected and can be obtained from the intercept at $\Delta H=0$ of a linear fit of the melting enthalpies vs. water content percentages (figure 2). From the fitting equation, $\Delta H=3.639 \times W - 130.8$ (where ΔH is the melting enthalpy per g of dry matter and W is the moisture percentage), the unfrozen water content of 35.9 % is estimated; note that the slope of the fitting equation (363.9 J g^{-1}) does *not* equate the melting enthalpy of pure water (334 J g^{-1}) thus confirming the notion [30] that the amount of frozen water cannot be calculated from the melting peak area using the heat of fusion of pure water.

4.5 NMR Measurements

The results of UPEN inversion [31] of the CPMG data obtained from freeze-dried chicken meat samples equilibrated at several a_w 's are shown in figure 3A. At every water content the T_2 relaxograms comprise a major water population whose average T_2 starts from about 0.2 ms at low hydration and gradually moves towards the "standard" value of 30-50 ms for raw meat [32,33].

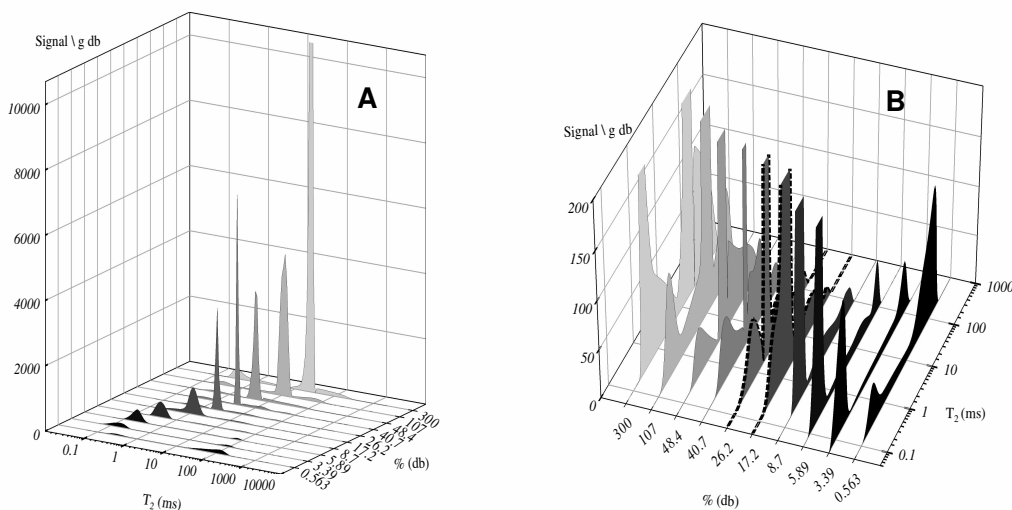


Figure 3. (A) T_2 relaxograms of freeze-dried chicken breast meat samples rehydrated at several water contents. (B) Close up view showing the appearance of the fast relaxing shoulder at $a_w=0.75$ (17.2%).

The width of the main peak also changes with water content, although not as monotonically. In fact, at $a_w=0.75$ (corresponding to a water content of 17.2 %) a sudden narrowing of the main water peak takes place, together with a shift to higher T_2 's, diagnostic of enhanced water mobility; a shoulder at about $T_2 = 0.3$ ms is also uncovered, revealing a faster-relaxing proton population (figure 3B). At $a_w=0.86$ (water content 26.2 %) the new peak is completely visible. At $a_w=0.99$ (water content 300%) the relaxogram resembles that of fresh meat.

A discontinuity is also observed in the plot of the major peak relaxation rate ($R_2 = T_2^{-1}$) vs moisture percentage (figure 4); an estimate [34] of the slope break point through linear fitting of 4 experimental points at low hydration and 3 points at high hydration yields 17.8%, a moisture content close to that at which the shoulder appears.

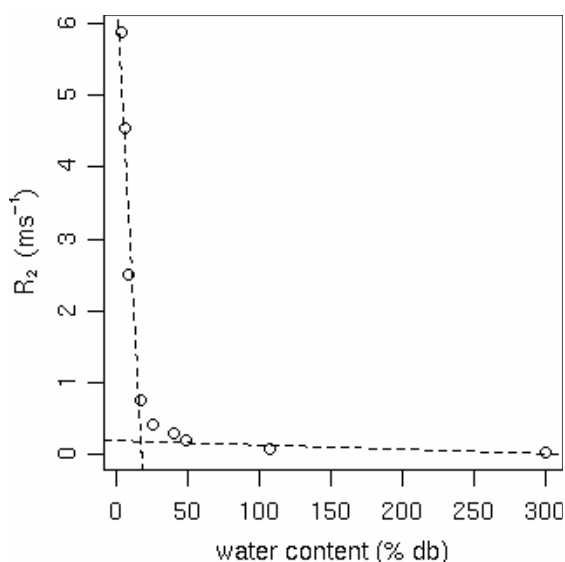


Figure 4. Relaxation rate vs. water percentage in freeze-dried chicken meat sample at several moisture contents. The two dashed lines cross at 17.8%.

4.6 Multianalytical Comparison

According to Wolfe et al., [18] hydration water of macromolecules or biomembranes is the one “whose physical properties [...] become different from those of pure water”. Under this view both our DSC and isotherm data point towards a situation where up to 30-40% of moisture water can be considered as “different from pure water” either because of low a_w or its inability to freeze at 0 °C. The value of 35.9% of unfrozen water provided by DSC lays within the range of estimated moisture contents at which bulk water appears (Tab. 1), thus confirming that both techniques detect the same hydration process. On the other side, the NMR results shown in figure 4, seem to contradict the above agreement because mobile water appears where it is reported by DSC to be still unfrozen (i.e. in the range 17.2 – 35.9%). Similar phenomena have been noted in starch and cellulose systems and ascribed to the presence of “metastable water” [12]. However, a simpler explanation is possible here. Water in meat may not freeze before 35.9% simply because the contemporary presence of small solutes, membranes and macromolecules depresses the freezing point according to mechanisms (i) and (ii) described in section 4.1; thus no DSC peak is visible between 17.2 and 35.9% of moisture despite water not being actually “bound”.

By looking at the plot in figure 4 it is clear that water mobility is much limited at low hydration. The high relaxation rate is the result of a combined effect of the higher water correlation time due to the slower reorientation of water close to the mesoscopic meat structures [18] and cross exchange of hydration water with the

extremely fast relaxing exchangeable matrix protons. Therefore, in the first part of figure 4, before the break point, R_2 decreases probably because the plasticizing effect of the added water enhances matrix mobility, thus reducing the R_2 of the matrix protons (exchangeable matrix protons included), in turn reducing also the R_2 of the main water population *via* proton exchange. After hydration completes R_2 keeps decreasing (albeit with a lower dependence on moisture content) because of exchange between the increasing amount of bulk water and water entrapped in matrix cavities [35] and/or labile matrix protons [36].

The small population of fast relaxing protons peaking at about $T_2 = 0.2$ ms and appearing at 17.2% moisture is usually assigned to water tightly associated with the matrix macromolecules. Nevertheless, this old interpretation has been reinvestigated in this thesis work and the results reported in chapter 2 and 3 show that origin of the fast relaxing component likely arise from the protein mobile side chains comprising both non-exchanging and labile protons in intermediate or slow exchange regime with water.

A further proof that the low T_2 signal is due to protons exceeding those added with water is obtained in this study from a comparison between the gravimetric water content and the water content inferred from the total NMR signal through a reference calibration (see methods).

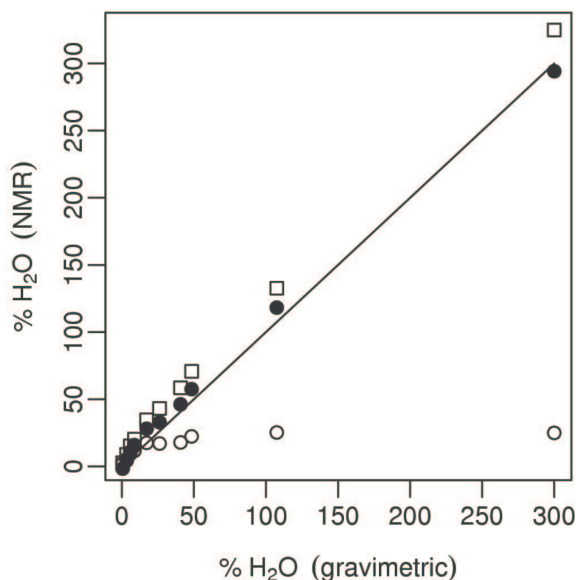


Figure 5. Comparison between actual water content and water content inferred from NMR signal through a reference calibration: (□) values obtained from total NMR signal; (●) values obtained from the NMR signal after subtracting the fast relaxing signal population; (○) difference between water obtained from total NMR signal and actual value.

It appears that water content obtained from the total NMR signal is higher than actual (figure 5). Subtraction of the low T_2 signal population from total NMR signal where possible (i.e. for samples at hydration higher or equal to 17.2 %)

greatly improves the agreement. It is also instructive to note that the difference between NMR- and gravimetrically-measured protons is not constant, but gradually increases with moisture until it reaches a plateau at 17.2% of actual hydration (figure 5). Beyond this point, the difference between NMR-inferred and actual water content is on the average 20.8%, i.e. about 6.4% of the total meat NMR CPMG signal. This behavior is again compatible with a model by which the solid matrix (whose NMR signal decays too fast to be detected by CPMG experiments in our conditions) is gradually plasticized by water and becomes more and more detectable in the low- T_2 region of the relaxograms as hydration proceeds. As soon as hydration is complete, plasticized chains have reached their maximum amount and mobility and do not change further upon water addition. This explanation is corroborated by the results very recently published for model systems of cross-linked proteins [37] for which a positive deviation between NMR and actual weight content was always obtained at high hydration, i.e. where side chain mobility was high as confirmed by dramatic reduction of the proteins' second moment.

Overall, the multianalytical comparison of water dynamic during the hydration of freeze-dried chicken breast meat revealed an agreement (between sorption isotherm and DSC experiments) and an apparent contradiction (between NMR and the other experiments) concerning the water content at which mobile water appears (30-40% for DSC and isotherm, and 17.2% for NMR). This contradiction can be reconciled by noting that frozen water may not appear in DSC experiments because of the presence of solutes and mesoscopic objects may depress the water freezing point so that it cannot form ice in our DSC conditions, for thermodynamic reasons. Furthermore, the NMR relaxation results confirmed that the fastest-relaxing part of the NMR signal detected in meat T_2 -relaxograms may not arise from the usually invoked "structural water", but from matrix protons located in meat structures that are plasticized by the addition of water; this view is strengthened by the finding that on the average 6.4% of the total ^1H CPMG-NMR signal of chicken breast meat is not due to the added water.

MATERIALS AND METHODS

Raw material

Twenty-four hours *post mortem* boneless chicken breast meat was collected from a local commercial processing plant (Amadori Group, Cesena, Italy), packed on ice, and transported to the laboratory. Upon receipt at the laboratory, the two fillets (*pectoralis major* muscle) of each whole breast were separated, trimmed of excess fat and connective tissue and held at 2-4°C throughout handling and measurements. About 200 g were immediately analyzed for fresh sample measurements, while the remaining portion (about 4 kg) was freeze-dried.

Freeze-drying

Freeze-drying was performed using a freeze-dryer mod. Lio2000 (CinquePascal S.r.l., Milano, Italy). The initial sample temperature was – 35°C, well below the glass transition temperature of the tissue (around – 16°C, [24]), and the pressure during the primary drying vacuum phase was 25.12 Pa. The freeze-drying process lasted for about 4 days and the surface to volume ratio of the product was around 0.9 cm⁻¹. Freeze-dried meat was packed under vacuum and stored at - 18°C until grinding and re-hydration.

Water Sorption Isotherm

Freeze-dried meat (at about 0.5% residual water) was ground using an universal mill mod. M20 (IKA, Staufen, Germany) at a speed of 20000 rpm for 15 s. During crushing, the milling chamber was maintained at 8-10°C with a water-cooling system. The ground sample was immediately transferred into glass desiccators, containing phosphorus pentoxide (P₂O₅) for two days in order to complete sample drying. A gravimetric method was employed for the determination of the sorption isotherm at 24°C. Moisture equilibration took place inside 10 sterilized glass jars (hygrostats) containing 10 different saturated salt solutions

covering relative humidity in the range 12-99% ($a_w = 0.12, 0.33, 0.44, 0.57, 0.75, 0.86, 0.91, 0.94, 0.97$ and 0.99). Dried samples of about 1 g were inserted into previously cleaned and oven dried glass bottles, 10 ml in volume. Each hydration experiment comprised nine bottles. The bottles were kept half-open on a plastic net inside the hermetically closed hygrometers containing, on the bottom, different saturated salt solutions at the required a_w [38]. The bottles were periodically taken (3 times a day) and weighed after closing, until they reached a constant weight for three consecutive weighings ($\Delta w < \pm 0.0005$ g) [39]. Equilibration time for each of the hydrated samples ranged from one ($a_w = 0.12$) up to 30 days for the samples at the highest a_w ($a_w = 0.99$). Note that for the latter group of samples it was necessary to brush the meat samples with a 0.02% solution of NaN_3 before hydration to avoid growth of molds, and to carry out the whole re-hydration under a laminar flow hood. a_w of the equilibrated samples was checked by an Aqualab water activity meter (Decagon Devices Inc., Pullman, USA). Dry matter content was determined gravimetrically according to [40]. Water content percentages are hereafter expressed on a dry matter basis.

Sorption isotherm data were analyzed using four different equations (Eqs. 1-4) according, respectively, to the GAB (11), BET (10), Caurie [25] and Ali-Asbi and Baianu [26] models:

$$X = \frac{X_m C_G K a_w}{(1 - K a_w)[1 + (C_G - 1)K a_w]} \quad (1)$$

$$X = \frac{X_m C_b a_w}{(1 - a_w)[1 + (C_b - 1)a_w]} \quad (2)$$

$$\ln(X) = \ln(X_m C^{1/n}) + \frac{2C^{1/n}}{X_m} \ln \frac{a_w}{1 - a_w} \quad (3)$$

$$X = n_I + C a_w + A a_w^B \quad (4)$$

In all equations X is the sample water content percentage and X_m is the percentage of water forming a monolayer of adsorbed water. In Eq. (1) C_G is the

Guggenheim constant and K is a constant related to the modified properties of the sorbate in the multilayer region; in Eq. (2) C_b is a constant related to the net heat of sorption; in Eq. (3) n is the number of adsorbed water layers and C is a constant related to C_b in Eq. (2); finally, in Eq. (4) all parameters have a mere empirical meaning. a_w at which water condensation takes place was estimated (i) according to Caurie ($a_{X_m^2}$, [25]) using Eq.(5)

$$\frac{1}{a_{X_m^2}} = 1 + \frac{1}{X_m^{n/2}} \quad (5)$$

and (ii) from the intersection between the linear and power-law tract of Eq. 4 (n_1 being close to zero, see Table 1).

DSC Measurements

Frozen water content was evaluated by a Pyris 6 DSC (Perkin Elmer Corporation, Wellesley, USA). The DSC was equipped with a low-temperature cooling unit Intacooler II (Perkin Elmer Corporation, Wellesley, USA). Temperature calibration was done with ion exchanged distilled water (m.p. 0.0°C), indium (m.p. 156.60°C) and zinc (m.p. 419.47°C); heat flow was calibrated using the heat of fusion of indium ($\Delta H = 28.71$ J/g). For the calibration, the same heating rate as used for sample measurements was applied under a dry nitrogen gas flux of 20 ml/min. Each sample (about 20 mg) was weighed in 50 μ l aluminum pans, hermetically sealed, and then loaded onto the DSC instrument at room temperature, using an empty pan of the same type for reference. Samples were then cooled at 5°C/min to -60°C, held for 1h and then scanned at 5°C/min to 20°C [41]. Unfrozen water was evaluated, according to Quinn et al. [30], as the maximum water content for which no enthalpic peak is detected and obtained from the intercept at $\Delta H=0$ of a linear fit of the melting enthalpies vs. water content percentages.

NMR Relaxation Measurements

Proton T_2 of the samples was measured in triplicate at each moisture level. Samples of about 350 mg of meat were placed inside 10 mm o.d. NMR tubes, in such a way as they did not exceed the active region of the RF coil and analyzed at 24 °C with the CPMG pulse sequence using a Bruker Minispec PC/20 spectrometer operating at 20 MHz. Each measurement comprised 3000 points, corresponding to 3000 echoes, with a 2τ interpulse spacing (*i.e.* between each couple of 180° pulses) of 80 μ s and a recycle delay of 3.5 s. The number of scans was varied depending on moisture content, in order to obtain a S/N ratio in the range 900-1400. The CPMG decays corresponding to the same moisture content were normalized to the sample weight, averaged and analyzed with the UPEN program [31]. UPEN *inverts* the CPMG signal using a continuous model *i.e.* it finds the less biased distribution of transverse relaxation times that fits the CPMG decay at best according to Eq. (6)

$$I(2\tau n) = \sum_{i=1}^M I_0(T_{2,i}) \cdot \exp(-2\tau n/T_{2,i}) \quad (6)$$

where 2τ is the CPMG interpulse spacing, n is the index of a CPMG echo and $I_0(T_{2,i})$ provides a distribution of signal intensities for each T_2 component extrapolated at $\tau=0$ (the relaxogram), sampled logarithmically in the interval $T_{2,\min} - T_{2,\max}$ set by the user. Default values for all UPEN parameters were used throughout this work. The behavior of UPEN in the presence of poorly sampled very fast relaxing signals together with slower components has been thoroughly studied by Moody and Xia [42]; it was found that UPEN is able to reproduce well synthetic data of this type when $S/N > 300$, *i.e.* well below the average S/N obtained in our experiments. Intensity of an NMR signal spanning a certain range of T_2 's on the relaxogram was obtained from the fraction of the "cumulative signal percentage" provided by UPEN in that range, multiplied by UPEN "total extrapolated NMR signal" (XSig).

It has been reported that when $T_2 \ll T_{1\rho}$ like in tissues or gels, the CPMG sequence at short interpulse spacing may induce spin-lock and lead to a marked increase in the measured T_2 values [15,36]. We have checked this possibility by comparing the relaxograms obtained by UPEN analysis of the CPMG and the alternating phase-CPMG (AP-CPMG, [44]) decays of the same meat sample in the same conditions ($2\tau = 80 \mu$ s) and found no significant differences. As the AP-CPMG sequence cannot induce spin-lock in the sample [44] we conclude that all our T_2

measurements are not contaminated by $T_{1\rho}$ effects. Similar results have been obtained [15] for cross-linked hydroxycellulose and carboxymethylcellulose networks.

Calibration of the NMR Signal

A calibration was attempted for determining the water content in meat from the measure of the absolute NMR CPMG signal intensity. Six samples of distilled H_2O spanning the range 52-398 mg were placed into 10 mm (o.d.) NMR tubes and analyzed with the CPMG sequence, collecting 5000 echoes with an interpulse spacing of 2 ms and a recycle delay of 10 s. The 90° pulse was carefully checked for each of the calibration points and found to be independent of the filling factor. This was expected, given the high homogeneity of the RF field within the several centimetres long solenoidal coil used in the Minispec probe (Fabio Tedoldi, Bruker Italy, private communication). Signal amplification was carefully adjusted along the series to take into account the different amounts of water in the samples and prevent signal clipping. Since we had planned to use UPEN for the analysis of all our meat signals, we calibrated the grams of water present into each sample vs. the NMR signal using the “total extrapolated NMR signal” (XSig) parameter provided by UPEN after inversion of the water CPMG decays. A plot of the intensity of the NMR signal vs the actual water content yielded a straight line ($R^2 = 0.9985$, $P < 0.001$) described by Eq. (7):

$$g H_2O = XSig' \times 5.4726 \times 10^{-4} - 6.3876 \times 10^{-3} \quad (7)$$

where XSig' is the signal obtained by UPEN XSig parameter and normalized to a Minispec amplification of 90. Eq. 7 was found to predict correctly the weight of water in samples containing various amounts of 10 mM $CuSO_4$ and 246 mM $FeCl_3$ solutions (having respectively $T_2 = 162$ and 16 ms) with an average relative error of 3.7%. It was assumed that also the amount of the water population appearing in the leftmost part of the meat relaxograms (i.e. at shorter T_2 's) could be predicted as reliably.

REFERENCES

1. E. Vittadini, L. C. Dickinson, J. P. Lavoie, X. Pham, P. J. Chinachoti, *Agric. Food Chem.*, **51**, (2003), 1647.
2. Van den Berg, C.; Bruin, S. Water activity and its estimation in food systems. Theoretical aspects. In *Water activity: Influences on food quality*; Rockland, L. B., Stewart, G. F., Eds.; Academic Press: New York, 1981; 1-43.
3. A. H. Al-Muhtaseb, W. A. M. McMinn, T. R. Magee, *A. Food Bioprod. Process.*, **80**, (2002), 118.
4. T. P. Labuza, L. McNally, D. Gallanher, J. Hawkes, F. J. Hurtado, *Food Sci.*, **37**, (1972), 154.
5. M.-L. Mateus, M. Rouvet, J.-C. Gumy, R. J. Liardon, *Agric. Food Chem.*, **55**, (2007), 2979.
6. M. A. Hossain, T. Ishihara, K. Hara, K. Osatomi, M. A. Ali Khan, Y. J. Nozaki, *Agric. Food Chem.*, **51**, (2003), 4769.
7. H. C. Bertram,; A. K. Whittaker,; H. J. Andersen, A. H. Karlsson, *J. Agric. Food Chem.*, **51**, (2003), 4072.
8. V. Morillon, F. Debeaufort,; M. Capelle,, G. Blond, A. Voilley, *J. Agric. Food Chem.*, **48**, (2000), 11.
9. L. Slade, H. Levine, *CRC-Critical-Reviews-in-Food-Science-and-Nutrition*, **30**, (1991), 115.
10. S. Brunauer, P. H. Emmet, E. Teller, *J. Am. Chem. Soc.*, **60**, (1938), 309.
11. R. B. Anderson, *J. Am. Chem. Soc.*, **68**, (1946), 686.
12. S. Li, L. C. Dickinson, P. Chinachoti, *J. Agric. Food Chem.*, **46**, (1998), 62.
13. P. Cornillon, *Lebensm.-Wiss. Technol.*, **33**, (2000), 261.
14. Z. H. Ping, Q. T. Nguyen, S. M. Chen, J. Q. Zhou, Y. D. Ding, *Polymer*, **42**, (2001), 8461.
15. D. Capitani, G. Mensitieri, F. Porro, N. Proietti, A. L. Segre, *Polymer*, **44**, (2003), 6589.
16. R. N. M. Pitombo, G. A. M. R. Lima, *J. Food Eng.*, **58**, (2003), 59.
17. Simatos, D.; Faure, M.; Bonjour, E.; Couach, M. Differential thermal analysis and differential scanning calorimetry in the study of water foods. In *Water Relations of Foods*; Duckworth, R. D., Ed.; Academic Press: London, UK, 1975, 193.
18. J. Wolfe, G. Bryant, K. L. Koster, *CryoLetters*, **23**, 1(2002), 57.

19. Z. Kantor, G. Pitsi, J. J. Thoen, *Agric. Food Chem.*, **47**, (1999), 2327.
20. A. M. Tocci, R. H. Mascheroni, *Lebensm. Wissen. Technol.*, **31**, (1998), 418.
21. B. P. Hills, *Annu. Rep. NMR Spectr.*, **58**, (2006), 177.
22. H. C. Bertram, H. J. Andersen, *Annu. Rep. NMR Spectr.*, **53**, (2004), 157.
23. N. Aktaş, Y. Tülek, H. Y. J. Gökalg, *Therm. Anal. Calorim.*, **50**, (1997), 617.
24. A. E. Delgado, D.-W. Sun, *J. Food. Eng.*, **55**, (2002), 1.
25. M. Caurie, *Int. J. Food Sci. Technol.*, **40**, (2005), 283.
26. B. Ali Asbi, I. C. Baianu, *J. Agric. Food Chem.*, **34**, (1986), 494.
27. R. R. B. Singh, Rao, K. H. Rao, A. S. R. Anjaneyulu, G. R. Patil, *J. Food Eng.*, **75**, (2006), 228.
28. R. R. B. Singh, Rao, K. H. Rao, A. S. R. Anjaneyulu, G. R. Patil, *Food Res. Int.*, **34**, (2001), 143.
29. Caurie, M. Derivation of full range moisture sorption isotherms. In *Water activity: influences on food quality*; Rockland, L. B., Stewart, G. F., Eds.; Academic Press: New York, 1981; 63-87.
30. F. X. Quinn, E. Kampff, G. Smyth, V. J. McBrierty, *Macromolecules*, **21**, (1988), 3191.
31. G. C. Borgia, R. J. S. Brown, P. Fantazzini, *J. Magn. Res.*, **132**, (1998), 65.
32. R. J. S. Brown,; F. Capozzi, C. Cavani, M. A. Cremonini, M. Petracchi, G. Placucci, *J. Magn. Res.*, **147**, (2000), 89.
33. H. C. Bertram, S. Dønstrup, A. H. Karlsson, H. J. Andersen, *Meat. Sci.*, **60**, (2002), 279.
34. M.-C. Vackier, B. P. Hills, D. N. Rutledge, *J. Magn. Res.*, **138**, (1999), 36.
35. F. Vaca Chávez, E. Persson, B. Halle, *J. Am. Chem. Soc.*, **128**, (2006), 4902.
36. F. Vaca Chávez, E. Hellstrand, B. Halle, *J. Phys. Chem. B*, **110**, (2006), 21551.
37. G. Diakova, Y. A. Goddard, J.-P. Korb, R. G. Bryant, *J. Magn. Res.*, **189**(2), (2007).
38. L. N. Bell, T. P. Labuza, In *Practical Aspects of Moisture Sorption Isotherm Measurement and Use*, 2nd Ed.; AACC Egan Press, Egan, MN, 2000.
39. W. E. L. Spiess, W. R. Wolf, The results of the COST 90 Project on water activity. In *Physical Properties of Foods*, Jowitt, R., Escher, F., Hallström, B., Meffert, H. F., Spiess, W. E. L., Vos G. Eds.; London and New York, Applied Science Publishers: London (UK), 1983, 65-91.

40. Anonymous, method n. 950.46. In *Official Methods of Analysis*, edition 15; Association of Official Analytical Chemists: Arlington, VA, USA, 1990.
41. N. C. Brake, O. R. Fennema, *J. Food Sci.*, **64**, (1999), 10.
42. J. B. Moody, Y. Xia, *J. Magn. Res.*, **167**, (2004), 36.
43. G. E. Santyr, M. J. Henkelman, R. M. Bronskill, *J. Magn. Reson.*, **79**, (1988), 28.
44. B. J. Suh, D. R. Torgeson, F. Borsa, *Phys. Rev. Lett.*, **71**, (1993), 3011.

CHAPTER 5

NMR DIFFUSION STUDIES ON MEAT

Part I: Probing Meat Microstructure through Bulk ^1H NMR Diffusion Measurements

5.1 Water Diffusive Studies and Microstructural Organisation of Compartmentalized Biological Samples

It is common knowledge that some microstructure characteristics of samples can be conveniently studied through the physical properties of the water they contain. Diffusion weighted ^1H NMR signals have been proved particularly informative at the purpose, especially when registered on systems where water diffuses in single, homogeneous regions of known shape [1]. The diameter of the droplets in an emulsion or the water diffusion coefficient inside a rock can at present be routinely estimated by means of affordable benchtop NMR instruments.

When barriers give rise to two regions with different characteristics it is still in principle possible to obtain structural information albeit a more difficult interpretation of the data based on chemical-physical considerations related to the sample under investigation. For instance, the highly degree of organisation characterizing meat gives rise to different water compartments or pools namely intra and extra-myofibrillar water. Between these two pools water molecules or protons are in exchange, resulting in partial averaging of the intrinsic relaxation times and the observed relative amplitudes. The amount of the averaging depends on the intrinsic relaxation times and exchange rates that in turn are influenced by the proton permeability of the cell membranes and diffusion process by which water molecules reach the membrane. Despite the complexity characterizing compartmentalized samples, such as meat, the extrapolation of microstructural information is still achievable through the application of a suitable fitting model incorporating all the main physical-chemical variables of the system.

With this regard, a frequent problem when dealing with such systems may arise from the poor free parameters-to-experimental points ratio [2]. At one hand, the models commonly employed require up to six free parameters: water pools ratio, each water pool diffusion coefficient, the possible contribution of the compartments shape to each diffusion coefficient and finally at least one exchange

parameter in case water exchanges between the two regions at a frequency comparable to the observations [3]. At the other hand, the degradation of the observed tissues at the experimental conditions may dramatically limit number and signal-to-noise ratio of the acquired experimental points. In practice it is not uncommon to find works where a 4 parameters model is fitted to less than 20 experimental points [4].

In the following sections are reported the results concerning water diffusion experiments performed on turkey *pectoralis major* muscle, based on low resolution nuclear magnetic resonance bulk measurements. The experimental data were interpreted in terms of a model characterized by anisotropic water diffusion through two exchanging compartments, intra and extra-myofibrillar (see section 1.3 of chapter 1 for further details). Results of measurements performed along and across the muscular fibers were combined, so to gain information about fibers' shape and diameter, the apparent diffusion of water inside and outside them and the exchanging rates between the two pools. Preliminary investigation related to changes of meat microstructure organisation upon freezing have also been attempted to assess the feasibility of the proposed model in future meat authentication studies.

In order to reduce the degrees of freedom of the model applied the parameters related to the intra and extra-myofibrillar water pools have been calculated through independent experiments by performing transverse relaxation analysis of the CPMG curves. This procedure has shown to be significantly effective in reducing the risk of over-fitting preventing the achievement of ambiguous physical parameters. Despite this simplicity, at the best of the author's knowledge, no works have been published to date combining transverse relaxation and diffusion experiments in this way.

5.2 The Choice of an Appropriate Fitting Model for Meat

A suitable model to interpret the obtained diffusion data was built from considerations about skeletal muscle morphology and its post-mortem evolution. Skeletal muscle cells are accepted to have a cylindrical shape, [5] with a length of centimeters and a radius which strongly depends on the observed animal. For a 100 days old female turkey selected for high lean meat this is around 32 microns [6]. The cells are parallelly grouped into bundles, the main structures that can be

observed in muscle light microscope images [7]. Their volume is mainly occupied by the myofibrils network, through which the cytoplasm is evenly distributed [8]. Following death, the muscle undergoes rigor which is expected to cause, as any contraction, water expulsion from the myofibrils network [9]. At the same time cell membranes undergo disintegration, as can be assessed by means of impedance measurements [10]. The two combined phenomena lead to the accumulation of water in the intercellular spaces, characterized by a width of hundreds of microns [5]. After the rigor phase such water is only partially reabsorbed by the myofibrillar network. As a consequence a T₂ spectrum shows two proton populations, at 45 and 170 ms, ascribable to intra-myofibrillar and extra-myofibrillar water respectively [11].

When diffusion weighted signals are analyzed, extra-myofibrillar water self-diffusion can be safely considered isotropic and unaffected by the shape of the huge compartments it is confined in. At the opposite the myofibrils, being parallelly stacked, are likely to give rise to an intra-myofibrillar water self diffusion which strongly depends on the orientation. Both longitudinal and transversal water diffusion are expected not to be prevented by the myofibrils. This can be deduced by observing that a free flow is possible in both directions even for globular proteins [12]. Transversal water diffusion is expected to be influenced by the myofibrils, as has been observed in other filamentous proteins solutions [13] At the opposite no structures have been found able to hinder longitudinal water diffusion.

The comparison with similar systems [14] and experiments performed on skeletal muscle with gadolinium doped water [15] demonstrate that an exchange between the two populations exists. The dependence of diffusion on fiber orientation and shape can be considered by using as a starting point a model describing such exchange. The most intuitive and applied protocol to do so is that described by Karger [16].

The expression describing the diffusion weighted signal of two non-exchanging water populations

$$\psi(g) = p'_{intra} e^{-\gamma^2 \delta^2 g^2 D'_{intra} (\Delta - \delta / 3)} + p'_{extra} e^{-\gamma^2 \delta^2 g^2 D'_{extra} (\Delta - \delta / 3)} \quad (1)$$

is modified to include the exchange, by considering both diffusion coefficients and water populations as apparent, because exchange rates dependent, according to the equations

$$D'_{intra(extra)} = \frac{1}{2} \left(D_{intra} + D_{extra} + \frac{1}{\gamma^2 \delta^2 g^2} \left(\frac{1}{\tau_{intra}} + \frac{1}{\tau_{extra}} \right) \right) \mp (a^2 + b^{1/2}) \quad (2)$$

$$a = D_{intra} - D_{extra} + \frac{1}{\gamma^2 \delta^2 g^2} \left(\frac{1}{\tau_{extra}} - \frac{1}{\tau_{intra}} \right) \quad (3)$$

$$b = \frac{4}{\gamma^4 \delta^4 g^4 \tau_{intra} \tau_{extra}} \quad (4)$$

$$p'_{intra} = 1 - p'_{extra} \quad (5)$$

$$p'_{extra} = \frac{1}{D'_{extra} - D'_{intra}} (p_{intra} D_{intra} + p_{extra} D_{extra} - D'_{intra}) \quad (6)$$

$$p_{extra} = 1 - p_{intra} \quad (7)$$

$$\tau_{extra} = \tau_{intra} \frac{p_{extra}}{p_{intra}} \quad (8)$$

where $D_{intra(extra)}$ are the true self diffusion coefficients, $\tau_{intra(extra)}$ are the water exit/entrance rates from/to the myofibrils, $p_{intra(extra)}$ are the two true water populations.

To include the myofibrils cylindrical shape effect on D_{intra} many modifications to the basic Karger model have been put forward [17]. Schoberth [4] offers the simplest approach, consisting in considering D_{intra} as an apparent coefficient for restricted diffusion, according to the equation

$$D_{intra} = \frac{\langle r^2 \rangle}{6t} \quad (9)$$

where $\langle r^2 \rangle$ is the mean square displacement and t is the diffusion evolution time.

For a time interval t-t' and a cylindrical compartment of infinite length, $\langle r^2 \rangle$ has been described by Meier [17] as

$$\langle r^2 \rangle = \frac{1}{4} R^2 + \sum \frac{2}{\alpha_m^2 (\alpha_m^2 R^2 - 1)} - e^{-D\alpha_m^2 t} - e^{-D\alpha_m^2 t'} \quad (10)$$

where α_m is the mth nonzero root of $J'(\alpha R)=0$ with J being the spherical Bessel function of the first kind and R the radius of the cylinder. The sum has been introduced to account for the spins that don't equally feel the effects of the restricting boundaries and still haven't lost their dependence on diffusion [3]. When $\frac{D\Delta}{R^2} \gg 1$ the sum can be safely ignored, so that

$$D_{intra} = \frac{R^2}{24t} \quad (11)$$

It should be now noticed that the relation (11) can be considered an acceptable simplification of equation (10) even when $\frac{D\Delta}{R^2}$ is lower than 1, as figure 2 of reference [18] shows.

5.3 Microstructure and Diffusive Considerations on Turkey Fresh Samples

Figure 1 shows, for the samples taken from one of the turkeys pectoral muscle analyzed, the signals weighted by diffusion along (panel A) and across (panel B) the muscle fibers, for the 3 diffusion times. Lines show the result of the simultaneous fitting to the six curves of the model outlined in the previous section.

In table 1 are summarized the results of the fitting procedure which seem to be in good agreement on the basis of chemical-physical considerations. In particular, the differences in the intra/extra-myofibrillar water diffusion coefficients reflects the different characteristics of the domains they are contained. Due to its size of hundreds of microns and the reduce solute concentration, the diffusion of water in the extra-myofibrillar space can reasonably be expected higher than in the cytoplasmatic environment where the contemporary presence of myofibrils and biological constituents significantly slower the diffusive process. Similar findings

have also been reported for diffusion of water in isolated rat heart cells [19] and phosphocreatine in rabbit leg muscle [20].

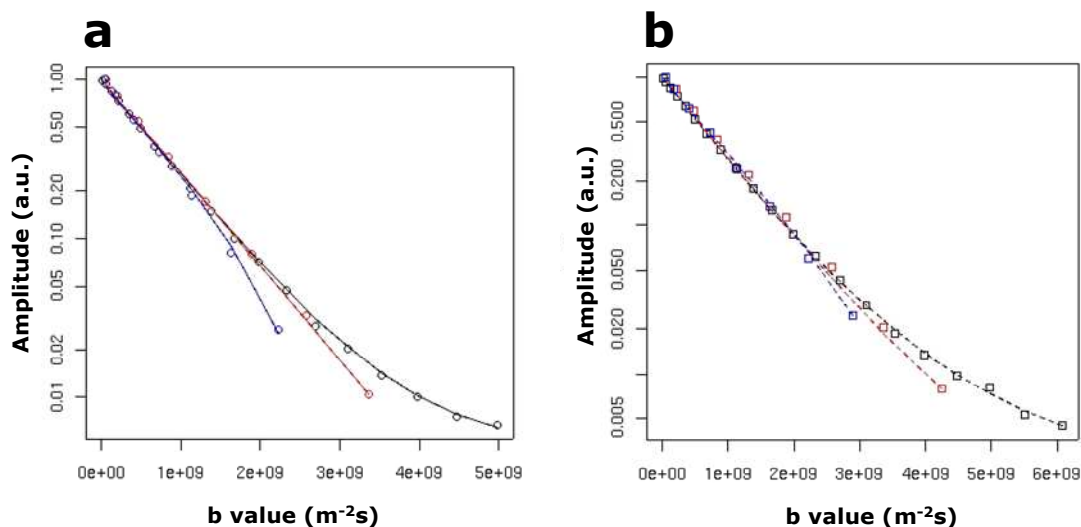


Figure 1. Normalized PFG NMR stimulated-echo amplitudes of the water signals measured in fresh turkey samples with diffusion sensitizing gradients applied (a) along and (b) across the muscle fibers at different observation times (54, 104 and 704 ms corresponding to the black, red and blue points respectively). Solid (a) and dashed (b) lines refers to the calculated values obtained through the simultaneous fitting of the six curves.

The data are also consistent with histological observation where an average cell radius of 32 microns is reported for female turkey meat samples [6] in agreement with the fitting value shown in table 1 (i.e. 22.3 microns).

Fresh Samples		
NMR Fitting Parameters	Mean	sd
Replicates n°	5	5
D_{intra} (m ² s ⁻¹)	6.47×10^{-10}	$\pm 6.87 \times 10^{-11}$
D_{extra} (m ² s ⁻¹)	1.59×10^{-9}	$\pm 8.61 \times 10^{-11}$
T_{intra} (s ⁻¹)	1.27×10^1	± 3.37
R (m)	2.23×10^{-5}	$\pm 5.16 \times 10^{-6}$

Table 1. Summary of the NMR parameters obtained through the simultaneous fitting of the six curves shown in figure 1.

5.4 Effect of Freezing on Meat Structure and Organisation

Freezing is one of the most common preservation method for meat and meat products. Unfortunately, its beneficial effects are to a certain extent counterbalanced by the damage caused by the formation of ice within the tissue resulting in a damage of overall meat cellular microstructure. Important quality parameters, such as exudates, texture and colour of the product are therefore influenced by the rate, final temperature and storage time at which the freezing process is conducted.

Five turkey meat samples – from the same batch previously discussed (see materials and methods) - have been analyzed through NMR experiments to assess the feasibility of this approach in detecting changes concerning the chemical-physical and microstructure properties of meat upon freezing. The response of relaxometric and diffusion measurements have been combined by fitting the experimental data with the model described in section 5.2.

In figure 2 are reported the results of the T_2 continuous distribution obtained after the inversion of the raw CPMG decays for fresh (solid line) and frozen-thawed (dashed line) turkey samples respectively.

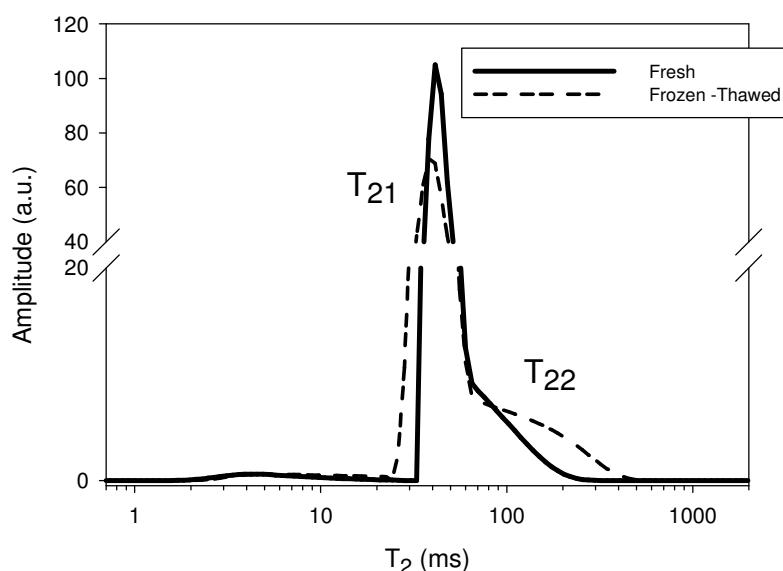


Figure 2. T_2 continuous distribution analysis of fresh (solid line) and frozen-thawed (dashed line) turkey breast meat samples.

The analysis of the relative signal percentages of intra (T_{21}) and extra-myofibrillar (T_{22}) water components has revealed a water re-distribution occurring

in the samples after freezing (see table 2). In particular, data of table 2 outline as the freezing process causes a reduction of the intra-myofibrillar water population of about 3.45% followed by an analogous increase of the moisture percentage located outside the contractile reticulum.

T₂ population	Mean Values (%)	
	Fresh	Frozen-Thawed
Intra-Myofibrillar Water (T ₂₁)	85.58 ± 2.47	82.13 ± 2.45
Extra-Myofibrillar Water (T ₂₂)	14.42 ± 2.47	17.86 ± 2.45

Table 2. Relative mean percentages of the T₂₁ and T₂₂ water populations obtained after the inversion of the raw CPMG decays.

The CPMG percentages of the two water components have been included in the fitting model (p_{intra} and p_{extra}) of the diffusion curves to reduce the risk of over-fitting caused by the poor free parameters-to-experimental points ratio. Figure 3 shows the results of the applied fitting procedure to the weighted diffusion curves measured along (panel a) and across (panel b) the muscle fiber for frozen-thawed meat samples.

In table 3 are reported the calculated values of the simultaneous fitting of the six curves seen in figure 3. A comparison of these values with those of fresh samples (table 1 vs table 3) reveals some interesting changes induced by the freezing process on meat structure. Beside a water re-distribution from the inside to the outside of the protein dense matrix (as seen in the discussion of the CPMG data) a main effect is also detectable on the diffusion properties of the intra and extra-myofibrillar water fractions characterized respectively by an average variation of -19.01 and +15.42% of their coefficients upon freezing. This modification is also associated to an average reduction of the cell diameter of 12.56% and a slight decrease in the exchanging rate of about 7.09% which is probably induced by modification of the cell membrane permeability or disrupting effects caused by the low temperature process.

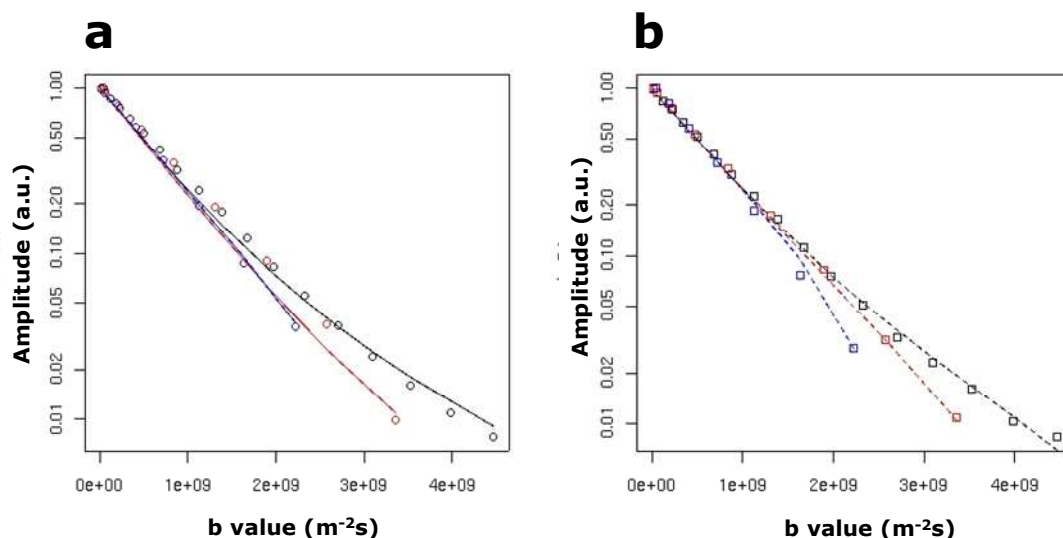


Figure 3. Normalized PFG NMR stimulated-echo amplitudes of the water signals measured in frozen-thawed turkey samples with diffusion sensitizing gradients applied (a) along and (b) across the muscle fibers at different observation times (54, 104 and 704 ms corresponding to the black, red and blue points respectively). Solid (a) and dashed (b) lines refers to the calculated values obtained through the simultaneous fitting of the six curves.

Frozen-Thawed Samples		
NMR Fitting Parameters	Mean	sd
Replicates n ^o	5	5
D_{intra} (m^2s^{-1})	5.24×10^{-10}	$\pm 9.76 \times 10^{-11}$
D_{extra} (m^2s^{-1})	1.88×10^{-9}	$\pm 1.60 \times 10^{-10}$
T_{intra} (s^{-1})	1.18×10^1	± 1.43
R (m)	1.95×10^{-5}	$\pm 2.14 \times 10^{-6}$

Table 3. Summary of the NMR parameters obtained through the best simultaneous fitting of the six curves shown in figure 3.

Generally, during a slow freezing process, such as that one employed in the analysis, the formation of ice crystals is mainly confined in the extra-cellular regions characterized by a lower osmotic pressure while the solute concentration of the unfrozen phase gradually increases, thus decreasing its vapour pressure. Previous histological studies conducted on air-blast frozen pork meat samples [21]

has revealed that such freezing method is responsible of the de-hydration of the cellular compartment since water diffuses outside the protein reticulum because of the vapour pressure difference. An analogous behaviour has been detected in the analysis of the CPMG curves where water re-distributes between meat domains with an increase of the extra-myofibrillar water population following the dehydration of the intra-cellular compartment. Though the extent of this process is influenced by many variables such as the freezing rate, the temperature and the storage time, it would generally lead to an increase of the sarcoplasm viscosity accounting for the reduction detected in the intra-myofibrillar water diffusivity (D_{intra}). On the other hand, the extra-myofibrillar component, in agreement with the NMR results, is expected to exhibit an enhancement of its diffusion rate (D_{extra}) as a consequence of the dilution effect induced by moisture migration. The fact that ice crystals formation and growth mainly occur in the extra-cellular space has also important implications in the changes related to meat structure. Usually, slow freezing results in a more severe tissue damage reflecting in a considerable shrinkage of the cells and disruption of fibers. The average reduction of 12.56% detected in the cell diameter is thus in agreement with previous histological observations and it is explainable in terms of a lateral pressure exerted on muscle cells by the formation of large, exclusively extra-cellular, ice crystals.

Overall, despite the preliminary nature of this work the model applied resulted in a good rationalization of the experimental data when compared to histological observations. In principle, the results demonstrate the potentials of NMR in future meat authentication studies. Nevertheless, more detailed investigations are needed to clarify the effect of different freezing methods and storage times on meat structure and organisation. To these aspects it will be turned in the next chapter where the tensor approach in the analysis of the diffusion coefficient is proposed for a more rigorous treatment of the anisotropic diffusion properties of meat.

MATERIALS AND METHODS

Samples Choice and Preparation

Full *pectoralis major* muscles of five 100 days old female turkeys were obtained within 24 hours of slaughter from a local factory. From the upper part of each muscle a 4 cm wide cube was dissected, which displayed parallel muscular fibers at a visual inspection. With a specially designed die-cutter two cylindrical samples were taken from each cube, one across and one along the fibers. The remaining flesh was frozen at -25°C for one week and then thawed at 4°C for 24h prior the analysis. At the end of the thawing process two cylindrical samples were taken, again across and along the fibers respectively.

NMR Measurements

The experiments were carried out using a 20-MHz single-coil pulsed ^1H NMR spectrometer from Bruker, equipped with 2T/m pulsed magnetic field gradients generator. The two series of samples were carefully placed in 10 mm NMR tubes so to observe water diffusion across and along the fibers.

The diffusion weighted signals were registered with a Pulsed Field Gradient Stimulated Echo (PFG-STE) sequence, by ramping the gradient pulse area for three evolution times, 54ms, 204ms and 704ms.

The transverse relaxation weighted signals were registered with a CPMG sequence, with 200 ms spaces between the echoes. A continuous multiexponential model was then fitted to the experimental values to derive the main proton populations [22].

REFERENCES

1. B. P. Hills, *Magnetic Resonance Imaging in Food Science*, John Wiley & Sons, Inc., New York, 242-264.
2. Y. Roth, A. Ocherashvilli, D. Daniels, J. Ruiz-Cabello, S. E. Maier, A. Orenstein, and Y. Mardor, *Magn. Reson. Imag.*, (2007), in press.
3. W. S. Price, A. V. Barzykin, K. Hayamizu, and M. Tachiya, *Biophys. J.*, **74**, (1998), 2259.
4. S. M. Schoberth, N. Bar, R. Kramer, and J. Karger, *Anal. Biochem*, **279**, (2000), 100.
5. N. F. S. Gault, (1992). Structural Aspects of Raw Meat. In: The chemistry of muscle based foods. (Eds. Johnston, D.E., Knight, M.K., Ledward, D.A.). The Royal Society of Chemistry, Cambridge, pp. 79-105.
6. F. V. Salomon, Th. Anger, H. Krug, U. Gille, and H. Pingel, *Anat. Histol. Embryol.*, **19**. (1990), 314.
7. H. C. Bertram, A. K. Whittaker, H. J. Andersen, and A. H. Karlsson, *Meat Sci.*, **68**, (2004), 667.
8. D. A. Nelson, and E. S. Benson, *J. Cell. Biol.*, **16**, (1963), 297.
9. K. Trombitas, P. Baatsen, J. Schreuder and G.H. Pollak, *Muscle Res. Cell. Motil.*, **14**, (1993), 573.
10. H. C. Bertram, A. Schäfer, K. Rosenvold, and H. J. Andersen, *Meat Sci.*, **66**, (2004), 915.
11. H. C. Bertram, P. P. Purslow, and H. J. Andersen, *J. Agric. Food. Chem.*, **50**, (2002), 824.
12. S. Papadopoulos, K. D. Jürgens, and G. Gros, *Biophys. J.*, **79**, (2004), 2084.
13. M. A. Cremonini, B. P. Hills, G. Placucci, "The effect of ageing on the egg white -a water proton transverse relaxation study-" In: XXXIII National Congress on Magnetic Resonance, Bressanone, Italy, 2003.
14. J. Pfeuffer, U. Floegel, and D. Leibfritz, *NMR Biomed.*, **11**, (1998), 11.
15. H. C. Bertram, J. Stagsted, J. F. Young, and H. J. Andersen, *J. Agric. Food Chem.*, **52**, (2004), 6320.
16. J. Karger, H. Pfeifer and W. Heink, in *Advances in Magnetic Resonance* (Waugh. J. S. Ed.), Vol. 12, Academic Press, New York, pp. 1-89.
17. C. Meier, Dreher W., and D. Leibfritz, *Magn. Res. Med.*, **50**, (2003), 500.
18. B. N. N. Achar, and J. W. Hanneken, *J. Mol. Liquids*, **114**, (2004), 147.

19. C. Liess, G.K. Radda and K. Clarke, *Magn. Res. Med.*, **44**, (2000), 208.
20. P. Van Gelderen, D. DesPres, P.C.M. Van Zijl and C.T.W. Moonen, *J. Magn. Res. ser. B*, **103**, (1994), 255.
21. M. N. Martino, L. Otero, P. D. Sanz and N. E. Zaritzky, *Meat Sci.*, **50**, (1998), 303.
22. G. C. Borgia, R. J. S. Brown, and P. Fantazzini, *J. Magn. Reson.*, **132**, (1998), 65.

CHAPTER 6

NMR DIFFUSION STUDIES ON MEAT

Part II: DTI Measurements of Meat Anisotropic Diffusion Properties upon Freezing

6.1 Previous NMR Meat Authentication Studies

Consumers perceive fresh meat as a premium quality item of their diet, because of its superior nutritional and organoleptic properties. Compared to it frozen meat is usually considered an inferior - yet cheaper - replacement. In recent years the repeated alerts about the possibility of SARS (bird flu) transmission from birds to humans have caused a sudden drop in the poultry meat sellings in the western countries. This fact has prompted wholesale sellers to store most of their unsold goods in frozen form with the hope of selling it once the alarm is over. While this practice is absolutely legal, cases may exist where unscrupulous retailers may want to take advantage of the consumers' trust and sell thawed meat for fresh. Unfortunately, testing if the meat product is actually fresh or has been previously frozen is a issue still open in analytical and forensic food chemistry. Besides, since consumers may hardly notice the changes occurring in meat upon freezing, they might put their health at risk by freezing and thawing again a previously frozen and thawed meat [1].

Nuclear magnetic resonance imaging (MRI) has been advocated in the past as a non-destructive and non-invasive tool able to discriminate between fresh and frozen-thawed meat. This unique capability of MRI arises from its sensitivity to local variations in water mobility resulting from modification of the interactions between water and macromolecules and changes in the meat structure upon freezing [2].

Pulsed-gradient spin-echo (PGSE) represents a common NMR method used to characterize the water mobility of biological systems through the measure of its effective diffusion coefficient (ADC). Unfortunately, as for other orderly tissues (i.e. skeletal, cardiac, uterine muscle [3-5] and white matter [6-8]), the high degree of organization of meat, whose fibers are mainly aligned in a specific direction, give rise to a directional dependence of diffusion, that is diffusion anisotropy.

In previous authentication studies of meat, the directional dependence of diffusion coefficients has been taken into account by measuring the water diffusion

axially ($D_{//}$) and radially (D_{\perp}) with respect to the fibers direction while denoting the anisotropy level as the ratio between these two parameters. Some authors [2,9] conducted a PGSE-MRI study in unfrozen and frozen/thawed trouts stored for different time periods. It was found that the freeze-thaw process affects significantly the D_{\perp} while no influence was detected in the $D_{//}$ after 41 days of freezing. These results are inconsistent with a previous study of Guiheneuf *et al.* [10] which found that the D_{\perp} and $D_{//}$ as well as the anisotropy measured on frozen meat samples exhibited higher but not significant values if compared to unfrozen ones. It is likely that the reasons of this apparent contradiction arise from the fact that the anisotropic diffusion properties are better expressed in the form of a tensor instead of a scalar measure [11]. In light of this, a more rigorous and suitable measure should involve the use of the diffusion tensor MRI technique (DTI-MRI). This approach permits characterization of the diffusion properties of a complex system by the effective diffusion tensor (\mathbf{D}) [12-13] and quantitative anisotropy indexes derived from it [14] (see appendix B for a more detailed description). The main advantage arises from the possibility of obtaining a number of diffusion indexes that are rotationally invariant or independent of the directions at which diffusion is measured, the position of the sample with respect to the laboratory frame and fibers distortions within the sample.

In the following sections of this chapter the results about frozen-thawed chicken breast meat analyzed by means of Diffusion Tensor Micro Imaging (μ DTI) are reported. Changes in the anisotropic diffusion properties of water were investigated by freezing the samples with two methods (domestic freezer and liquid nitrogen) and for different storage periods. To the best of the author's knowledge, this represents the first attempt of meat authentication based on the μ DTI-MRI technique.

6.2 Effect of Different Freezing Methods and Storage Time on Meat DTI Parameters

Figure 1 represents the canonical bi-plot of fresh and frozen meat samples groups calculated through the generalized discriminant analysis. Blue arrows represent the correlations of the original DTI parameters with the canonical axes 1 and 2 and can be considered as a measure of their discriminating power. Note that the pointing directions of arrows are consistent with increasing values of the

relative DTI parameter while decreasing values of it are associated to the opposite direction.

The statistical test revealed a significant difference among the multivariate location of the sample groups ($P < 0.0001$) that was achieved with $m = 3$ (see materials and methods for a more detailed description of the statistical test) resulting in the smallest cross-validation error; see table 1.

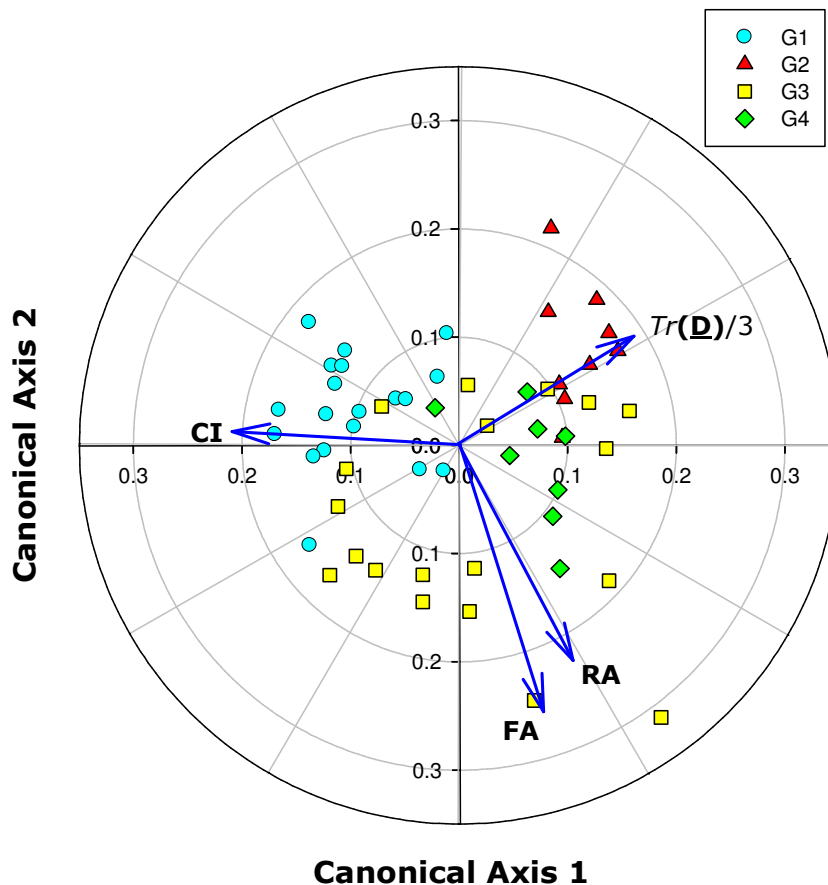


Figure 1. Constrained ordination of the multivariate meat samples obtained by application of generalized canonical analysis, $m = 3$. Blue arrows have been scaled to ease visualisation of the multivariate location of the samples. (G1: Fresh samples; G2: samples frozen in liquid N_2 and stored at $-30^\circ C$ for 1 day; G3: samples frozen in liquid N_2 and stored at $-30^\circ C$ for 11 days; G4: samples frozen at $-30^\circ C$ then stored at the same temperature for 11 days).

Particularly interesting is the multivariate location of fresh (G1 group) and frozen (G2-G4 groups) samples which are clearly discriminated by the first two canonical axes of figure 1 (misclassification error of 14.6%; data non shown). The main differences arises from the changes occurring in the intra-voxel anisotropy indexes upon freezing. In fact, a generalized increase of the mean anisotropy value

(i.e. FA and RA; see also table 2) is detectable in the frozen groups especially at longer storage times. According to experimental observations this effect is likely attributable to a reduction (-1.59% and -3.36% respectively, data not shown) of the lateral water diffusion tensor components (i.e. D_2 and D_3) occurring upon freezing leading to a concomitant elongation of the diffusion tensor ellipsoid whose shape is more oblate (i.e +12.17%) compared to the fresh group (G1).

	G 1	G2	G3	G4	Total	% correct
Meat groups						
G1	16	1	2	0	19	84.2
G2	0	8	0	1	9	88.9
G3	3	3	9	3	18	50.0
G4	2	1	2	4	9	44.4

Table 1. Results of cross-validation for the DTI data; rows are true groups, columns are predicted groups.

Table 2. Mean and SD of the DTI parameters displayed by the four groups of meat samples.

DTI parameter	Experimental group			
	G1	G2	G3	G4
Replicates n.	19	9	18	9
$Tr(\underline{\mathbf{D}}) / 3$ (10^{-9} m ² /s)	1.145 ± 0.028	1.217 ± 0.022	1.160 ± 0.065	1.163 ± 0.042
FA	0.260 ± 0.013	0.264 ± 0.013	0.291 ± 0.023	0.273 ± 0.023
RA	0.203 ± 0.011	0.210 ± 0.012	0.230 ± 0.023	0.215 ± 0.024
CI	1.354 ± 0.038	1.294 ± 0.010	1.317 ± 0.054	1.294 ± 0.016

It is worth to note that these findings are consistent with the observations reported in the previous chapter in section 5.4. Despite the different nature of the analytical approach the results seem to suggest a common origin of the meat structure modifications occurring upon freezing in terms of a lateral shrinkage undergone by meat fibers. In particular, water migration outside the intra-cellular protein reticulum- as demonstrated by the analysis of the CPMG distribution

discussed in section 5.4- might be responsible for the reduction of the meat fibers diameter (through de-hydration), reflecting in a measurable decrease of radial diffusivity. Higher system anisotropy in frozen samples also accounts for a contribution derived from principal diffusivity (i.e. D_1) which has the overall effect of increasing the mean diffusivity (i.e. $Tr(\mathbf{D}) / 3$) of the system. However, this result may also be an artefact due to the incorporation of part of the extra-myofibrillar water component in the computation of the diffusion coefficient, as the population of this kind of water increases in the system upon freezing.

Particularly severe are the anisotropy changes detected in G3 and G4 samples compared to the G2 group. Their similar location on the canonical axes suggest that a possible explanation could be consistent with the time (11 days) they have been stored at -30°C . This hypothesis is in agreement with a previous study [15] which has confirmed that further modifications occur during freezing when the process is extended over time. Particularly effective on meat structure might have been the damage caused by the re-crystallization process in the G3 group which was exposed to a large temperature fluctuation (frozen at -196°C then stored at -30°C). This evidence is not surprising since other studies [16-17] have demonstrated that the beneficial effect of ultra-fast freezing method (usually associated with the formation of smaller and uniformly distributed ice crystals in the intra/extra-cellular space) might be neutralized by an inappropriate storage temperature resulting in a subsequent re-crystallization to bigger ice-crystals. According to the literature [16-17], these detrimental effects can result in a structural damage of meat comparable or even more pronounced than that obtainable with slow freezing process (such as the one employed for the G4 samples) where a production of large, exclusively extra-cellular ice crystals is usually reported [18-19].

The macrostructural measure of similarity or coherence index (CI) lends partial support to this explanation. In fact, lower CI values have been detected in G3 samples, thus indicating a deterioration in the local order of fibers probably due to the presence of gaps between and within cells as previously observed in histological studies [18-19]. The fact that also the G2 samples have lower CI than fresh ones, but comparable diffusion anisotropy to them, suggests that the time scale for the structural modification affecting CI and RA (or FA) may be different; while one day at -30 degrees is sufficient for producing a relevant variation of CI, more days are needed for ice crystals to grow to a dimension that modifies the

radial dimension of the fibers. Unfortunately not much can be said about the G3 samples which are very much scattered in the direction of the CI canonical variate.

These observations have been finally tested by conducting an additional trial on a new batch of samples (see materials and method). This time the number of experimental variables was reduced by keeping constant the freezing storage time and temperature and considering only the effect of the freezing method. In table 3 are reported the mean values and standard deviation of the DTI parameters for each sample group.

DTI parameter	Experimental group			
	H1	N	H2	F
replicates n.	3	3	3	3
$Tr(\underline{D}) / 3$ (10^{-9} m ² /s)	1.20 ± 0.061	1.213 ± 0.035	1.217 ± 0.015	1.403 ± 0.195
FA	0.366 ± 0.021	0.355 ± 0.011	0.353 ± 0.011	0.396 ± 0.050
RA	0.223 ± 0.009	0.223 ± 0.008	0.215 ± 0.009	0.257 ± 0.023
CI	0.764 ± 0.017	0.742 ± 0.059	0.729 ± 0.046	0.694 ± 0.063

Table 3. Mean and SD of the DTI parameters displayed by the four groups of meat samples analyzed in the second trial.

The results of the multivariate discriminant analysis are shown in figure 3 together with the correlations displayed by the original DTI parameters reported as blue arrows. Figure 3 shows that no separation occurs between the group frozen in liquid nitrogen (i.e. N group) and the fresh ones (H1 + H2 groups). This can be taken as a proof of a reduced structural damage or modification concerning the N group samples as a results of the ultra-fast freezing method. This evidence also supports the explanation by which the similar multivariate location observed for the G3 and G4 groups in the first batch of samples was likely ascribable to the temperature fluctuation following the ultra-rapid freezing of the G3 group and not a real effect caused by the method itself.

The results related to the remaining group (i.e. F group) are consistent with the data obtained in the previous trial. According to figure 2 and 3, slow freezing rate has shown to affect the structure of meat in terms of a significant increase of the water diffusion anisotropy (i.e. FA and RA). The deterioration of meat tissue is mainly explainable as a result of the formation of bigger, exclusively extra-cellular ice crystals which restrict the radial translation motion of water molecules by

reducing the cell diameter through a lateral pressure exerted on cell membrane. The analysis of the coherence index (i.e. CI) supports these observations confirming that this parameter is generally lower in slow-frozen samples (i.e. F group) as a result of a more severe freezing damage reflecting in a open structure of the tissue and a loss of compactness of fibers throughout the sample [18-19].

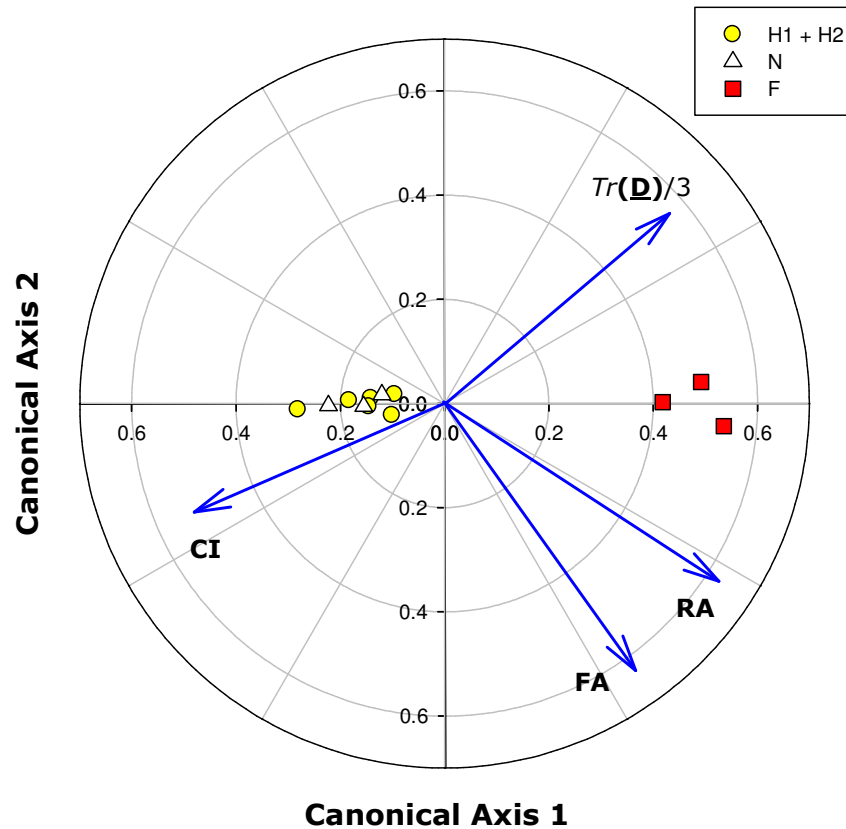


Figure 3. CAP biplot of the constrained ordination of multivariate meat samples analyzed in the second trial. Arrows representing the contribution that each of the 4 original DTI parameters has in discriminating among groups have been scaled to allow an easy visualisation of the multivariate location of the samples. (H1 + H2: fresh samples; N: samples frozen in liquid nitrogen and immediately thawed; F: samples frozen at -30°C for 7 days)

Overall, despite data of the two trials have been acquired with different equipments and sequences, the consistency of the results emphasizes the importance of both freezing rate and storage time as critical factors for the quality control of frozen meat in agreement with a previous observation [20].

MATERIALS AND METHODS

Raw Material

Boneless chicken breast meat was bought from different local dealers in different times. The samples were divided into 4 groups accordingly with the treatment they were subjected. Group (G1) was evaluated as fresh, group (G2) was pre-frozen in N₂ then stored at -30°C for 1 day, group (G3) was pre-frozen in N₂ then stored at -30°C for 11 days and, finally, group (G4) was frozen at -30°C and stored for 11 day. The frozen samples, before NMR analysis, were let thawing overnight at 5°C.

The additional trial was conducted only on a single chicken breast. A total of 6 samples were excised with a specially designed die-cutter. Three of them (H1 group) were analysed and then frozen in liquid nitrogen (N group) and the remaining three samples (H2 group) were put in a domestic freezer at -30°C for 1 week (F) after the analysis. The liquid nitrogen samples were immediately thawed after freezing and analyzed while the F group samples were let thawing overnight at 5°C prior to the analysis.

NMR Measurement

Experiments on the first batch of samples were performed on a Bruker Avance 9.4 T (400 MHz ¹H resonance frequency) microimaging system equipped with a MICRO 5 probe (insert = 10 cm) and gradient units capable of a maximum amplitude of 40A (200 Gauss/cm).

For each chicken sample the signals from 10 different slices were acquired using a multiple spin-echo sequence (Multiple SE). Voxel matrix was 128 X 128 with a FOV of 12 X 12 mm² corresponding to a 93.8 X 93.8 X 500 μm³ voxel resolution. The diffusion tensor **D** was estimated from the acquisition of one image without diffusion attenuation (B₀) and a set of diffusion-weighted images with gradients applied in 6 different non-collinear directions. The diffusion encoding gradients were applied with a duration $\delta = 2$ ms and separated by a time $\Delta = 20$ ms. The other acquisition parameters were as follow: TR = 5000 ms, TE = 26.376 ms and number of scans = 1.

The additional trial was conducted on a Bruker AM WB spectrometer (200 MHz ^1H resonance frequency) microimaging system. The diffusion encoding gradients were applied with a duration $\delta = 3$ ms and separated by a time $\Delta = 50.8$ ms. The other acquisition parameters were as follow: TE = 26.376 ms (time between the first and second 90° pulse of figure 4) and number of scans = 4. Voxel matrix was 128 X 128 with a FOV of 12 X 12 mm^2 corresponding to a 93.8 X 93.8 X 500 μm^3 voxel resolution. For each sample the signal of 1 slice was acquired and the apparent diffusion coefficients (ADCs) were calculated from signal attenuation obtained for one **b** value with a set of 6 diffusion gradients directed along the vertices of a sphere.

The entire DTI protocol was developed in house. For this purpose a STEAM sequence was chosen as the one reported in figure 4.

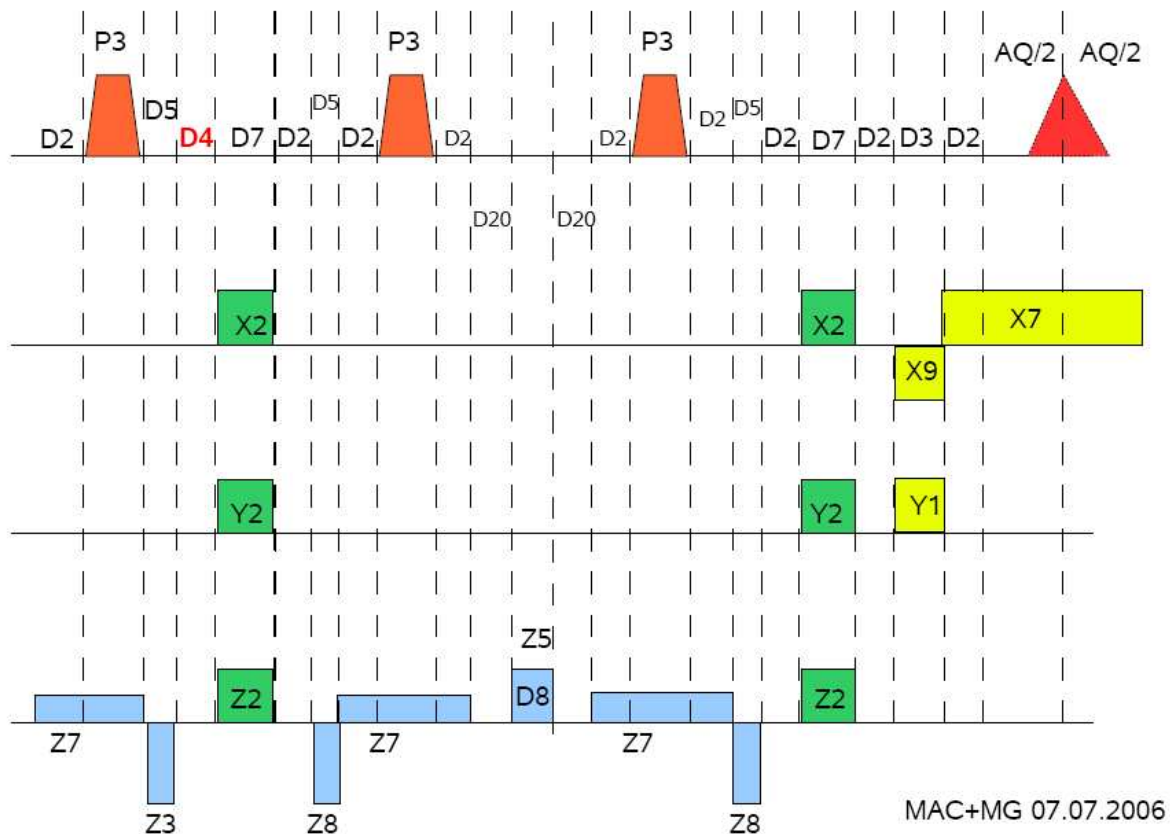


Figure 4. Schematic representation of the STEAM sequence used to acquired the DTI images of the second batch of samples. In green are depicted the diffusion sensitizing gradients applied along the laboratory frame coordinate system (i.e x, y, z axes). The yellow rectangles represent the read and the phase gradients while the blue colours refer to the crashing gradients inserted in the sequence to avoid inferences from spurious signals. In red are reported the slice selective pulses and acquisition.

Postprocessing

Since the DW images of the first trial were acquired with 1 scan a gaussian smoothing (kernel size of 5 X 5 voxels corresponding to a FWHM of 220.43 μm) was applied before tensor calculation in order to improve the signal to noise ratio and to increase the validity of statistical inference. The tensor elements were then calculated from each voxel using the Biimage suite software (<http://www.bioimagesuite.org/public/Running.html>) by applying a multivariate linear regression routine. A threshold mask was applied in the procedure to avoid background noise being included in the calculation. In addition to the tensor principal diffusivities (eigenvalues D_1 , D_2 and D_3) and directions (eigenvectors ε_1 , ε_2 and ε_3) other rotationally invariant DTI parameters has been considered. The intra-voxel diffusion characteristics have been evaluated by calculating the mean diffusivity $\langle D \rangle$ ($= \text{Tr}(\mathbf{D})/3$), the most common anisotropy indexes (FA and RA) and also the coherence index (i.e. CI) was determined as a measure of macrostructural (diffusive) anisotropy of the system.

Since the reduced number of replicates analyzed, each slice of a sample was treated as a repetition unit within the corresponding group. This was realized by averaging the considered DTI parameter over each slice before performing statistical analysis. Table 4 summarizes the experimental design of the work.

Sample group	Number of samples	Total repetition units
G1	2	19
G2	1	9
G3	2	18
G4	1	9

Table 4. Unbalanced experimental design of this work. Due to the reduced number of samples analyzed, each meat slice was treated as a repetition unit within the corresponding group.

Since the data of the additional batch of samples were acquired with an higher number of scans the application of a smoothing procedure was not performed before data processing. The tensor elements were then calculated from each voxel using the Biimage suite software

(<http://www.bioimagesuite.org/public/Running.html>) by avoid negative value being included in the computation.

Statistical Analysis

The main purpose of the statistical analysis was to test the changes related to the whole set of DTI parameters in response to the freezing treatments. Multivariate constrained ordination procedures are particularly appropriate in such cases where data are classified into *a priori* groups allowing to visualize potential patterns of differences in the location or relative dispersion among groups. In this work the software CAP (**C**anonical discriminat **A**nalysis of **P**rincipal coordinates) has been used to perform a generalization of the most common canonical discriminat analysis (CDA) [21-22]. The main advantage of the CAP method arise from the possibility of maximizing the differences among groups basing on any distance measured while the CDA approach is relegated to the use of Mahalanobis distances. The CAP constrained ordination can be summarized as follows: (i) data reduction by performing a principal coordinate analysis (PCO) on the DTI parameters using a dissimilarity measure based on Euclidian distances; (ii) non-arbitrary choice of an appropriate number of PCOs (m) leading to the minimum error of the observations correctly classified. The place of a new observation into the canonical axes is done trough the leave-one-out cross validation procedure; (iii) do a traditional canonical analysis on the first m PCOs.

The hypothesis of no significant difference in multivariate location among groups is done by using the trace statistic (sum of canonical eigenvalues = sum of squared of canonical correlations) obtained a P value by permutation. This has been tested among fresh and frozen groups with a number of permutations equal to 9999.

APPENDIX B

DTI (Diffusion Tensor Imaging)

Water self-diffusion is the microscopic random motion of water molecules driven by internal kinetics energy. Since the majority of solutes dissolved in biological and food systems are transported by water its translational diffusion properties have been extensively studied because capable of influencing the chemical-physical composition and modification occurring in these systems over time. Due to its non-invasive nature, nuclear magnetic resonance spectroscopy is a unique tool for studying molecular dynamics in chemical and biological systems. Generally, the self diffusion coefficient of water is extrapolated through application of a set of **pulsed field gradients (PFG)**. In a PFG experiment, the attenuation of a spin-echo signal resulting from the dephasing of nuclear spins due to the combination of the translational motion of the spins and the imposition of spatially well-defined gradient pulses is used to measure motion [23]. The mechanism of how a PFG spin-echo sequence qualitatively works is depicted in figure 5. First, the net macroscopic magnetization (orientated along the z axis) derived from spin diffusing ensemble is tipped along the x - y plane through application of a $\pi/2$ pulse. During the first τ period at time t_1 , a gradient pulse of duration δ and magnitude g is applied along the z axis so that at the end of the first τ period, individual spin experiences a phase shift.

At the end of the first τ period, a π rf pulse is applied to reverse the sign of the precession (i.e. the sign of the phase angle) before the application, at time $t_1+\Delta$, of a second magnetic pulse gradient of the same duration and magnitude of the one previously applied. If the spins have not undergone any translational motion with respect to the z -axis, the effect of the two gradients pulses cancel and all spins refocus. Conversely, if the spins have diffused the degree of dephasing due to the applied gradient will be proportional to their displacement along the gradient direction (i.e. z axis) in the period Δ (i.e. the duration between the leading edges of the gradient pulses).

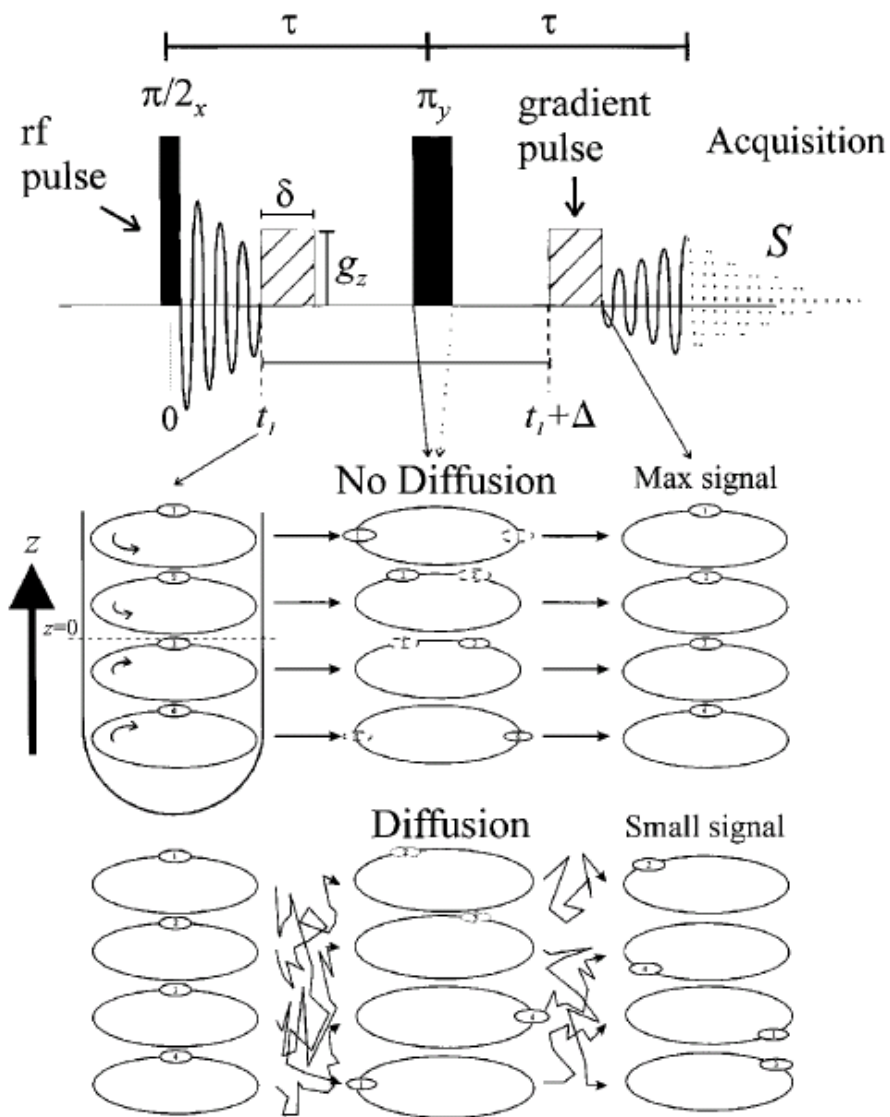


Figure 5. A schematic representation of how a spin-echo PFG or Stejskal and Tanner pulse sequence measures diffusion. In this figure it is assumed that the centre of the gradient coincides with the centre of the sample inside the NMR tube (i.e. $z=0$). Accordingly, the spins above and below this point acquire phase shifts owing to the gradient pulses, but in opposite senses. In the absence of diffusion, the effect of the first gradient pulse, denoted by the curved arrows in the first phase diagram, is to create a magnetization helix (i.e. the solid ellipses in the centre phase diagram) with a pitch of $2\pi/\gamma\delta g$. The π pulse reverses the sign of the phase angle (i.e. the dotted ellipses in the centre phase diagram), and thus, after the second gradient pulse, the helix is unwound and all spins are in phase, which gives a maximum echo signal. In the presence of diffusion, the winding and unwinding of the helix are scrambled by the diffusion process, resulting in a distribution of phases, although it is not easily seen since the sample consists of only four spins. Larger diffusion would be reflected by poorer refocusing of the spins, and consequently by a smaller echo signal. (Figure taken from [23])

In practice, it is possible to calculate the water self-diffusion coefficient (D) by fitting the echo NMR signal attenuation following the application of a set of diffusion gradients:

$$S = S_0 \exp(-bD) \quad (1)$$

where S_0 is the NMR signal intensity in the presence of no gradients applied and b takes into account the diffusion sensitizing gradients strength and duration [24].

Unfortunately, a single D value can not univocally characterize the translational motion of water since it exhibits a high dependence on the chemical-physical composition of the system under investigation as well as on its structural organisation. Usually, in macromolecular solutions (such cell cytoplasm, polymer solution, protein solution) the water molecules have to skirt around the “obstructing” molecules (i.e. organelles, proteins) as well as perhaps interacting with protein hydration shells and this lead to a lower measured diffusion coefficient (namely apparent, ADC or D_{app}) in comparison with that measured in the pure liquid (i.e. true diffusion coefficient or D).

In addition, further complications may arise when the water molecules dynamics are restricted by the system’s boundaries in which they are contained [23]. In figure 6 is schematically reported what happens when the diffusion coefficient of water is measured under free or restricted regime (i.e. within a sphere of radius R). In the case of freely diffusing water particles (left part of figure 6), the diffusion coefficient determined will be independent on Δ and the displacement measured in the z -direction will reflect the true diffusion coefficient, since the mean-squared displacement scales linearly with time. However, for the particle confined to the sphere, the situation is entirely different. For short values of Δ such that the diffusing water particle has not diffused far enough to feel the effect of the boundary (i.e., $\xi < 1$), the measured diffusion coefficient will be the same as that observed for the freely diffusing water molecule. As Δ becomes finite (i.e., $\xi \approx 1$), a certain fraction of the water particles (i.e. in a real NMR experiment there is an ensemble of diffusing species) will feel the effects of the boundary and the mean squared displacement along the z -axis will not scale linearly with Δ ; thus, the measured diffusion coefficient (i.e. D_{app}) will appear to be (observation) time dependent. At very long Δ (i.e., $\xi > 1$), the maximum distance that the confined water particle can travel is limited by the boundaries, and thus the measured mean-squared displacement and diffusion coefficient becomes independent of Δ .

Thus, for short values of Δ the measured displacement of a particle in a restricting geometry observed via the signal attenuation in the PFG experiment is sensitive to the diffusion of the particle while at long Δ the signal attenuation becomes sensitive to the shape and dimensions of the restricting geometry (see figure 7).

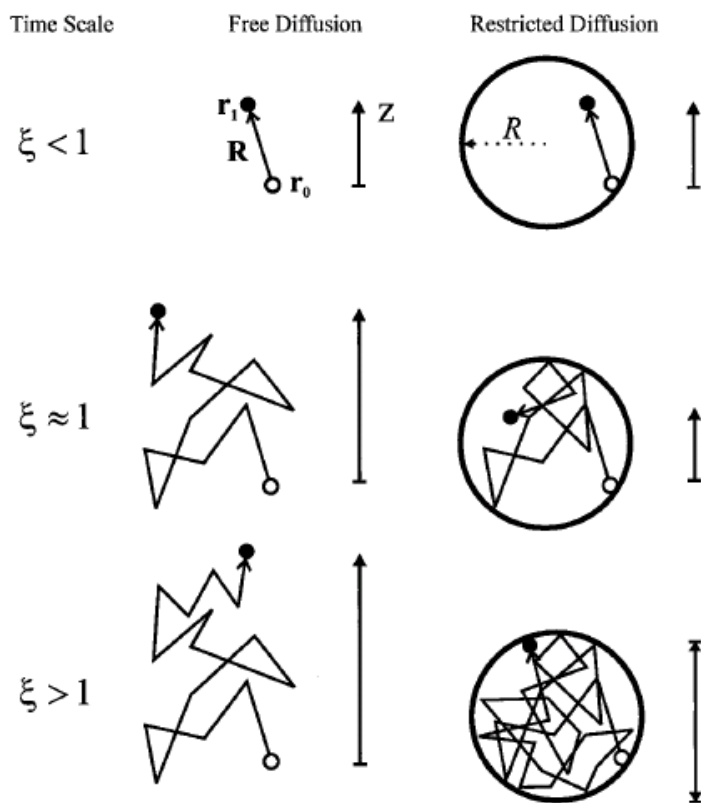


Figure 6. In the diagram it is schematically represented what happens when a the diffusion coefficient of a water molecule undergoing free diffusion or restricted diffusion in a sphere of radius R is measured. r_0 denotes the starting position (\circ), and r_1 denotes the position (\bullet) at a time Δ later. The length of the arrows (\mathbf{R}) denotes the measured displacement in the direction of the gradient which is in the z direction in the present diagram. Three relevant time scales can be considered for the measurement of the effects of the restricted diffusion; (i) $\xi (= D\Delta/R^2) \ll 1$ (the short time limit); the particle does not diffuse far enough during Δ to feel the effects of restriction. Measurements performed within this time scale lead to the true diffusion coefficient (i.e. D). (ii) $\xi \approx 1$; some of the particles feel the effects of restriction and the diffusion coefficient measured within this time scale will be apparent (i.e. D_{app}) and be a function of Δ . The fraction of particles that feel the effects of the boundary will be dependent on the surface-to-volume ratio S/V . (iii) $\xi > 1$ (the long time limit); all particles feel the effects of restriction. In this time scale, the displacement of the particle is independent of Δ and depends only on R . Thus, restriction causes a (measuring-time)-dependent diffusion coefficient in which at Δ the displacement is limited by the embedding geometry. (Figure taken from [23])

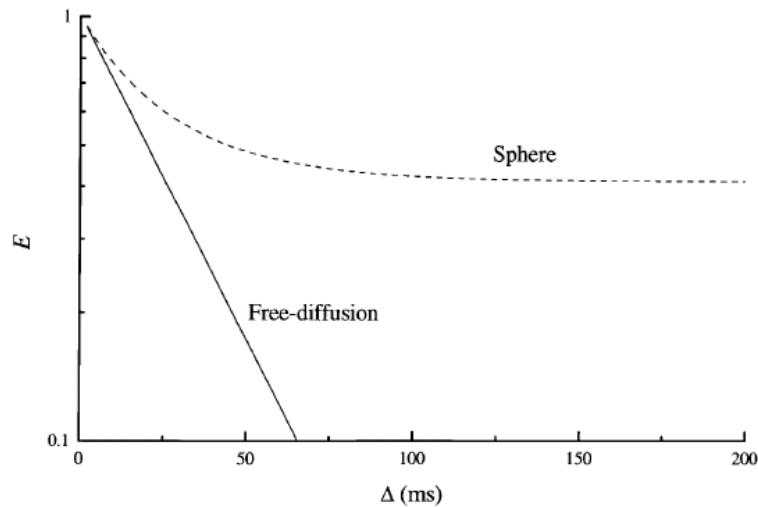


Figure 7. A plot of simulated echo attenuation in the case of free diffusion (—) and diffusion in a sphere (---) versus Δ . The parameters used in the simulation were $\delta=1$ ms, $D = 5 \times 10^{-10}$ m²s⁻¹, $g = 1$ Tm⁻¹, $R = 8$ μ m and $\gamma = \gamma^H$. The echo attenuation in the case of diffusion in the sphere can be seen to go through three stages: (i) when $\xi < 1$, the diffusion appears unrestricted and the result is the same as that of free diffusion, (ii) as Δ increases the spins begin to feel the effects of the surface, and (iii) when $\xi > 1$, the diffusion is fully restricted and the attenuation curve plateaus out. (Figure taken from [23])

Free and restricted diffusion inside a sphere represent special cases of random motion under isotropic conditions. Usually, a condition of “isotropic diffusion” is fulfilled every time the measured diffusion coefficient is independent on the directions of the applied magnetic gradients (i.e. diffusion within a sphere) as for instance in liquid samples or more generally in microscopically homogenous media.

Unfortunately, the majority of biological samples (such as skeletal and cardiac muscle and in white matter) violate the isotropic diffusion condition since they display a diffusivity that is dependent upon orientation of the sample (i.e. $D_{\perp} \neq D_{//}$) with respect to the direction of the diffusion sensitizing gradients. This is the case for highly organized tissue samples, such as skeletal muscle, whose anisotropic diffusion properties arise from the peculiar fiber cell architecture so as a single D can no longer characterize the water mobility in these samples. An appropriate model to describe anisotropic diffusion has been proposed by Bassler

and co-workers [12-13] where the scalar diffusion coefficient D of water has been replaced with a symmetric diffusion tensor \underline{D} .

The simplest model of such a tensor representation is to think of the diffusion as composed by three principal diffusivities corresponding to the diffusion of water in the three main directions. In case of free and isotropic diffusion, these three principal diffusion values are equal (i.e. $D_1 = D_2 = D_3$) and the tensor shape can reasonably be approximated to that one of a sphere (figure 8a). On the contrary, in highly orientated samples where water diffusion is constrained by microscopic structures the three tensor values will be different (i.e. $D_1 \neq D_2 \neq D_3$) displaying a dependence upon geometry architecture of the system. In particular, for a general case of diffusion inside a muscle cell a cylindrical geometry can be assumed so as the tensor representation would be described by an ellipsoid (figure 8b) with D_1 conventionally denoted as the largest diffusion coefficient so that $D_1 > D_2 = D_3$.

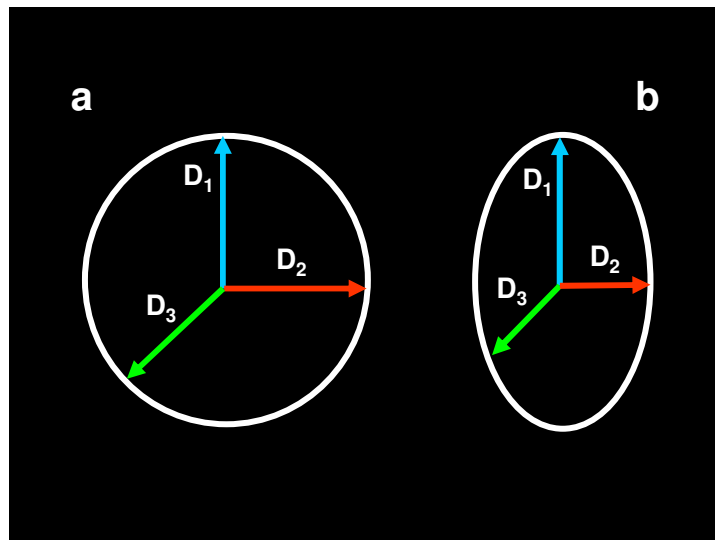


Figure 8. Graphical representation of the three main tensor diffusivities values in case of (a) isotropic and (b) anisotropic diffusion. Case b resembles the particular condition of diffusion inside a cylinder where D_1 is conventionally denoted as the largest diffusion coefficient and $D_2 = D_3$.

For the sake of simplicity, it can be hypothesized a situation where the diffusion ellipse is orientated such that D_1 is along the z axis, D_2 is along the x axis and D_3 is along the y axis, then the diffusion coefficient (D_z) measured with a diffusion gradient along the z axis will be $D_z = D_1$ and $D_x = D_2$ and $D_y = D_3$ (see figure 9, left panel). In this simple case, the diffusion tensor (\underline{D}) is described as a diagonal matrix:

$$\underline{\mathbf{D}} = \begin{pmatrix} D_1 & 0 & 0 \\ 0 & D_2 & 0 \\ 0 & 0 & D_3 \end{pmatrix} \quad (2)$$

The values D_1 , D_2 , D_3 are the eigenvalues of the tensor. At each eigenvalue are associated three eigenvectors of the matrix that describe the vectors pointing along the principal directions of diffusivity. In other words, the eigenvectors represent the spatial coordinates (x , y , z) of each diffusivity (D_1 , D_2 , D_3) with respect to the laboratory frame. In the above case, since the main diffusivities directions are aligned to the NMR coordinate system the corresponding eigenvectors will exactly point along x , y , and z axes. Unfortunately, this is not the case for real samples where their high degree of heterogeneity and internal architectural variability might lead to misalignment with respect to the reference laboratory frame. For example, in muscle tissue the cell fibres tract often rotates as it moves from one spatial point to the other causing a spatial shift of the tensor coordinate system indicated as a ρ , θ , and Φ rotation angles with respect to the reference x , y and z axes (right panel of figure 9). In such a condition the mathematical formalism of the diffusion tensor would account for cross terms as reported in the following:

$$\underline{\mathbf{D}} = \begin{pmatrix} D_{xx} & D_{xy} & D_{xz} \\ D_{yx} & D_{yy} & D_{yz} \\ D_{zx} & D_{zy} & D_{zz} \end{pmatrix} \quad (3)$$

The diagonal tensor elements of this new matrix represent the projections of the original D_1 , D_2 and D_3 coefficients onto the laboratory reference system. To obtain an exact estimation of the three main diffusivities is therefore sufficient to diagonalize the matrix by a ρ , θ , and Φ rotation of the corresponding eigenvectors. Thus, in general there are six quantities to be calculated: the diffusivities D_1 , D_2 and D_3 and the rotation angles ρ , θ , and Φ that describes the directions of the eigenvectors. These measures depend on the gradient b value that, as previously described, take into account the diffusion sensitizing gradient strength and duration; in a diffusion tensor situation, this is expressed as a gradient b -value matrix (\mathbf{b}).

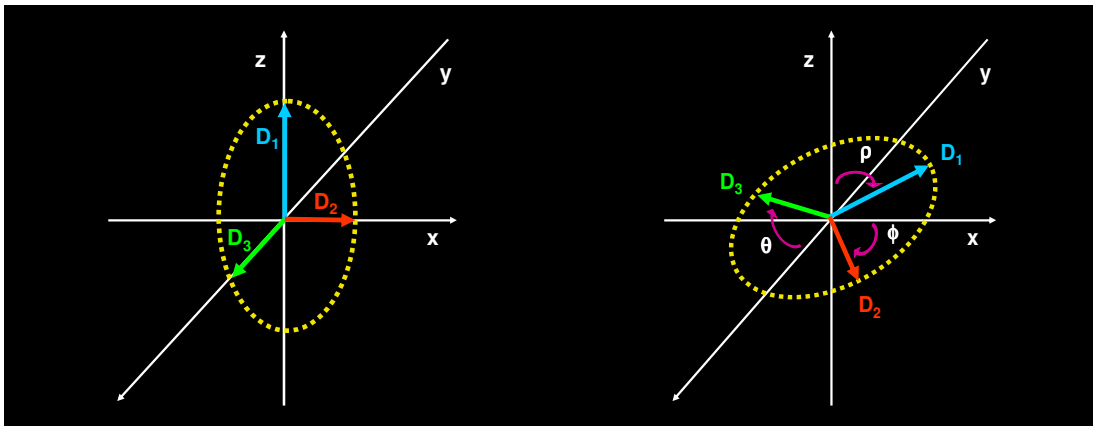


Figure 9. Ellipsoidal representation of the three main tensor diffusivities in case of (left panel) perfect alignment with the reference x , y and z axes and (right panel) ρ , θ , and Φ spatial shift of the tensor coordinate system with respect to the laboratory frame.

When a DT protocol is performed the measurements need to be acquired with six different b -value matrices. In addition, a seventh experiment is required with no diffusion weighting to provide a reference measure of signal intensity without a diffusion gradient (S_0). These seven measurements are the minimum needed to calculate the full diffusion tensor, although more are often used to improve the stability of the calculation. It is important that the measurements be taken with gradient directions that are independent and not coplanar. A popular way to distribute the gradient directions is to use vectors in which the endpoints are uniformly distributed on a sphere centered at the origin. Nevertheless, other schemes are possible as shown in figure 10.

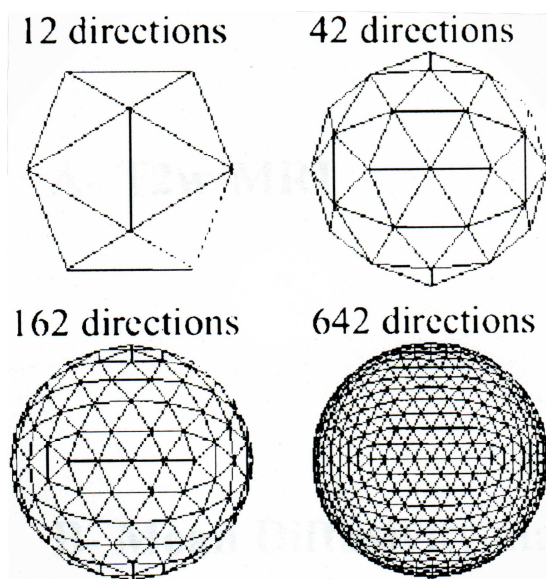


Figure 10. Different gradient encoding directions schemes employed in fiber orientation mapping [25]

The Diffusion Tensor approach was originally introduced in bulk diffusion measurements where it has been proven useful to better describe the properties of orientated tissue [12-13]. Nevertheless, potential clinical applications of the diffusion tensor in MRI (Magnetic Resonance Imaging) were suggested very early [25]. The most successful application of the diffusion tensor imaging (also known as DTI) since the early 1990s has been brain ischemia[26] when it was discovered that the water diffusion drops at the very early stage of the ischemic event allowing suitable treatment of patients at a stage when the brain tissue might still be salvageable. The application of the diffusion tensor protocol in the MRI field basically provide tensor information for each voxel of the image.

Mean Diffusivity

Once a gradient direction scheme has been chosen and suitable measurements taken, the diffusion tensor will yield the D_1 , D_2 and D_3 coefficients and the three eigenvectors that correspond to the spatial orientation of the main diffusivities in each voxel. The overall evaluation of the apparent diffusion coefficient (ADC, also indicated as mean diffusivity $\langle D \rangle$) in a voxel or region can then be easily calculated as:

$$\langle D \rangle = (D_1 + D_2 + D_3) / 3 = \text{Trace}(\underline{\mathbf{D}}) / 3 \quad (4)$$

It is an interesting result of the mathematics of tensor that the Trace is an invariant, or the same in all coordinate systems. By applying a DTI protocol is thus possible to obtain an estimation of the diffusion coefficient of an orientated sample that is independent from its position inside the instrument as well as from the directions of the applied weighting gradients. The mean diffusivity has been one of the first DTI rotationally invariant parameters to be successfully used in clinical study in assessing the diffusion drop following brain ischemia [27].

Diffusion Anisotropy Indices

In the past, several scalar indices has been proposed to characterize diffusion anisotropy. One of the simplest measure is the ratio between perpendicular

diffusion directions (i.e. D_x/D_y , D_x/D_z , ecc.). Isotropic material would have this ratio equal to 1 while anisotropic material would exhibit values smaller than unity. Another proposed approach was to take as a measure of anisotropy the standard deviation of D_x , D_y and D_z divided by their mean value [27]. Unfortunately, none of these indices are really quantitative since they don't correspond to a single meaningful physical parameter and, more importantly, are clearly dependent on the choice of directions made for measurements. In fact, with these indices the degree of anisotropy would vary according to the direction of the applied gradients and the tissue frame of reference and would generally be underestimated. Rotationally invariant indices of anisotropy have been introduced by Pierpaoli *et al.* [14] through the combination of the diagonalized diffusion tensor elements (D_1 , D_2 and D_3). The most commonly used invariant indices are summarized in table 5.

The FA index (**F**ractional **A**nisotropy) measures the fraction of the "magnitude" of the tensor **D** that can be ascribed to anisotropic diffusion while the RA parameter (**R**elative **A**nisotropy) is described in terms of the tensor standard deviation representing the ratio of the anisotropic part of it to its isotropic part. Both anisotropy indices vary between 0 (isotropic diffusion) and 1 ($2^{1/2}$ for RA) (infinite anisotropy). Finally, VR (**V**olume **R**atio) represents the ratio of the ellipsoid volume to the volume of the sphere whose radius equals the mean diffusivity value. Its range of variation is between 1 (isotropic diffusion) and 0 (infinite anisotropy) so that some authors prefer to use $(1-VR)$ for easier comparison with the other anisotropy invariant parameters [24].

The concept of voxel-by-voxel anisotropy indices (also known as *intra-voxel* anisotropy) can also be extended to a family of *intervoxel* or lattice measures of diffusion anisotropy which allows neighboring voxels to be considered together in a region of interest [28]. The physical meaning of this *intervoxel* parameter is slightly different from that one discussed above for the classical *intra-voxel* anisotropy indices. In fact, the coherence index (CI) has to be thought as a measure of the coherence of the diffusion orientation across voxels composing the region of interest. The more the diffusion orientation will be respected passing from one voxel to the other, the higher the structural organization exhibits by the sample will be (CI = 1, perfect alignment of diffusion orientations, infinite *intervoxel* anisotropy condition). On the contrary, if the system under investigation is characterized by a large scattering of diffusion orientations across voxels (for instance in low structured samples) its coherence will be low and the relative CI index will tend to assume the value 0 (isotropic *intervoxel* diffusion condition). The *intervoxel*

measure of anisotropy has been extensively applied in clinical studies allowing the visualization of the human brain areas characterized by a higher degree of organisation such as the *corpus callosum* and the pyramidal tract in the white matter [24].

Anisotropy Measure	Formula	Range of Variation
Fractional Anisotropy (FA)	$FA = \frac{\sqrt{3}}{2} \sqrt{\frac{(D_1 - D)^2 + (D_2 - D)^2 + (D_3 - D)^2}{D_1^2 + D_2^2 + D_3^2}}$	$0 < FA < 1$
Relative Anisotropy (RA)	$RA = \frac{\sqrt{1}}{3} \sqrt{\frac{(D_1 - D)^2 + (D_2 - D)^2 + (D_3 - D)^2}{D^2}}$	$0 < RA < 2^{1/2}$
Volume Ratio (VR)	$VR = \frac{D_1 \times D_2 \times D_3}{D^3}$	$1 < VR < 0$

Table 5. Summary of the three main rotationally invariant intra-voxel anisotropy indexes. D = Apparent Diffusion Coefficient (ADC) = $(D_1 + D_2 + D_3) / 3$

Fiber Tracking

One of the most important achievement of the DTI protocol has been the possibility of mapping the orientation in space of sample structure. This has opened a completely new way to gain direct and in vivo information on the organisation in space of orientated tissue, such as muscle, myocardium, and brain or white spine white matter which are of particular interest in clinical studies.

As previously explained, the diagonalization of the tensors yields its eigenvalues and eigenvectors corresponding respectively to the principal diffusivities values and orientations (in terms of x, y and z spatial coordinates) with respect to the laboratory frame. The most intuitive approach of fiber tracking is **to consider the orientation of the fastest water diffusion (conventionally indicated as D_1) collinear with the local fiber direction of the tissue**. Since the orientation of the main water diffusivity is indicated by its eigenvectors (x, y and z spatial coordinates) the fiber tracking operation is simply performed by connecting the directional trajectories of eigenvalue 1 between the neighboring

voxels in order to trace out the underlying tissue fiber pathway or “tracts” of the entire imaging volume.

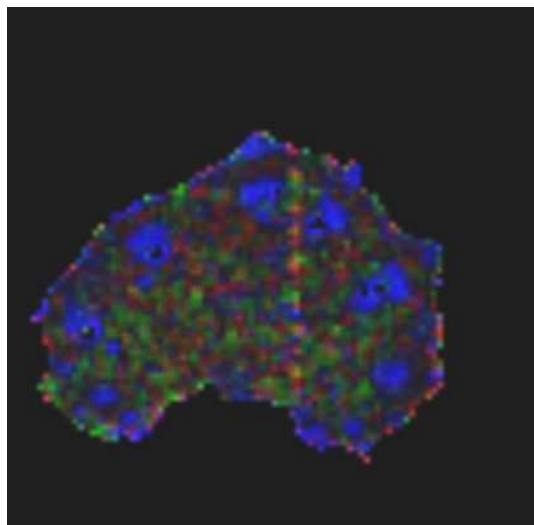


Figure 11. Representation of the main eigen-vector direction in a 1 mm slice thickness celery sample (coronal view) using a colour scale (red = x axis, green = y axis, blue = z axis). This image was acquired on a Bruker AM WB spectrometer (200 MHz ^1H resonance frequency) microimaging system. The diffusion encoding gradients were applied with a duration $\delta = 3$ ms separated by a time $\Delta = 50.8$ ms.

Common ways to visualize fiber orientation are based on colour encoding maps (figure 11), ellipsoid representations, streamlines and arrows (figure 12) pointing along the main diffusion direction.

Visualisation of specific sample tracts can be achieved by selecting the regions where fiber streamlines will begin or by applying “filtering” steps to interactively select among computed streamlines only those characterized by a specific range of intra-voxel anisotropy in order to recognize areas with higher structural organisation (see figure 13). This approach allows visualisation of the major biological sample tracts in a manner that is qualitatively consistent with the expected tissue structure as shown in figure 12.

Despite its enormous potentials diffusion tensor imaging is an inherently low-SNR technique. The noise level in DTI images can therefore have a direct impact on the accuracy of the estimated diffusion tensor and its eigenvalues and eigenvectors. Poor image SNR leads to erratic fiber streamlines behaviours. Fiber tracking accuracy can be achieved by employing more encoding directions or signal averaging; optimized sets of gradients directions for encoding anisotropic diffusion; or novel acquisition strategies such as reduced encoding DTI.

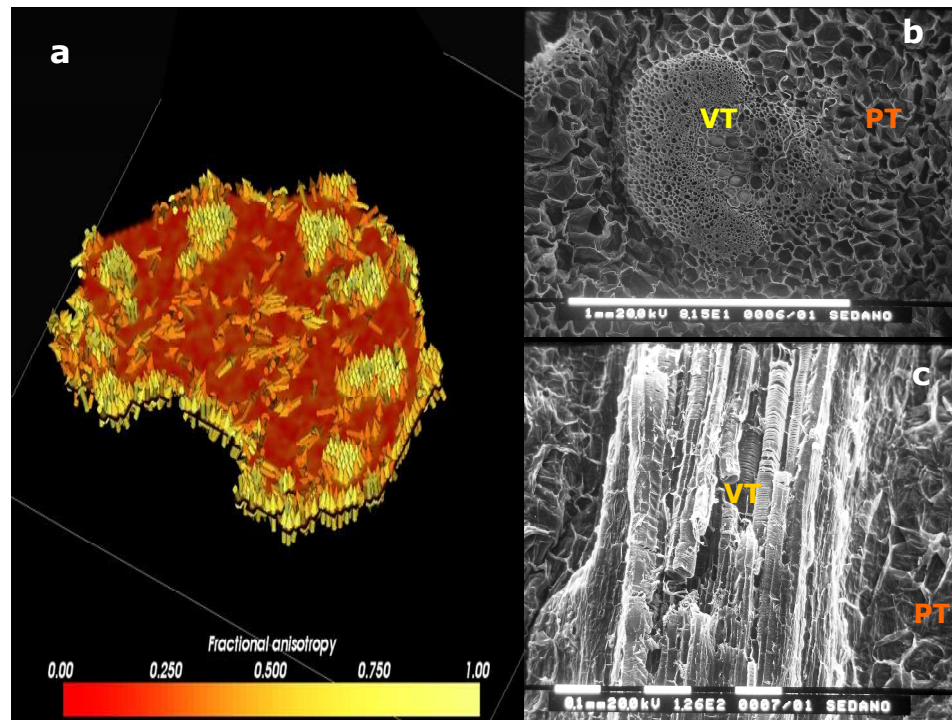


Figure 8. (a) 3-D arrows representation of the principal eigen-vector direction in a 1 mm slice thickness celery sample (transversal view). Since celery vascular tissue (VT) is more anisotropic than parenchyma (PT) these two areas can be readily delineated by the application of a fractional anisotropy (FA) colour encoding map (i.e. yellow vs red arrows respectively). The results are qualitative consistent with the tissue architecture observed in transversal (b) and longitudinal (c) SEM micrographs. This image was acquired on a Bruker AM WB spectrometer (200 MHz ^1H resonance frequency) microimaging system. The diffusion encoding gradients were applied with a duration $\delta = 3$ ms separated by a time $\Delta = 50.8$ ms.

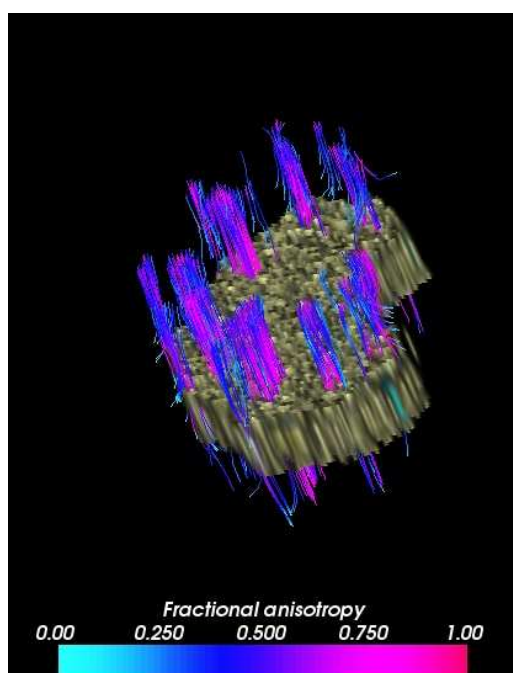


Figure 9. Fiber tracking representation of the major vascular tissue tracts in a 10 slices celery sample.

Fiber streamlines were computed from local diffusion tensor eigen-vectors and displayed as continuous tubular objects coded in colour as a function of their inherent fractional anisotropy index.

This image was acquired on a Bruker AM WB spectrometer (200 MHz ^1H resonance frequency) microimaging system. The diffusion encoding gradients were applied with a duration $\delta = 3$ ms separated by a time $\Delta = 50.8$ ms.

REFERENCES

1. L. D. Hall, S. D. Evans and K. P. Nott., *Magn. Reson. Imag.*, **16**, (1998), 485.
2. J. P. Renou and J. M. Bonny, *Food Chem.*, **82**, (2003), 35.
3. G. G. Cleveland, D.C. Chang, C. F. Hazlewood and H.E. Rorschach, *Biophys. J.*, **16**(9), (1976), 1043.
4. L. Garrido, V. J. Wedeen, K. K. Kwong, U. M. Spencer and H. L. Kantor, *Circul Res.*, **74**(5), (1994), 789.
5. J. E. Tanner, *Biophys. J.*, **28**, (1979), 107.
6. R. M. Henkelman, G. J. Stanisiz, J. K. Kim and M. J. Bronskill, *Magn. Reson. Med.*, **32**(5), (1994), 592.
7. M. E. Moseley, Y. Cohen, J. Kucharczyk, J. Mintorovitch, H. S. Asgari, M. F. Wendland, J. Tsuruda and D. Norman, *Radiology*, **176**(2), (1990), 439.
8. M.E.Moseley, J. Kucharczyk, H. S. Asgari and D. Norman, *Magn. Reson. Med.*, **19**(2), (1991), 321.
9. Foucat L., R. G. Taylor, R. Labas and J. P. Renou, *American Laboratory*, **33**(16), (2001), 38.
10. T. M. Guiheneuf, A. D. Parker, J. J. Tessier and L.D. Hall, *Magn. Reson. Chem.*, **35S**, (1997), 112.
11. T. Saotome, M. sekino, F. Eto and S. Ueno, *Magn. Reson. Imag.*, **24**, (2006), 19.
12. P. J. Basser, J. Mattiello and D. LeBihan, *Biophys. J.*, **66**, (1994), 259.
13. P. J. Basser, J. Mattiello and D. LeBihan, *J. Magn. Reson. Series b*, **103**, (1994), 247.
14. P. J. Basser and C. Pierpaoli, *J. Magn. Reson. Series b*, **111**, (1996), 209.
15. H. C. Bertram, R. H. Andersen and H. J. Andersen, *Meat Sci.*, **72**(1), (2006), 34.
16. T. M. Ngapo, I. H. Babare, J. Reynolds and R. F. Mawson, *Meat Sci.*, **53**, (1999), 149.
17. M. Mortesen, H. J. Andersen, S. B. Engelsen and H.C. Bertram, *Meat Sci.*, **72**, (2006), 34.
18. R. J. Carrol, J. R. Cavanaugh and F. P. Rorer, *J. Food Sci.*, **46**, (1981), 1091.
19. M. N. Martino, L. Otero, P. D. Sanz and N. E. Zaritzky, *Meat Sci.*, **50**(3),

(1998), 303.

20. M. M. Farouk, K. J. Wieliczko and I. Merts, *Meat Sci.*, **66**, (2003), 171.
21. M. J. Anderson and J. Robinson, *Australian and New Zealand Journal of Statistics*, **45**(3), (2003), 301.
22. M. J. Anderson and T. J. Willis, *Ecology*, **84**, (2003), 511.
23. W. Price, *Concepts Magn. Reson.*, **9**, (1997), 299.
24. W. D. Taylor, E. Hsu, K. R. R. Krishnan and J. R. MacFall, **55**(3), (2003), 201.
25. D. LeBihan, J. F. Mangin, C. Poupon, C. A. Clark, S. Pappata, N. Molko and H. Chabriat, *J. Magn. Reson. Imag.*, **13**, (2001), 534.
26. S. Warach, D. Chien, W. Li, M. Ronthal, R. R. Edelman, *Neurology*, **42**, (1992), 1717.
27. P. Van Gelderen, M. H. M. De Vleeschower, D. Des Pres, et al., *Magn. Reson. Med.*, **31**, (1994), 154.
28. T. Klingberg, C.J. Vaidya, J. D. Gabrieli, M. E. Moseley, M. Hedehus, *Neuroreport*, **10**(13), (1999), 2817.

CONCLUSIONS AND PERSPECTIVES

In past years NMR has successfully contributed with basic knowledge within essential areas of meat science. In particular, the NMR relaxation data have been proved to be highly sensitive to meat quality traits as revealed by the significant correlations found between the transversal relaxation time of meat and its water holding capacity (i.e. WHC), cooking loss, pH, colour indexes and other quality factors. These evidences suggested that NMR could potentially be used as a rapid, non-invasive and non-destructive on-line technique for the quality control of meat. Nevertheless, the development of generally NMR-based industrial applicable models and simple quality parameters is far to be achieved due to the complexity of meat exhibiting multicomponent and multiphase organisation.

In the present Ph.D. work the biophysical aspects related with the mobility and availability of water in meat in relation to its structural organisation have been investigated by NMR to reach a deeper understanding of the mechanisms underlying phase, water distribution and compositional changes of meat.

The theoretical studies conducted on reference concentrated BSA solutions and gels have highlighted the potentials of rationalizing the complexity of a real multiphase, multicomponent system such as meat through the analysis of a model protein system. The 1-D transversal relaxation distribution of a 24% BSA gel have revealed the presence of three proton populations identical to those previously reported for muscle and pork meat samples and respectively ascribed to myofibrillar (T_{21}), extra-myofibrillar (T_{22}) and structural water (T_{2b}). An approximately reduction of 90% in the signal of the two major proton pools (i.e. T_{21} and T_{22}) has been detected after deuteration of the BSA and meat samples confirming the water origins of the two populations. On the other hand, the minor decrease (19-21 %) characterizing the fast relaxing part of the signal (i.e. T_{2b}), has raised doubts about its assignment to the water fraction, let alone "structural water" suggesting a different origin. One possible hypothesis is that the T_{2b} population belongs to mobile macromolecular protons, for example protein side chains, whose mobility remains sufficiently high, despite cross-linking, and that for this reason can be detected in a CPMG decay, provided that the interpulse spacing is short. Under this view, the decrease of the T_{2b} population is but an effect of the deuteration of the labile protons present on the mobile chains and in intermediate or slow exchange with water, as this figure is comparable to the actual percentage of exchangeable protons in BSA (19.3 %).

Hydration experiments conducted on freeze-dried chicken samples seems to confirmed the macromolecular proton origin of the T_{2b} population. Particularly, this proton pool becomes more and more detectable in the low- T_2 region of the relaxograms as hydration proceeds exhibiting a behaviour compatible with a model by which the solid matrix is gradually plasticized by water. As soon as hydration is complete, plasticized chains have reached their maximum amount and mobility and do not change further upon water addiction. It is interesting to note that this mobility level approximately coincides with the water content at which freezable water is detected through calorimetric analysis and it might thus be considered as a reliable indicator of the physical-chemical and reological changes occurring in meat samples upon moisture variation.

Water-biopolymer interactions have been taken into account by extending the conventional 1-D relaxometric analysis of BSA to a higher number of dimensions. Particularly, the multidimensional experiments conducted on model BSA samples have been extremely effective in elucidating the different pathways involving magnetization transfer between the meat proton pools. Patterns of intermediate hydrogen exchange were visualized for the first time in cod meat samples between the macromolecular and the myofibrillar water pool in T_1 - T_2 and T_2 -store- T_2 multidimensional experiments. In addition, the possibility of directly detecting diffusion exchange between different microdomains in heterogeneous systems, such as BSA gels and meat samples, have been demonstrated by stepping out the store time in the T_2 -store- T_2 experiment to one second. This is especially interesting because the experimental observation of the water redistribution and microphase compositional changes during processing and storage of meat is an outstanding problem that affects the quality of the final product. Since structural and biophysical attributes of meat are generally modified by an increase number of factors (i.e. genetic, enzymatic chemical and mechanical) the future application of multidimensional protocols in the meat industry would allow the control of the microscopic water distribution and the prediction of how the modified biopolymer composition and matrix microstructure will affect the functional behaviour -such as texture and shelf life- of the raw product and its processed derivates. However, experimental imperfections, noise and sub-optimum regularisation in the inverse Laplace transform in addition to long acquisition times of the multidimensional cross correlation pulse sequences are a barrier to such on-line industrial quality control and novel pulse sequences for the ultra-fast acquisition of the multidimensional relaxation data are required to support this application.

Since the majority of solutes dissolved in meat are transported by water its translational diffusion properties have been studied because capable of influencing the chemical-physical composition and modification occurring in meat over time. The NMR diffusion decays of turkey samples have been interpreted in terms of a two sites (myofibrillar-extramyofibrillar water) exchange model assuming a cylindrical geometry of the system. The microstructural information inferred from experimental data have demonstrated a good level of agreement with histological observations reported in the literature. The consistency of the model has also been tested in assessing the effect of microstructure changes of meat induced by its storage at low temperature (i.e. freezing). The results have shown a reduction of the cell diameter (i.e. 12.56%) exhibited by the samples frozen at -30°C for 1 week. It has been hypothesized that this evidence might be interpreted in terms of the de-hydration of the cellular compartment on the basis of vapour pressure differences existing between the inside and outside of the cytoplasmatic environment. This explanation is consistent with the analysis of the CPMG curves where water re-distribution between meat domains occurs upon freezing with an increase in the extra-myofibrillar water population following the dehydration of the intra-myofibrillar compartment.

Since the high degree of organisation of meat, whose fibers are mainly aligned in a specific direction, the directional dependence of water diffusion (anisotropy) has rigorously been treated by application of the diffusion tensor MRI (DTI-MRI) technique. The analysis of meat self-diffusion coefficients and the most common diffusion rotationally invariant parameters have supported the results obtained in previous bulk NMR measurements confirming how meat overall organisation changes upon perturbation induced by low temperature treatments (i.e. freezing) conducted at different regimes. In particular, a generalized increase in the level of anisotropy has been detected in frozen samples compared to the fresh groups. This evidence is mainly attributed to the de-hydration of the intra-cellular compartment which reflects into a lateral shrinkage of the fibers. The random translational properties of water would thus be much more restricted across the diameter of the meat cells reflecting in a measurable decreased of radial diffusivity (i.e. D_2 and D_3) if compared to fresh data. This effect is even more severe in samples subjected to a slow freezing process if compared with ultra-fast methods (i.e. liquid nitrogen). The formation of large, exclusively extra-cellular, ice crystals associated to slow freezing process is responsible for a lateral pressure exerted on muscle cells which accelerates the water expulsion from the contractile

reticulum with a more pronounced reduction of the cell radius. On the contrary, when ultra-fast freezing is conducted the formation of smaller ice crystals uniformly distributed in the intra/extra-cellular space affects to a less extent meat microstructure. However, our data also demonstrate that large temperature fluctuation during storage of frozen samples can even out and exceed the positive effects exerts by the ultra-fast freezing procedure since re-crystallization phenomena occur leading to the formation of extra-cellular bigger ice crystals causing cells damage and strong compaction of fibers.

Acknowledgements

I express special thanks to my tutor Professor Claudio Cavani for the possibility that he has given to me. Together I also thank Dr Mauro Andrea Cremonini for having introduced me to the fascinating and mysterious world of NMR with genuine passion and high competence.

My gratitude also goes to all the members (Kevin Wright, Ben Pigott, Niusa Marigheto and Joshua Warner) of the MRI exploitation platform of IFR (UK). I particularly acknowledge Dr Brian Hills for the constant support I received during and after our six months collaboration.

I also acknowledge all the other members of our research group namely Professor Giuseppe Placucci and Dr Luca Laghi.

I finally would like to thank those with whom I shared the rest of the time out of the lab: my friends Armando, Checco, Andrea, Sylvain, Enea and Barbara.